Feasibility for lifting from a feeder vessel for a Tetrahedron crane

H.B. Kronenberg

Technische Universiteit Delft

TU Delft

Feasibility for lifting from a feeder vessel for a Tetrahedron crane

by

H.B. Kronenberg

to obtain the degree of Master of Science
at the Delft University of Technology,
to be defended publicly on Wednesday August 27, 2021 at 9:00 AM.

Student number:	4371852	
Project duration:	August 1, 2020 – August 27, 2021	
Thesis committee:	Prof. dr. ir. A.V. Metrikine,	TU Delft, Chairman
	Ir. J. S. Hoving,	TU Delft, Supervisor
	Ir. K. Kuipers,	TU Delft, Supervisor
	Ir. A. Ronse,	Tetrahedron B.V., Supervisor

TU Delft

Abstract

Due to the increasing demand for sustainable wind energy, larger wind farms with more giant turbines are required. Therefore, more is expected of the existing installation vessels for wind turbines. These changes make it increasingly difficult to find capable jack-up vessels to transport and install these new ”mega turbines”. Another trend in the wind industry is that the demand for wind farms is increasing outside of Europe, where protective laws often apply, such as the Jones Act. The Tetrahedron crane can lift higher without increasing the weight or size of the crane. Installing wind turbines with a Tetrahedron crane whilst supplying the wind turbine components with a feeder vessel would mitigate most problems with the current trends in the offshore wind industry. However, no research is done on performing lifts with a Tetrahedron crane from a moving vessel. This research aims to determine whether it is feasible to perform lifts from a feeder vessel subjected to heave motion with a Tetrahedron crane and analyse this feasibility for large quantities of data points in a relatively short period.

A case study is used to assess the feasibility of executing feeder lifts. The case study is used to provide constraints and parameters for two models that simulate a lifting operation. Both models describe the location of the load from the start of the lifting process till it is safely suspended far above the deck of the feeder vessel. The first model, the 1D model, is based on a free body diagram that provides a simplified representation of the Tetrahedron crane. This model can assess the feasibility of executing feeder lifts for entire data sets. The second model, the 2D model, represents the Tetrahedron crane as a system of elements and nodes. This model is used to validate the single lifting operations of the first model. Both models generate output data that provides insight into the dynamic forces that the crane and components endure during a lifting operation and if the load that is lifted experiences a re-hit or not. From this, it can be concluded whether a lifting operation is successful or not. Successful in this sense means no re-hit takes place, and the dynamic forces remain within limits set by the turbine and crane manufacturer.

While comparing the results of the two models, the 2D model approximates reality better because the dead weight of the crane construction is included where the 1D model does not. By adjusting the 1D model to account for the dead weight, results can be determined for entire data sets. A Tetrahedron crane has a higher lifting speed and a lower crane stiffness than a commonly used luffing boom crane. When both cranes have a comparable re-hit percentage, the results showed that the dynamic forces in the lift operations with the Tetrahedron crane are lower than with a luffing boom crane. In addition, analyses were made regarding the re-hit percentage for varying wave heights, wave periods and masses.

The outlined case study represents a realistic situation, and re-hit percentages within this case study are low. The re-hits that occur can be indicated, and it is also evident in which period lifting operations can be started safely. However, measures must be taken to ensure that the dynamic forces remain within the limits of the crane and turbine components. For the crane, this means that a greater lifting capacity is required. For the vulnerable turbine components, the dynamic forces must be reduced by, for example, a passive heave compensator.

Preface

Graduating during a global pandemic. The isolation, quarantines, and restricting measurements made the whole experience of graduation not only intellectually challenging but also mentally challenging. As someone who thrives on social interaction and collaboration. The many days of sitting alone behind a desk in my room were sometimes hard. Although I have had less contact with my colleagues at Tetrahedron as I would have wanted to. I would like to thank everyone for all the explanations and stories about cranes and the industry, clearly driven by an infectious passion and enthusiasm.

A big thank you to my committee. First of all, I want to thank my daily supervisor at Tetrahedron, Ir. Alexander Ronse. His technical insights have helped me time and time again. I have a lot of respect for his thorough and calm approach to solving problems. Secondly, I would like to thank Ir. Kaj Kuipers for his advice and especially for the Friday afternoon video calls. These conversations were not only helpful but also made the entire graduation process more social. In addition, I would like to thank Ir. Jeroen Hoving for making the necessary decisions and pointing me in the right direction. Finally, I would like to thank Prof. dr. Andrei Metrikine for his critical eye and for putting me at ease during meetings that I initially could be pretty nervous about.

I have learned a lot about cranes in the past year, and I also got to know myself better. Learned where my strengths and weaknesses lie. I am also sure that this experience has given my analytical and technical thinking a huge boost. I am proud of the thesis I have delivered, and I am sure it will be of value to Tetrahedron.

H.B. Kronenberg
Delft, August 2021

Contents

List of Figures

List of Tables

Nomenclature

List of Abbreviations

ACE	Automatic Crane Engineer
API	American Patroleum Institute
COG	Centre of Gravity
DAF	Dynamic Amplification Factor
DFT	Discrete Fourier Transform
DNV-GL	Det Norske Veritas - Germanischer Lloyd
DOF	Degree of Freedom
DOT	Delft Offshore Turbine
EOM	Equation of Motion
F&G	Friede and Goldman
FFT	Fast Fourier Transform
GE	General Electric
HVL	Heavy Lift Vessel
JONSWAP	Joint North Sea Wave Project
LAT	Lowest Astronomical Tide
LBC	Luffing Boom Crane
NDOF	Number of Degrees of Freedom
OWF	Offshore Wind Farm
PSD	Power Density Spectrum
SAE	Society of Automotive Engineers
SDOF	Single Degree of Freedom
SMC	Salvage and Marine Contractors
SSCV	Semi-Submersible Crane Vessel
T&I	Transport and Installation
U.S.	United States
WTG	Wind Turbine Generator

List of Symbols

$\ddot{z}$	Acceleration in vertical direction [m/s^2]
$\Delta l_{main-hoist}$	Extension of the main hoist cable [m]
ω	Frequency of oscillations of the load [rad/s]
$\tilde{p}$	Frequency of oscillations of the load [rad/s]
A	Cross-sectional area [m^2]
a	Acceleration [m/s^2]
DAF	Dynamic Amplification Factor [-]
E	Young's modulus [Pa]
$F_{dynamic}$	Dynamic force [N]
F_{static}	Static force [N]
g	Gravitational acceleration [m/s^2]
$K_{cable,single}$	Single cable stiffness [kN/m]
$K_{cable,total}$	Total cable stiffness [kN/m]
K_{crane}	Crane stiffness [kN/m]
K_{total}	Total stiffness [kN/m]
L	Length of main hoist cable [m]
l	Length of main hoist cable around winches [m]
M	Mass [kg]
NH	Number of falls of hoisting cable [-]
p	Frequency of oscillations of the load [rad/s]
T	Period [s]
t	Time [s]
V_{deck}	Velocity of the vessel deck [m/s]
V_{line}	Velocity of the cable at the winch [m/s]
x	Location in x-direction [m]
y	Location in y-direction [m]
z	Location in z-direction [m]
z_0	Initial location of the load [m]
H_s	Significant wave height [m]
V_L	Maximum steady hoisting velocity for the rated lifting capacity [m/s]
V_R	Relative velocity [m/s]
V_t	Velocity of the jib top [m/s]
V_{in}	Initial velocity [m/s]
W	Working load [N]

1 Introduction

1.1. Tetrahedron B.V.

1.1.1. Company

Due to the increasing demand for sustainable wind energy, larger wind farms with larger turbines are required. Therefor, more is expected of the existing installation vessels for wind turbines.

These changes make it increasingly difficult to find capable jack-up vessels to transport and install these new ”mega turbines”. Furthermore, the affordability of these specific vessels is also a concern.

Tetrahedron B.V. offers a solution for this by offering a new type of crane that can lift ultra-high offshore wind turbines, the Tetrahedron crane. That is why the slogan of Tetrahedron B.V. reads, ”Simply Lifting High” [3]. This crane can lift higher without an increase in weight or size, and is designed to be installed on existing wind turbine installation vessels, as can be seen in Figure 1.1. This figure shows that luffing boom cranes, traditionally used in offshore oil and gas, cannot lift high enough for the newer, and larger turbines. The common practice when it comes to installing offshore wind turbines is that these oil and gas cranes, which are designed to lift heavy loads at a limited height, are re-dimensioned for the wind industry. The Tetrahedron crane is designed from the ground up, and specific attention is paid to all the requirements for performing installations in the wind industry. Globally, customers have expressed their interest in this specialised crane. Section 1.1.2 provides a further explanation of the design and operation of the crane.

Due to the increasing size of the wind turbines, the number of turbines that fit on the deck of the jack-up vessels will decrease, the sailing velocity of the jack-up vessels is also very low, and the costs are often high. A feeder vessel could offer a solution for this by transporting the parts of the wind turbine. If a feeder vessel is used to transport wind turbine components to the installation site, transport will be faster, and the vessel costs will be lower. In addition, it would decrease the installation time.

The current offshore wind industry is mainly based in Europe. However, more recently, countries such as the United States and Japan are offering tenders to the offshore wind market [4]. This new market entry is positive for European companies with more experience, but these new markets have their own rules and regulations, such as the Jones Act. The Jones Act requires that all goods shipped between U.S. ports have to be transported by U.S. vessels. However, if a jack-up vessel with a Tetrahedron crane can perform a feeder lift, this problem is mitigated because there is no need for the jack-up to enter a foreign harbour or quay.

1.1.2. Tetrahedron crane

The crane developed by Tetrahedron has a unique design with certain parts that are not common in luffing boom cranes. Figure 1.5 and Figure 1.6 depicted, respectively, the crane’s side and top view with the accompanying terms of the components. The crane is offered and designed in three different sizes: Tetrahedron 25, 45, and 65. However, the company does not rule out that other sizes will follow in the future. The number behind the name refers to the maximum overturning moment at the slew bearing in thousands of tonne-meter. The name Tetrahedron comes from the luffing assembly, shown by the orange triangle in Figure 1.3, which has a tetrahedron shape. The largest crane, the Tetrahedron

Figure 1.1: Comparison of the lifting height of a luffing boom crane with the lifting height of a Tetrahedron crane.

65, can lift loads up to 200 meters above the waterline, and has a maximum lifting capacity of 1250 metric tons.

While installed in the same jack-up vessel, a Tetrahedron crane can lift higher than a luffing boom crane due to the luffing mechanism. A conventional luffing boom crane luffs from derrick cables at the top of the A-frame, as can be seen in Figure 1.2. The pivoting point for the boom of the crane is at the inner side of the slew bearing, depicted in the figure at the point where the yellow plateau connects to the blue bar. The Tetrahedron crane rotates around the hinge at the back of the base frame. Furthermore, the luffing comes forth out the tetrahedron hoist that lifts the tetrahedron part of the crane at the heel from the mast. Compared to the luffing boom crane, the rotational point of the Tetrahedron crane is located behind the slew bearing and is also placed higher above it. The location of the rotational point allows the crane to have a much longer luffing assembly than that typically could fit onto a jack-up vessel. A higher pivoting point and a much longer jib results in the crane reaching enormous lifting heights.

Another advantage this crane has, compared to luffing boom cranes, is that the structure is relatively slender due to its members having small cross-sectional areas. Tetrahedron B.V. achieves these small cross-sectional areas by designing the crane with the help of an in-house software program: ACE, which stands for Automatic Crane Engineer. Typically customising or designing a new crane takes a very long time, as engineers need to execute many computations for each modification. This is because every ship is slightly different, and load cases are unique in every situation. The ACE software program aims to speed up this design process. ACE calculates the forces acting on the crane during lifting, optimises the crane for these specific forces. This results in a crane where the allowable stresses and the minimalisation of the cross-sectional areas of the members are closely matched. A lightweight crane with a high lifting capacity is the end product.

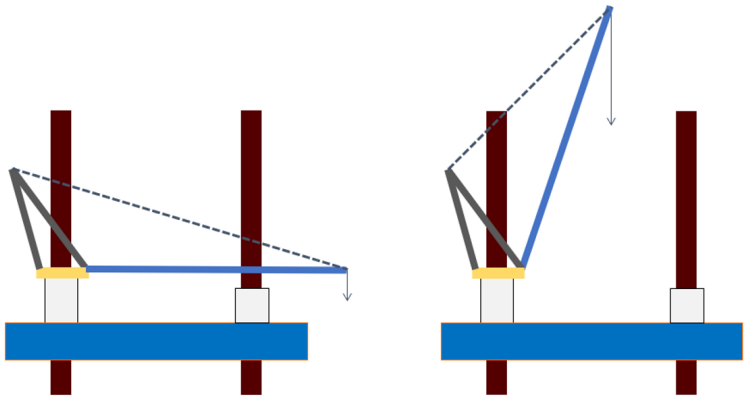

Figure 1.2: A luffing boom crane in rest position on the left and in lifting position on the right.

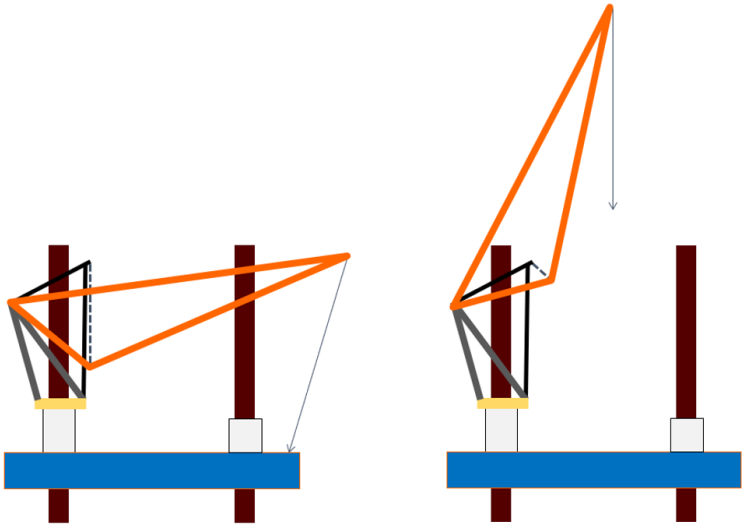

Figure 1.3: A Tetrahedron crane in rest position on the left and in lifting position on the right.

1.2. Problem statement

After developing and achieving DNV-GL design verification on the crane principle and concept design, Tetrahedron B.V. investigates alternative crane capabilities. The capability to lift higher and the competitive lifting speed promises a high installation rate compared to conventional installation configurations. However, the crane installed on a jack-up vessel causes the necessary inconvenience because of its low sailing speed and the time needed for the jack-up vessel to prepare for lifting operations and lowering back down before sailing to the harbour or following location. To achieve a higher installation up-time and pressing costs, the jack-up vessel with the Tetrahedron installed will remain at the location where the construction of the offshore wind farm takes place for the entire duration of the project. The supply of wind turbine components will be done by a so-called feeder vessel. This vessel has a higher sailing speed and will retrieve all the necessary components from the quayside and transport these to the jack-up vessel. However, this feeder vessel is subjected to wave motion which requires the crane to lift a load that is moving up and down.

Jack-up vessels are not able to carry as much wind turbine components as they used to, this is due to the growing turbine size. More trips to the quayside are needed and the relative up-time of the jack-up vessels decreases. Furthermore, to install the ever growing wind turbines, there is a need for more giant cranes leaving less deck space to store wind turbine generator components. Therefor, the Tetrahedron crane would be a viable solution. However, the capability, associated safety and effectiveness of feeder lifts of the Tetrahedron crane needs to be investigated.

1.3. Scope of work

The aim of this research is to investigate the feasibility of feeder lifts, executed by a Tetrahedron crane, providing wind turbine generator components to a jack-up vessel. The following research question needs to be answered:

What is the feasibility of executing feeder lifts with a Tetrahedron crane, and what are the limiting sea states in which these feeder lifts can be executed?

The process of executing the feeder lifts is limited to the offloading of the wind turbine generator components from a feeder vessel to either the deck of the jack-up vessel or onto the substructure of the, to be assembled, wind turbine. Only the heavy lifts of the wind turbine blade, nacelle and tower, together called the superstructure, shall be assessed. Lifts may include additional weight and size due to frames and rigging. The definitions of the wind turbine generator components can be found in Figure 1.4. The substructure is assumed to be installed in place and ready for installation of the superstructure. The placement and installation of these substructures are therefore considered out of scope. The type of substructure does not influence this thesis's research but is assumed to be a monopile because this is the most common used substructure.

The Tetrahedron crane, the jack-up vessel, the deck layout of the feeder vessel and the specific wind turbine generator with installation procedure will be described in Chapter 3. These will be used to sketch a realistic case study but may be subjected to changes. This case study contains the essence of the problem. The solutions can be used and implemented to different jack-up vessels, feeder vessel and wind turbine generators as long as the Tetrahedron crane is used to execute the heavy lifts. Additionally, the method used to analyze the potential for performing feeder lifts must be able to analyze large amounts of data, preferably in a relatively short time, and to assess feasibility if these lifts. This additional purpose of the analysis is important to determine the timing of the performance of the feeder lifts.

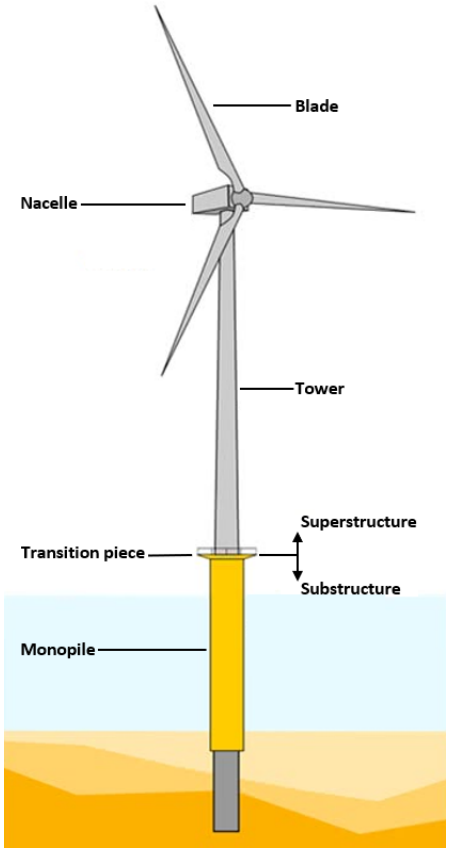

Figure 1.4: Components of a wind turbine generator.

1.4. Layout of the study

In order to successfully complete the thesis and answer the main question, a series of sub-questions need to be answered.

1. What is the common practice of installing wind turbine generators in the wind industry, and why is it relevant to start installing wind turbine generators (WTG's) with a feeder vessel?
2. Which turbine model, crane size and wind farm can be combined into a case study that represent a realistic feeder lift operation?
3. What boundary conditions apply to this case study?
4. What are the most critical activities involved in this case study?
5. How can a single degree of freedom (SDOF) model simulate lifting from a feeder vessel and why use such a simplified model of the crane?
6. What are the limiting conditions where the Tetrahedron crane can lift safely according to the 1D model?
7. How can a 2D NDOF model simulate lifting from a feeder vessel and what advantages does this model have in comparison to the SDOF model?
8. In what manner can these results be optimized to improve workability of feeder lifts with a Tetrahedron crane?
9. Is it possible to implement the results outside of the case study?

1.5. Methodology

A case study is used to answer the research questions from the previous section. Based on this case study, the feasibility of feeder lifts can then be assessed together with the extent in which feeder lifts are feasible outside this case study. However, first a case study must be determined and it must be determined to what extent the case study sketches a realistic situation. The case study is based on the available literature and data within Tetrahedron B.V. Subsequently, this case study is used as the basis of the models that are used to assess the feasibility, it will provide the constraints and parameters that are used.

To assess the case study a 1D and a 2D python-model are constructed to mimic the performance of a Tetrahedron crane executing feeder lifts. Both models describe the location of the load from the start of the lifting operation. Here the load is initially located on the vessel deck, after which it is gradually transferred from the vessel deck to the Tetrahedron crane before a lift-off occurs. From this moment onward the load is suspended in the crane hook. Analyses are performed concerning force, motion and velocities.

The 1D model is based on a free body diagram where the equation of motion and general solution are derived. This free body diagram is a simplified representation of the Tetrahedron crane. The equations derived from this model are used to simulate the location of the load from the moment of lift-off, the moment the load is fully suspended in the crane. Prior to this moment, the weight hanging in the crane hook increases until the entirety if the load is suspended in the crane. The moment of lift-off is used to obtain the initial conditions that the load has as a result of lifting from a moving feeder vessel. These initial conditions consist of the location and the velocity of the load at the moment of lift-off and are used as parameters in the general equation for the simplified dynamic 1D model and help determine the trajectory of the load whilst suspended in the crane. The simplified representation of the Tetrahedron crane in the 1D model makes it possible to assess the feasibility for large amount of data in a relatively short amount of time.

The 2D model represents the Tetrahedron crane with a system of elements and nodes. The elements are modelled as Euler-Bernoulli beam elements with possible axial extension. Based on this representation, a mass- and stiffness-matrix can be determined for the system. Together with the known forces caused by the weight of the structure, additional weights and external loads, the displacements of the nodes over time can be computed. This model uses the direct stiffness method to compute the mass- and stiffness matrix. Furthermore, the state-space formulation is used to re-write and simplify the equations of motions. The Runge Kutta 4th order method is used to execute the numerical integration. Resulting in the locations of the nodes over time. The most critical node, the node resembling the crane hook, is used to conclude whether or not a lifting operation results in a re-hit.

Results obtained from both the 1D- and 2D-model are used to access the feasibility of executing feeder lifts for the case study. The case study is concluded by validating and discussion the obtained results. Next, the feasibility of feeder lifts in situations outside the case study are examined. Conclusions for performing feeder lifts with a tetrahedron crane in general are made, and to conclude the thesis recommendations for further investigations are made.

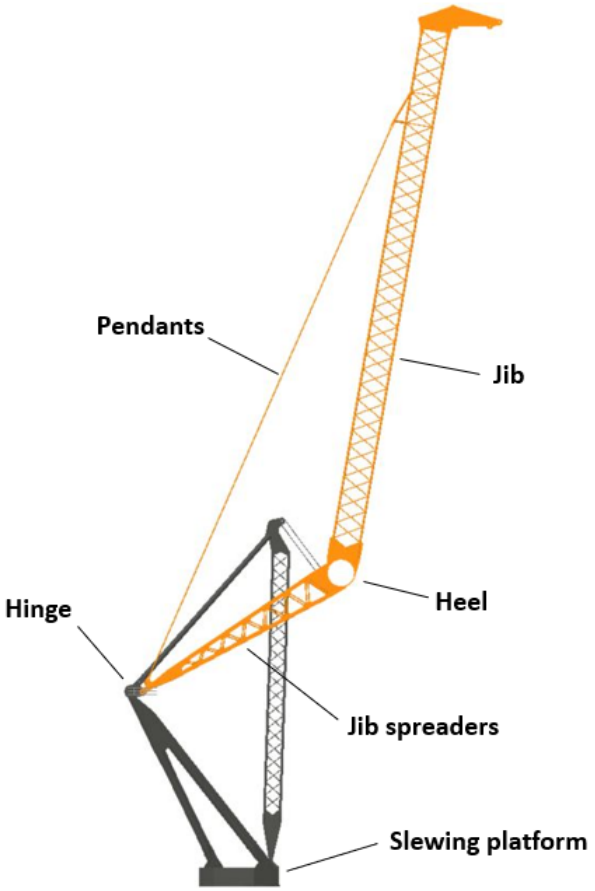

Figure 1.5: Tetrahedron crane - side view

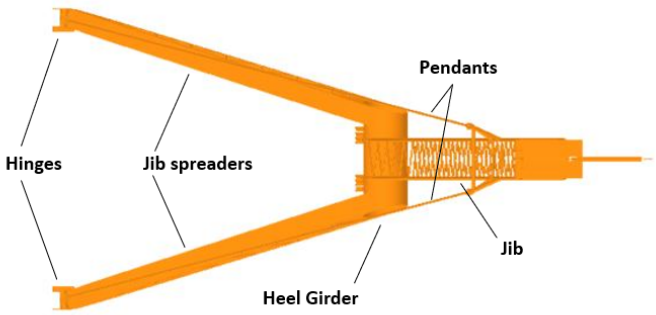

Figure 1.6: Tetrahedron crane - top view

2

State-of-the-Art of Feeder Lifting

For Tetrahedron B.V., being a new company entering the offshore wind installation market, it is helpful to understand the current trends in the development of offshore wind turbines as is the current way these turbines are being installed. Furthermore, it is helpful to know what lessons are learned from previous projects and how they worked out for the competitors when they changed their installation approach. Moreover, possible technical challenges are addressed. The information on the current market, future developments and possible competition will help to assure a competitive and profitable entry into the wind installation industry.

2.1. Current installation of wind turbine generators

Offshore wind farms consist of several turbines connected in loops or array through cables underneath the seabed. These cables transport the electrical energy to one or more converter stations, from which a more significant power cable transports the electrical energy to shore, where it is utilised. As explained in Section 1.3, before the WTG installation, the substructures are built. The substructure construction is usually done by a wind-dedicated jack-up vessel or a floating heavy lift vessel. In general heavy lift vessels, like Boskalis' Bokalift 1 and the Oleg Strashnov from Seaway Heavy Lifting, are more common used for these kinds of installation.

2.1.1. Installation procedure

The most common practice to install wind turbine generators is with wind dedicated jack-up vessels. These vessels provide the transport of the turbine components from quayside to the destined location (Figure 2.1), where often the substructure is already in place. Subsequently, the vessel can install the wind turbine (Figure 2.2). The flow diagram depicted in Figure 2.3 shows the steps usually taken in the transport and installation (T&I) cycle with a wind dedicated jack-up vessel. The cycle starts with the supply of components onto the vessel deck. Before the supply commences, the vessel first jacks up onto its legs. The components building up the wind turbine are, in general, one tower, one nacelle, and three blades. Resulting in a total of 5 significant lifts needed to install one turbine. When the jack-up vessel arrives at the pre-installed substructure, it jacks up before installing the tower, nacelle, and blades in that order. However, with more giant turbines, it occurs that blades and towers can consist out of multiple parts [5], but mostly these are pre-assembled in the marshalling yard. Limited deck space on the jack-up vessel causes a maximum amount of turbine components to be fit and loaded onto the vessel at the marshalling yard. Components are sea-fastened and transported on unique frames and grillages to protect them along the T&I. In addition to the turbine parts, the necessary tools for the installation must also be taken on the vessel deck. Furthermore, distances between all components on the deck must be taken into account to ensure workability and safety on the vessel.

Figure 2.1: Transport to installation side by jack-up vessel Aeolus of Van Oord.

Figure 2.2: Installation of a wind turbine blade by jack-up vessel Aeolus of Van Oord.

The main advantage of installing wind turbines with a wind dedicated jack-up vessel is that whenever the vessel executes a lift, it is in a jacked-up position. This largely mitigates the vessel motion due to currents, waves, and wind. This results in a higher workability. The number of wind turbines that make up the installed wind farm determines the number of voyages the jack-up vessel has to make from and to the marshalling yard. The world largest wind farm, when looking at the number of wind turbines, is London Array, with 175 turbines which have a combined capacity of 630 MW [6]. The second and third wind farms consisting out of the most wind turbines are the Hornsea 1 and Gwint y môr with 174 and 160 wind turbines, having a capacity of respectively 1218 and 576 MW [7][8]. This makes Hornsea 1 the wind farm with the largest installed capacity to this date. However, plans are underway for wind farms with even greater capacities. For example, the Sinan offshore wind farm, when completed, will have an installed capacity of 8.2 GW [9].

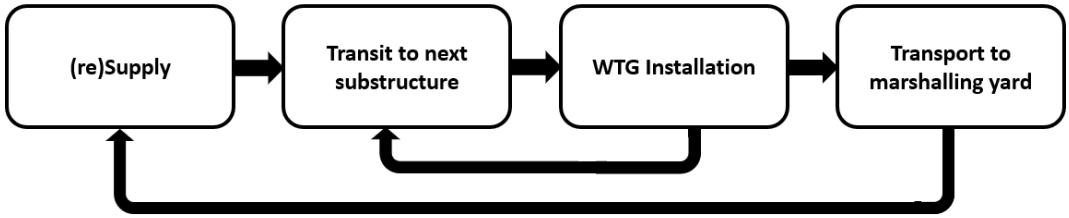

Figure 2.3: Flow-diagram of the WTG installation process with a jack-up vessel.

2.1.2. Jack-up vessel developments

Over the years, the wind turbine generators that need to be installed offshore have grown in size, and the installation has moved further offshore into deeper waters. This trend is further explained in Section 2.4.2. With these trends, also the installation vessels have changed. The first jack-up vessels to install offshore turbines were jack-up barges. These floating platforms had tubular poles with which the vessel could hold itself in place during installation. Sometimes, these vessels had a mounted crane installed on an elevated structure, but, more often, the cranes were mobile at the beginning. The next generation of dedicated wind installation jack-up vessels used larger tubular structures as jack-up poles. Cranes were installed around one of these jack-up legs to have a smaller footprint on the vessel deck. A larger area of the deck could be used to store the components needed to install the wind turbines. The latest and most modern wind turbine installation vessels use lattice structures as their jack-up legs. The lattice structures as legs allowed the jack-up vessels to install turbines in deeper waters. An overview of all the jack-up vessels used in the wind industry is shown in Table 2.1 [10]. This table gives an overview of all the active jack-up vessels with a maximum operational water depth of a minimum of 50 meters. Components of the latest generation of wind turbines are heavier than the crane capacity of some of these vessels but are shown in the table to complete the overview.

Company	Vessel name	Leg type	Depth [m]	Crane capacity [mT]
GeoSea	Neptune	Tubular	50	600
Jan de Nul	Vole Au Vent	Tubular	50	1500
A2Sea	Sea Challenger	Tubular	55	900
A2Sea	Sea Installer	Tubular	55	900
Fred. Olsen Windcarrier	Brave Tern	Tubular	55	640
Seajacks	Zaratan	Tubular	55	800
Fred. Olsen Windcarrier	Bold Tern	Tubular	60	640
Swire Blue Ocean	Pacific Orca	Lattice	60	1200
Geosea	Innovation	Lattice	65	1500
Seafox	Seafox 5	Lattice	65	1200
Seajacks	Scylla	Lattice	65	1500
Swire Blue Ocean	Pacific Osprey	Lattice	70	1425
Geosea	Apollo	Lattice	106,8	800

Table 2.1: Jack-up vessels involved in the installation of WTG's, as of 2018.

2.2. Alternative wind turbine installation

2.2.1. Transport of turbines while suspended in the crane

Apart from the conventional method, using an installation vessel with all the necessary components on it, for the installing of wind turbine generators, several other methods have been used to supply installation vessels with components. Furthermore, projects can be found where the installation of wind turbines was executed by vessels previously only used in the oil and gas industry, so vessels that are not dedicated to installing wind turbines. An example of such a project can be found in Figure 2.4. This figure shows a sheerleg barge named Rambiz, owned by Scaldis SMC for the Beatrice project on the coast of Scotland. The project consisted of the placement and installation of two jackets with two onshore-assembled, 5 MW wind turbines. The Rambiz is mainly used as an installation vessel for, among other things, topsides, jackets, and gravity-based foundations. The lift and installation of these two wind turbines as a whole were possible because of the relatively small size of the turbines and the gigantic transition piece connecting the bottom founded jacket with the turbine tower [11].

Figure 2.4: Transport and Installation of two 5MW Wind Turbine Generators for the Beatrice Demonstrator Project.

Figure 2.5: Installation of the first offshore WTG with a slip joint by floating heavy lift vessel, the Aegir.

The second case where a floating vessel provides the transport and the installation of a wind turbine generator is the installation of a turbine that was directly placed on a tapered monopile with a slip-joint connection commissioned by Delft Offshore Turbine (DOT). Heerema Marine Contractors executed the transport and installation (T&I) with its heavy lift vessel, the Aegir, shown in Figure 2.5. The installation was done at the Prinses Amalia wind farm, which is on close sailing distance to a quayside which allowed the Aegir to lift the turbine as a whole and transport the turbine while freely hanging in the turbine crane to the already installed, customized monopile. Again, the installed wind turbine was tiny in size and was meant as a proof-of-concept project.

A final example of a project executed by a floating vessel is the Hywind project commissioned by Equinor and performed by the Saipem 7000, a semi-submersible crane vessel (SSCV). The project consisted of 5 turbines installed on floating substructures. At the moment of installation, this project was the first floating wind farm in the world [12]. The 6MW turbines were installed in an in-shore bay. That the installation took place close to shore can also be seen in Figure 2.6. Therefore the distance from the quayside to the harbour was minimal. Also, the sea conditions are more forgiving nearshore. This combination made it possible to lift the pre-assembled turbines as a whole from the quayside, sail to the desired installation location, and installed on top of the floating substructures.

To summarize, all three projects are executed with a floating heavy lift vessel in very favourable weather conditions, as can be seen in Figure 2.4, 2.5, and 2.6. The turbines were already assembled onshore and transported in one piece. All the projects were executed with relatively small wind turbine generators, and also the number of turbines per project was not higher than five. The installation of more significant numbers or more giant turbines have not yet been executed with floating installation vessels. Also, no such project has been executed in less forgiving weather conditions.

Figure 2.6: Saipem 7000 installing a 6 MW inshore wind turbine on a floating substructure.

2.2.2. Feeder lifts from jack-up feeder vessels

A different way of supplying the installation vessels with wind turbine components, rather than sailing back and forth to the harbour, is by using a different kind of vessel to transport the components to the installation vessel. A project where they used a feeder vessel for the supply of wind turbine components is the Block Island wind farm near Rhode Island in the United States. The Block Island wind farm consists out of 5 turbines, each having a capacity of 6 MW [13]. Since this is the first offshore wind farm ever built in the United States, no experience and specialized vessels were available in the United States [14]. Fred. Olsen Windcarrier's wind dedicated jack-up vessel, the Brave Tern, has executed the installation of the turbine's. To do this, this ship had to sail across the Atlantic Ocean first, with the five nacelles already loaded onto the deck. The transport of the turbine blades and tower parts from an American port was carried out by a jack-up barge to circumvent the Jones Act (elaborated in Section 2.4.3). However, this barge was only big enough to handle the components for one turbine, as can be seen in Figure 2.7, three turbine blades and one tower. Once both jack-up vessels arrived at the jacket substructure and transformed to their jacked-up position, shown in Figure 2.8, the installation could commence. Then both vessels jacked down, the Brave Tern sailed to the next installation side, and the jack-up barge sailed back to the harbour to get the components for the next turbine. This process repeated itself five times. The solution used for the Block Island wind farm installation was politically driven, and it was certainly not the most productive solution.

Figure 2.7: Jack-up feeder barge transporting a tower section and three blades.

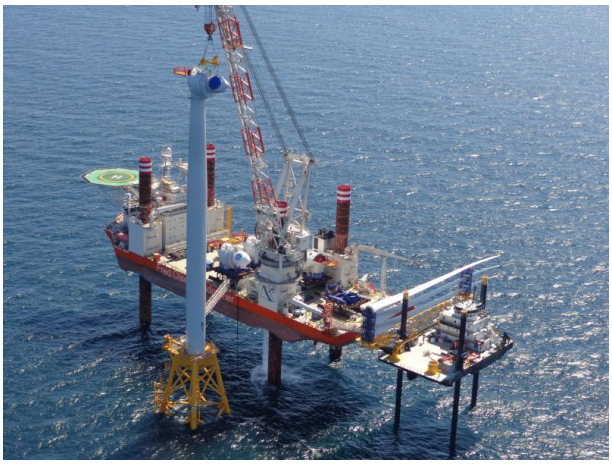

Figure 2.8: Brave Tern installing a nacelle for the Block Island wind farm.

2.2.3. Feeder lifts from floating feeder vessels

The last uncommon way of supplying installation vessels with wind turbine components is by using a floating feeder vessel instead of a jack-up feeder vessel. However, supplying components involves more risks since the feeder vessel is subjected to wave, tidal, and wind forces and therefore is constantly moving. Feeding components from a floating feeder vessel is done multiple times in the oil and gas industry; however, only a few examples are reported in the wind industry. All of them being in Chinese water and executed by Chinese company's.

The first example of a project where a floating feeder vessel is used is at the Xinghua Gulf demo project [15]. The project involved the construction of three 6MW wind turbines from General Electric. Figure 2.9 shows the one turbine that is just installed together with the wind turbine installation vessel and the feeder vessel that supplied the components behind it. Figure 2.10 shows another example of a floating feeder vessel supplying the turbine blades to the installation vessel. This figure shows a jack-up vessel of China's General Nuclear Power Corporation installing a 5.5 MW wind turbine on a pre-installed jacket substructure in the South China Sea for the Yangjiang Nanpeng Island Offshore Wind Farm [16]. The wind farm will consist out of 18 turbines.

Little is known about how these lifting operations were performed and what preliminary work was performed to ensure that all lifts were done safely and without damaging crane, vessels and turbine components. What does stand out in Figure 2.9 and 2.10 is that the sea surface is relatively calm, waves seem almost absent, and therefore, the motion of the feeder vessel is probably minimal.

Figure 2.9: Installation of 6MW turbine for the Xinghua Gulf demo project.

Figure 2.10: Installation of 5.5MW turbine for the Yangjiang Nanpeng Island Offshore Wind Farm

2.3. Technical challenges

The previous section showed there is little experience in the industry with installing offshore wind turbines using feeder lifts. Only a few projects are known that used a feeder vessel to supply the components for the turbines. All of these projects dealt with very forgiving weather conditions. When the weather conditions are less favourable, the motions of the feeder vessel increase and can lead to higher forces being exerted on the crane, feeder vessel and turbine components. In this section, the magnitude of the forces due to feeder vessel motions are discussed and how these forces can be taken into account computationally.

A dynamic factor or dynamic amplification factor (DAF) is used to multiply with the static load to account for dynamic effects caused by, for instance, crane movement or the motion of the load [17]. The static load, or working load, can be described by the load due to the static weight of an object plus the additional load due to the weight of accessories. For example, rigging, lifting beams, sheave blocks and hooks. The dynamic force (in N), which is exerted on the crane due to operational motions of the crane and feeder vessel, can be obtained through Equation 2.1.

In the DNV standard for "Offshore and platform lifting appliances", the dynamic amplification factor is described as Equation 2.2 [18]. In this equation, V_R represents the relative velocity (m/s) between the load and the hook at the lift-off time, W is the working load in kN, and g is the standard acceleration of gravity ($9,81\ m/s^2$). Finally, K_{total} is the stiffness coefficient defined by force at the hook needed to produce unit deflection at the hook (kN/m). This stiffness coefficient is calculated by taking into account all elements from hook to pedestal support structure.

$$F_{dynamic} = F_{static} * DAF \tag{2.1}$$

$$DAF = 1 + V_R \sqrt{\frac{K_{total}}{W * g}} \tag{2.2}$$

The relative velocity (V_R) between the load and the hook at the time of lift-off is described in Equation 2.3. This equation shows that the relative velocity is built up out of three velocity components. The maximum steady hoist velocity for the rated lift capacity(V_L), the downward velocity of the load at the moment of lift-off (V_{in}), and a velocity component describing the velocity of the crane's jib top V_t, all have m/s as their unit.

$$V_R = 0.5 * V_L + \sqrt{V_{in}^2 + V_t^2} \tag{2.3}$$

$$V_R = V_H + \sqrt{V_{in}^2 + V_t^2} \tag{2.4}$$

DNV states that in a situation, where there is no need to use the maximum hoist velocity, the crane operator will only use half of the maximum hoisting velocity. A situation without the need for the use of the maximum hoist velocity is when the occurrence of re-hits and snap loads are disregarded. When a lifting operation requires the use of the maximum lifting velocity, Equation 2.4 can be used instead of Equation 2.3. In this equation the velocity term dependent on the maximum steady hoist velocity ($0.5V_L$) is replaced with V_H. This adjustment can only be made if $0.5V_L$ is lower than V_H. This new term, V_H, in the equation can be calculated by; $V_H = 0.1(H_s + 1)$. The value for V_H is prescribed such that there is enough clearance with the next wave crest to avoid a re-hit, the impact probability with the next wave crest is reduced to an acceptable level of $< 2\%$. The reasoning behind the equation that describes V_H can be found in the SAE J1238 guideline [19]. This guideline states that the crane operator often starts his hoist operation at the trough of a wave. However, the hoist speed often cannot follow the wave and lift the load clear from the vessel deck before the wave crest that succeeds the through. Because of this relationships between hoisting velocity and the velocity of the wave, the lift-off will usually be while the ship is falling after the first crest. The velocity, V_H, is determined under the assumption that the least favorable condition occurs. The least favourable condition is that the lift-off occurs at maximum downward speed. The velocity that is determined with the equation for V_H is set up such that the probability that, after this unfavorable lift-off, a re-hit occurs with the next wave crest is less than 2 percent.

The second component, the downward velocity of the load at the moment of lift-off, can be obtained using three different methods. First, it can be obtained using direct measures of the deck velocity on the vessel. Or it can be estimated through motion studies for ships at sea. The last, most straightforward and widely used method, also the method used in the DNV standard, is by estimating the water surface velocity based on the sea state. DNV describes the downward velocity of the cargo vessel as $V_{in} = 0.6H_s$ for a significant wave height up to three meters. For wave heights higher than three meters, this velocity component may be assumed to be equal to $V_{in} = 1.8 + 0.3(H_s - 3)$. These equations are set up so that the exceedance level of the calculated wave velocity is 2%, so the chance of non-exceedance is 98%. The exact formulation for the vessel velocity is found in API Specification 2C - Specification for Offshore Cranes [20]. A general assumption both DNV and API make is that the wave velocity is equal to the vessel's velocity. This is only valid for relatively small vessels. Larger vessels typically experience smaller deck velocities than the wave velocity is where they are located. The probability of non-exceeding the calculated velocity of the vessel would be even higher, making the calculation of DNV even more conservative.

The last velocity component that impacts the relative velocity, the velocity caused by the motion of the crane's jib top (V_t), is only of significance for cranes located on mobile or floating offshore units. If the crane is located on a bottom supported platform or vessel, this velocity component may be assumed to be zero and can be left out of Equation 2.3 and 2.4.

Two out of the three velocity components that make up for the relative velocity between hook and load at the moment of lift-off are dependent on the significant wave height. They depend on the possibility of exceeding this significant wave height. The probability of exceeding that has been taken into account by DNV is very low, less than 2%, and is taken into account for both velocity components. Furthermore, the assumption that the vessel's velocity at the moment of lift-off is equal to the wave velocity at lift-off is only valid for relatively small vessels. This assumption would lead to an even more conservative determination of the DAF for larger vessels and thus for the dynamic forces.

The dynamic amplification factor is also described in "Dynamic Factors for Offshore Cranes" by D.E. Charett (1976). D.E. Charett describes the DAF as can be found in Equation 2.5. In this equation, the relative velocity is based on the actual lifting velocity (V_L) and the velocity of the feeder vessel's deck (V_D) at the moment of lift-off, both in m/s, and these components are not conservative estimates based on the significant wave height and the chance of exceeding this significant wave height. This makes it possible to find a different value for the DAF for each lifting operation in a specific sea state. The velocity of the feeder vessel at the moment of lift-off can vary significantly per lifting operation. This would probably give a closer estimate of the dynamic force that occurs during a lifting process. However, the downside of this way of determining the DAF is that the true velocity of the vessel at the moment of lift-off can only be estimated in advance. The actual velocity during the lift-off can only be obtained by monitoring the lifting operation and retroactively determining the velocity and thus the dynamic force. It could therefore happen that the value of the DAF estimated in advance is exceeded during the actual lifting operation.

$$DAF = 1 + (V_L - V_{deck}) \sqrt{\frac{K_{total}}{W * g}} \tag{2.5}$$

2.4. Future challenges and opportunities

2.4.1. Larger wind turbine generators

The design of the turbines might vary between different projects and wind farms, but the general trend is that the size of the turbines is growing, as can be seen in Figure 2.11. More giant turbines can harvest energy from the wind more efficiently and compete with fossil-fuel alternative energy sources. On average, a wind turbine had a rated power of 1,77 MW in 2010, and due to the growing size of the WTG's, this grew to an average of 2,77 MW in 2017 [21]. However, this is not only due to the increasing size of the turbines but also due to technological progress. The disadvantage of the ever-increasing wind turbines is that fewer and fewer installation vessels can install these mega turbines. It is estimated that around the year 2030, there will be turbines with a hub height of far more than 125 meters. Only a handful of vessels can install this [22].

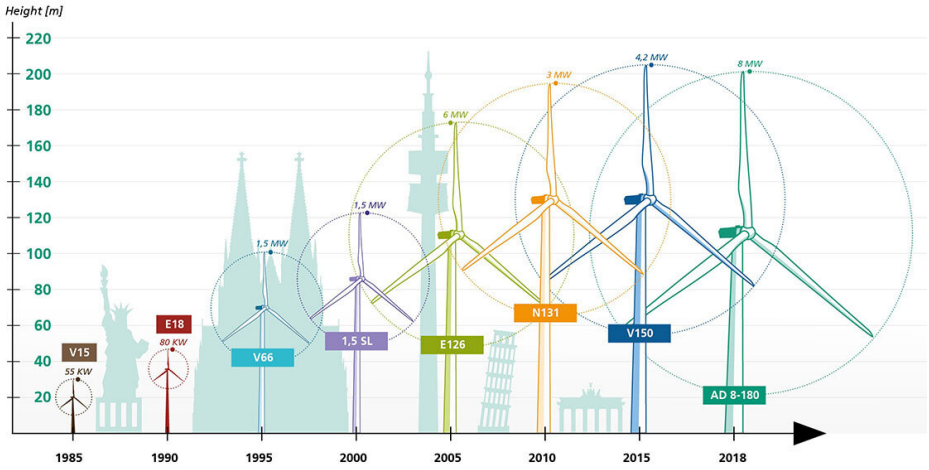

Figure 2.11: Growth of wind turbines over the last decades.

2.4.2. Further and deeper offshore

Wind farms are moving further offshore and into deeper waters. This can be seen in figure 2.12 and 2.13. Reasons for these trends are that the wind sources further offshore are more stable. Furthermore, there are fewer and fewer near-shore locations available for building an offshore wind farm [1]. In addition, technical progress makes it possible to build substructures for offshore turbines in deeper water. A positive effect of this movement to deeper, more remote locations is that horizon pollution is mitigated. The downside of this trend is that the project costs increase, mainly caused by the wind turbine installation vessels having to travel further to and from the installation site. The installation vessels are the most expensive assets in the installation procedure. If nothing is done about the supply chain of wind turbine components, costs and project duration will increase.

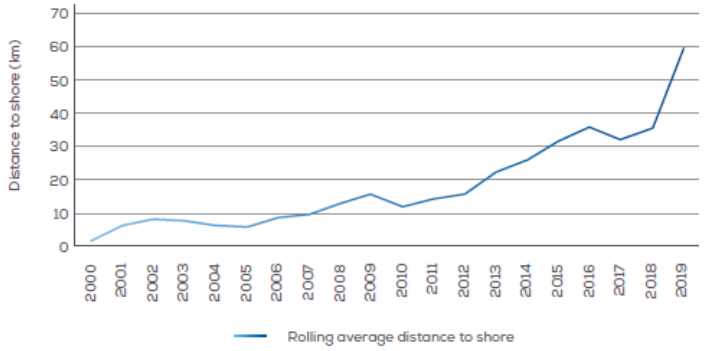

Figure 2.12: Rolling average distance to shore of online offshore wind farms. [1]

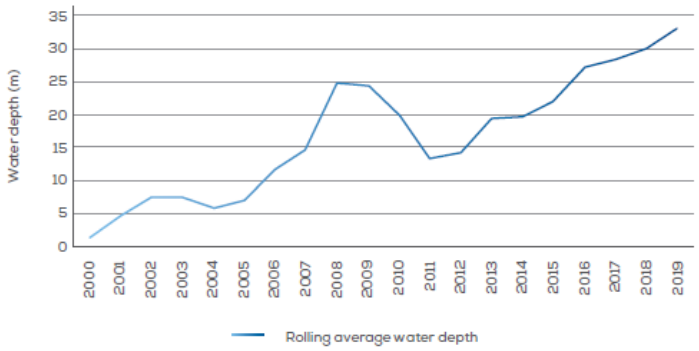

Figure 2.13: Rolling average water depth of online offshore wind farms. [1]

2.4.3. Jones Act

The Jones Act is a protective law that requires waterborne transport of goods and merchandise between two points in the United States of America to be executed by a U.S.-built, owned, crewed and flagged vessel [4]. This result in difficulties in order to achieve the level of ambition set out in the Biden Administration's offshore wind goal of 30 GW by 2030 because there is no U.S. coastwise qualified vessel specialised in installing offshore wind turbines [23]. The United States can solve this in two ways. The first solution is by building new vessels specialised in the installation of offshore wind turbines, a very expensive and time-consuming solution. The second solution is by using a solution as shown in Figure 2.14. This figure shows an example of how non-U.S.-flagged wind turbine installation vessels can jump into the emerging U.S. offshore wind market by using a Jones Act-compliant feeder vessel that transports the components between U.S. ports and wind farms. Even in this scenario, new feeder vessels might have to be built to transport the newest "mega" turbines.

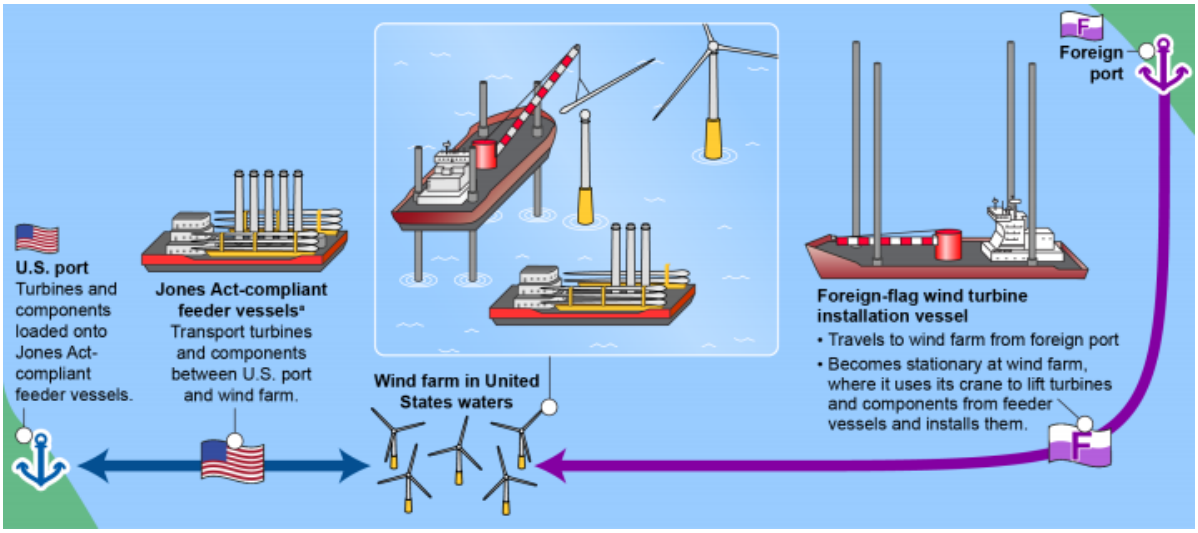

Figure 2.14: Example of an offshore wind installation in U.S. waters using a foreign-flag installation vessel and Jones Act-compliant feeder vessels. [2]

2.4.4. Opportunities

Preforming the installation of WTG's with the help of a feeder vessel rather than with a jack-up vessel would be a great solution to the problems and trends mentioned above. If a jack-up vessel remains on the installation side instead of going back and forth to a marshalling yard, the location for new OWF's will become less of a limiting factor. In contrast, the feeder vessels that supply the dedicated installation vessels with components have higher sailing velocity. Also, multiple feeder vessels can travel at the same time. The increasing size of the turbines and the increasing number of turbines per wind farm makes it almost impossible for most of the jack-up vessels in the industry to keep up with the installation demand. Suppose the feasibility for the execution of feeder lifts with a Tetrahedron crane can be proven, then Tetrahedron B.V. would have the solution to all the problems mentioned above. Its capability to lift higher than conventional cranes in the industry would give jack-up vessels with a Tetrahedron crane a considerable advantage compared to jack-ups with luffing boom cranes. Furthermore, if the feasibility of feeder lifts is proven, it would open an emerging market with many growth opportunities. The U.S. market can be entered using non-U.S.-flagged wind installation vessels and feeding them turbine components and parts with a U.S. coastwise qualified vessel.

3

Research Specifics

A case study is set up to simulate a real-life situation that would prove the feasibility of the execution of feeder lifts by a Tetrahedron crane. The choices made for this case study needs to be well-grounded to obtain relevant results. Among other things, the turbine, jack-up vessel and the location are highlighted in this chapter. Guidelines, constraints and assumptions that are set or assumed to be valid define the boundaries of this research.

3.1. Case study

One of the market leaders in the WTG market is General Electric Renewable energy or GE for short. GE has designed one of the most powerful wind turbine generators on the market, the Haliade-X. The turbine has received Full Type Certification by DNV. A prototype located in Rotterdam has set a new world record for generating the highest yield of continuous power with 312 MWh in one day. This type of turbine has been selected for numerous OWFs that will be built in the upcoming years, including large projects in Europe and the United States [24]. The Haliade-X is, therefore, an exemplary model for this research. An installation method that includes using a European flagged jack-up vessel equipped with a Tetrahedron crane is chosen because of the reasons mentioned in the previous chapter. The specific crane chosen is the Tetrahedron 45 because its rated power of 900 tons slightly exceeds the most significant weight of the components for the Haliade-X and therefore makes for a challenging case study. The crane used for the case study will be further explained in Section 3.2.1.

The location picked for the OWF to be installed using feeder lifts is the Vineyard Wind I project located near the islands of Nantucket and Martha's Vineyard, around 250 kilometres east of New York. Using a US-flagged barge can be shown that using feeder lifts as an installation method, the Jones Act can be circumvented, and non-US companies can enter the American wind market. The combination of this wind project and the Haliade-x wind turbine appears to be realistic because it has also been decided to use this turbine in the existing Vineyard Wind I project [25]. A map that gives more insight into the project regarding the location, ports, and the existing and planned infrastructure can be found in Appendix A. Also, the natural heave motion response of a barge is made available by Friede and Goldman collected around a similar area.

3.2. Boundary conditions and constraints

In order to constraint the thesis results, several values, measurements, and data are assumed to be applicable. These constraints are picked and chosen to sketch a situation that could come close to reality and might be a reality in a couple of years from now. The various constraints are elaborated in this section.

3.2.1. Tetrahedron crane

The design of the crane that will be used can be found in Figure 3.1. This figure shows that the Tetrahedron crane is placed around one of the legs of the Jack-up vessel and displays the most critical nodes and elements. The axis system displayed above the legend finds its origin in the middle of the slew bearing depicted by the yellow circle. The grey part of the crane can only rotate around the z-axis and cannot move along the axis.In addition to the freedom of movement of the gray part of the construction, the orange part can also move in the xz-plane.

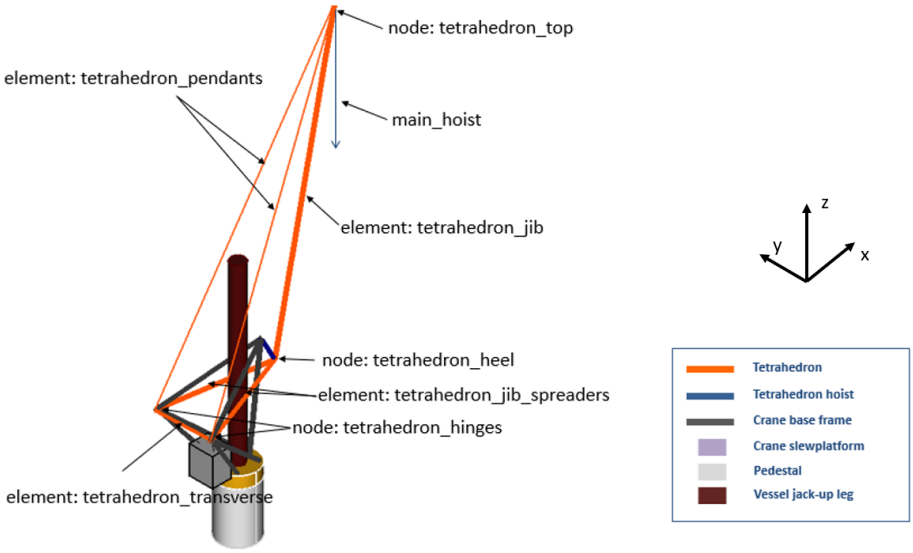

Figure 3.1: Orientation, and the names of important elements and nodes of the Tetrahedron crane.

The specific crane that will be used for the calculations in the following chapters is a Tetrahedron crane. The crane used is the Tetrahedron 45, the crane has a maximum load capacity of 900 tons, and the maximum distance between the water level and the hook is 180 meters. The number 45 in the name of the crane represents the maximum overturning moment onto the slewing platform in tonne-meter. The general arrangement of the crane, together with some technical specifications, can be found in Appendix B.

The main hoist can lift at a radius of 21 to 80 meters, measured from the heart of the slew bearing, and can reach a lifting speed of up to 16 m/min using its SmartHoist, but this speed can be doubled when lifting reduced loads. The SmartHoist is a single hoist block, combining the main hook and forward hook to increase the hoisting velocity. The luffing time from up to down or the other way around is about 10 minutes. The slewing speed is 0.2 rounds per minute, so a full round around its axis would take 5 minutes. Figure 3.2 shows the reeving diagram for the Tetrahedron 45. What can be seen in this diagram is that not all the available positions are used. These additional reeving positions would increase the maximum lifting capacity but decrease the maximum distance between the water level and hook.

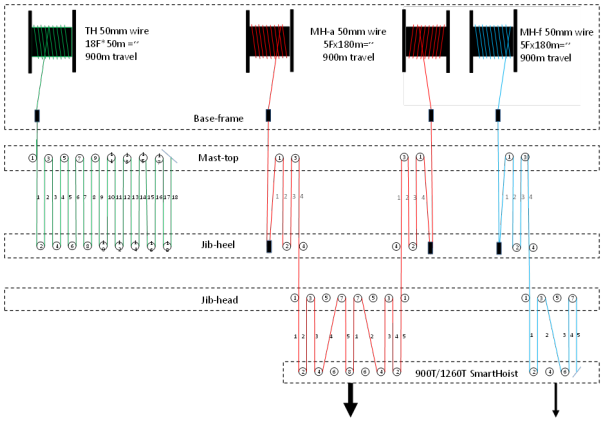

Figure 3.2: Reeving diagram of the Tetrahedron 45.

3.2.2. Jack-up vessel

The jack-up vessel used for the calculations in the following chapters is the Adventure of Van Oord. This vessel is sailing under the Dutch flag and is therefore not allowed to transport goods and merchandise between two ports or harbours in the United States. However, this is necessary to install the Haliade-X turbines in the Vineyard Wind project. Travelling back and forth to Europe would take a long time, cost a fortune, and lead to problems as the cargo could be damaged during the long journey across the Atlantic. This is not an option. The Adventure is the same jack-up vessel as displayed on the general arrangement of the Tetrahedron crane that is found in Appendix B. This Jack-up vessel is built in 2011, has a length of 136 meters, a width of 40 meters. Figure 3.3 shows the jack-up vessel during one of its previous wind turbine installation tours. The wind turbines on these previous tours were smaller, and more turbines could fit on the vessel itself. With modern turbines growing in size and the Tetrahedron crane being larger than the crane shown in Figure 3.3, little space is left for the wind turbine components on the deck of the Adventure. The general arrangement of the current MPI jack-up vessel can be found in Appendix B.1 and B.2. These figures clearly show that the crane intended for the heavy lifts executed to install the offshore wind turbines is located at the centerline of the jack-up vessel. The weight of the crane and its carrying load is transferred to the ground, first via the deck and then through the legs. The difference in the general arrangement with the luffing boom crane and the arrangement with the Tetrahedron crane can also be found in appendix B, is that the crane is mounted on one of the legs of the jack-up. The weight of the crane and the load are therefore directly transferred to the ground via the leg. The deck is not subjected to this heavy load anymore. The advantage of this configuration is that the boom encloses around the other two legs, on the same side of the vessel and that it can rest on a newly built frame next to all the sleeping quarters, galley and, other facilities. In this way, the Adventure can be equipped with a larger and heavier crane than it used to.

Figure 3.3: Former MPI adventure, jack-up vessel.

3.2.3. Wind turbine

In this section, the wind turbine and its characteristics will be described together with the technical requirements needed to install these turbines. The chosen wind turbine used in the rest of this case study is the General Electric Haliade-X, 12MW wind turbine generator. The turbine consists of a tower consisting of three parts, a nacelle transported on a special frame and three blades. All the numbers for the weight of the different components are the values for the minimum required lifting capacity of the crane on the turbine installation vessel for the offshore installation of the Haliade-X turbines.

Tower

The tower characteristics are displayed in Figure 3.4, the weight as shown in Table 3.1 is including a 10% weight contingency. The tower can be lifted in a different combination. If tower sections are combined, the pre-assembly must be executed on the quayside before loading the feeder vessel. Also important to note is that when the entire tower is transported and lifted as a whole, a complete tower lifting tool needs to be applied. This tool weighs 55 tons.

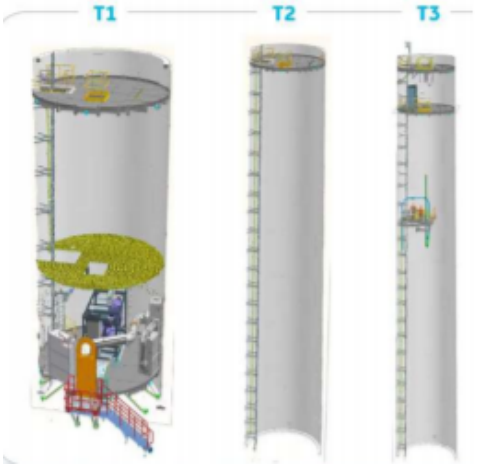

Figure 3.4: Tower configuration.

Tower section	Weight [tons]	Length [m]	Bottom diameter [m]
T1	274	26,69	8
T2	282	40,97	8
T3	238	43,54	6,83
Full tower	793	112,2	8

Table 3.1: Main characteristics of the tower components.

Nacelle

The nacelle of a wind turbine is the heaviest component. It needs to be transported on a particular frame to prevent the nacelle from tipping over and getting damaged during transport. The nacelle, together with the transport frame, weighs, including 10% weight contingency, 801 tons. The dimensions of the, to be transported, the nacelle is 22 meters in length, has a width of 10 meters and a height over 18.5 meters. A unique rigging tool needs to be used to lift the nacelle together with the transport frame. This tool weighs an extra 40 tons. The total weight of the nacelle, together with frame and rigging, becomes 841 tons. The rigging also adds 6.4 meters to the height of the, to be lifted, wind turbine section. Figure 3.5 shows the nacelle together with the transport frame and the rigging.

To install the nacelle onto the tower, first, the nacelle and the transport frame need to be lifted on the deck of the jack-up vessel. Here the nacelle will be detached from the transport frame and installed on top of the tower. The combination of nacelle and rigging weighs 794 tons and has a height of 17.5 meters, but this lift will not be considered in this thesis because this lift is not a feeder lift and the weight of the normative lift for this operation.

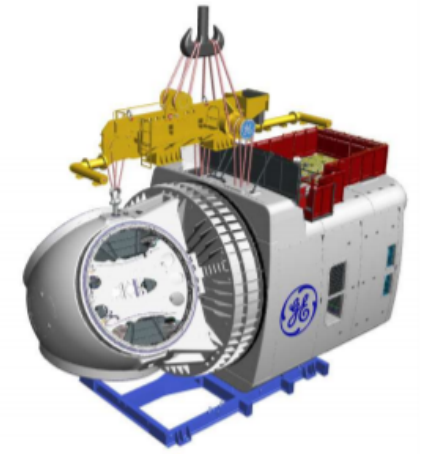

Figure 3.5: Nacelle with transport frame and rigging.

Blades

The Haliade-X has three blades with a length of 108 meters. The diameter at the root is 5 meters. A single blade weighs 61 tons. The blades are transported in a blade rack, a supporting frame that keeps the blades in place and allows transport of multiple blades on top of each other. An example of a blade rack staking three blades on top of each other is shown in Figure 3.6. The three blades together with the blade rack would weigh approximately 300 tons. The combination with blades and blade rack is twice the weight of just the blades. A single blade is installed by using a tool called a blade yoke or blade eagle (Figure 3.7), a device used to stabilize the turbine blade when lifting and installing. It prevents the blade from most of the rotational motions due to wind or eccentric weight. Because the entire blade rack together with the blades is lifted and placed on the jack-up vessel, the lifts executed with the blade eagle are out of scope for this thesis at this moment.

Figure 3.6: A blade rack that can hold 3 wind turbine blades.

Figure 3.7: A wind turbine blade lifted with a blade yoke.

Installation

Two key lifts mainly drive the needed capacity to install the Haliade-X wind turbine. First, the lift of the nacelle is critical because this component is the heaviest and needs to be lifted to a height of at least 149 meters above the lowest astronomical tide (LAT). This lift is vital because it pushes the crane towards the maximum load curve. The turbine regulations describe a minimum outreach with which the nacelle must be installed of 30 meters. However, installing the turbine blades with this outreach is impossible because the margin to the crane is too small. The tetrahedron 45 can reach its maximum lifting capacity up to an outreach of 40 meters. It is advisable to perform the lifts at the maximum outreach where the crane can still assess its maximum lifting capacity. With an outreach of 40 meters, both the heavy components can be lifted, and there is enough margin with the crane to install the turbine blades.

The second essential lift is that of the blades. The blades need to be installed at a 30-degree angle above the horizontal. The crane, therefore, needs to reach a height of at least 168 meters above LAT. This lift pushes the crane to its limits regarding the hook height.

The most probable installation methodology that will be used is that the tower is split into two pieces. One piece will consist of tower component T1 and the other piece will consist of the tower component T2 and T3 together. The tower components T2 and T3 are assembled on the quayside. This will mean that the entire procedure of building the Haliade-X wind turbine consists of 6 heavy lift. Apart from the two lifts needed to put the tower in place, one lift is needed for the nacelle, and three lifts will be needed to install the blades. If the components are transported and delivered with a feeder vessel, two more heavy lifts will be needed, so eight heavy lifts in total. One extra lift is needed for the nacelle because it first needs to be lifted to the jack-up vessel to get rid of the transport frame. The other extra lift is needed to transport the blade rack with the blades from the feeder vessel to the jack-up vessel. An overview of the steps needed to install the wind turbine generator can be found on the next page, Figure 3.8 to 3.13.

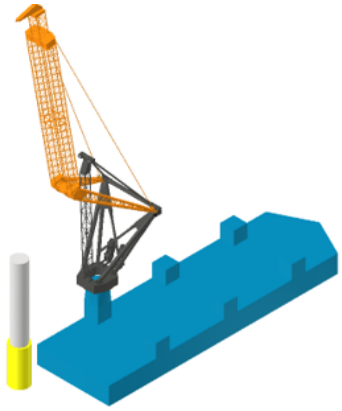

Figure 3.8: Installing T1 onto substructure.

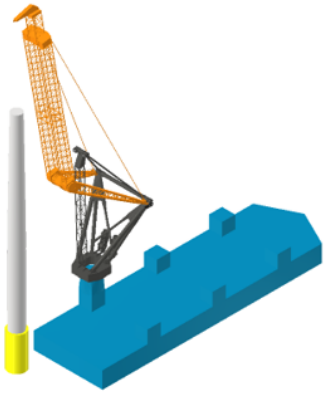

Figure 3.9: Installing T2 and T3 onto T1.

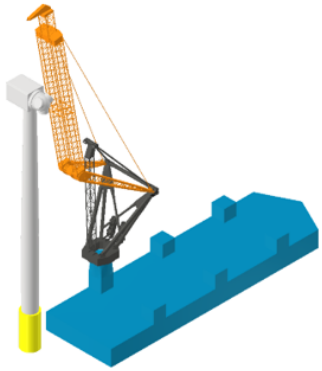

Figure 3.10: Installing the nacelle on T3.

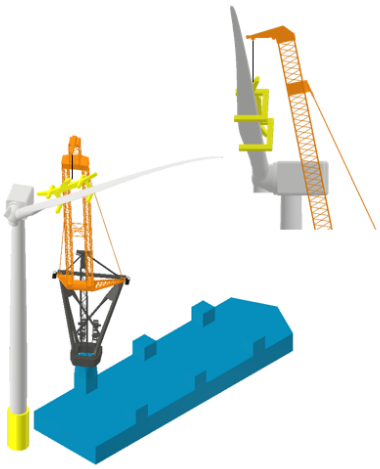

Figure 3.11: Installing blade 1.

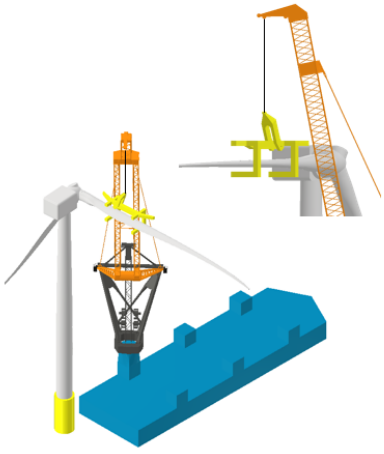

Figure 3.12: Installing blade 2.

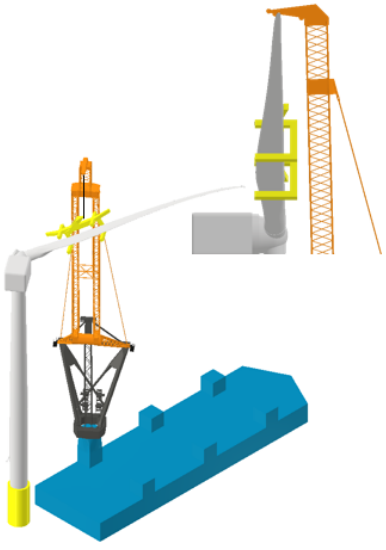

Figure 3.13: Installing blade 3

3.2.4. Feeder vessel

The chosen barge to perform as a feeder vessel during the feeder lift operation has a length of 400 feet and a width of 100 ft and sails under the flag of the United States of America. These distances translate to a length of around 122 meters and a width of 30.5 meters. Figure 3.14 shows the size of the feeder vessel compared to the size of the Adventure equipped with the 900 tons Tetrahedron crane.

The deck layout of the feeder vessel is of the essence to keep all components positioned within the reach and capacity of the Tetrahedron crane. The chosen deck layout for the operation described in this thesis is shown in Figure 3.14. The deck of the feeder vessel is displayed with the green, rectangular outer line and holds all the components needed for the installation of two 12 MW, Haliade-X wind turbines. The positioning of the nacelles is the decisive factor when arranging the deck layout. The nacelle's (number 5 and 6 in Figure 3.14) need to be placed within the limits where the Tetrahedron crane can reach its maximum load capacity, so between 21 and 40 meters. The combined tower components T2 and T3 are displayed in Figure 3.14 by numbers 2 and 3. Tower components T1 are numbered 1 and 4. The blade racks, each containing three blades, are depicted with the numbers 7 and 8.

Also of importance when arranging the deck layout, the roll and pitch moments around the centre of buoyancy are essential. It is assumed that the feeder vessel is symmetric in both x- and y-direction and, thus, the centre of gravity and the centre of buoyancy are located in the middle of the barge. The deck layout is chosen so that the cargo is also distributed almost symmetrically around this centre point. This prevents the feeder vessel from being tilted around the x- and y-axis. The components are also arranged by weight. The heaviest components are closest to the COG. This is done so that the weight and the moment around the COG change as little as possible when offloading the feeder vessel. Overall resulting in smaller roll and pitch motions of the vessel than when the heavier components were located near the edges of the feeder vessel and then removed.

Furthermore, General Electric has set several specific requirements for the transport of the Haliade-X wind turbine components. Constraints that need to be taken into account when making the deck layout, according to GE, are that a minimum space of 1 meter needs to be reserved between the wind turbine components and any adjacent obstacles. This is done to prevent damage and to facilitate access and movements. Another restraint is that there needs to be enough clearance around the nacelle to allow access for a scissor lift.

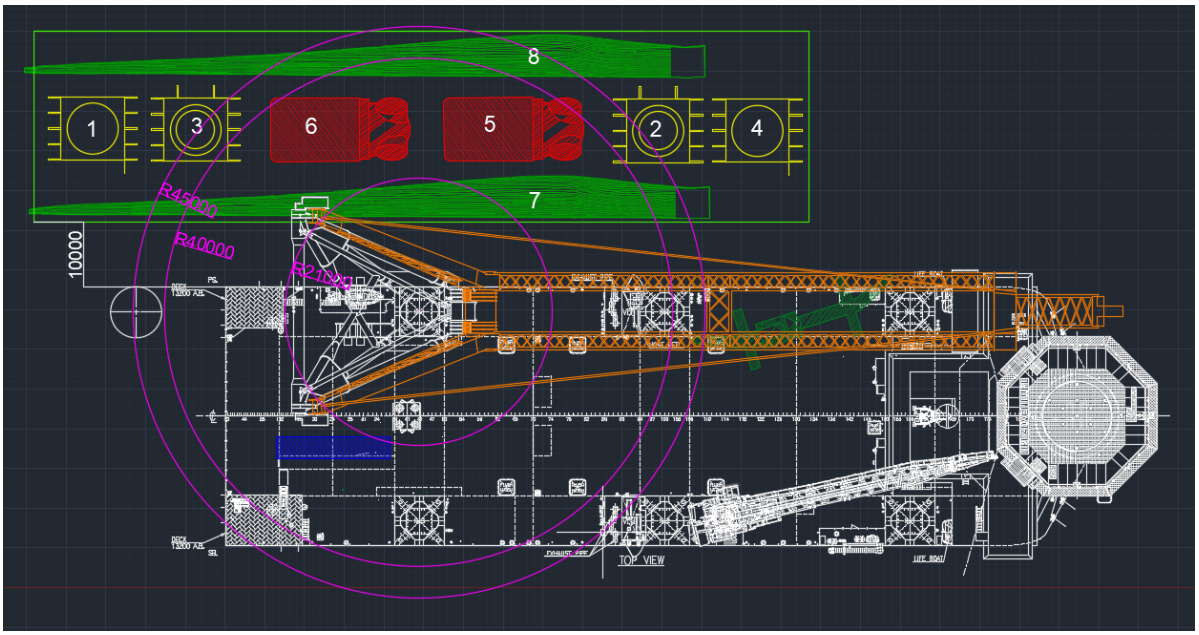

Figure 3.14: Arrangement of the Adventure with Tetrahedron crane and a feeder vessel with Haliade-X wind turbine components.

3.2.5. Sea state

This case study's location is the Vineyard Wind project located near the islands of Nantucket and Martha's Vineyard, around 250 kilometres east of New York. A location on the east side of the United States in the Atlantic ocean. Friede & Goldman, a vessel designer from the United States, have provided heave motion data on one of their barges at the east coast of the United States of America. The obtained heave motions data comes from a barge located in waves with a significant wave height of 1.5 meters. The two directions from which the waves were coming during the recording of the heave data are indicated with the orange arrows. The directions are called; beam sea direction and head sea direction. The average periods from which the heave data is recorded are 5.59, 7.64 and 9.13 seconds. The first 5 minutes of heave motion of every dataset can be found in Appendix C. Figure 3.15 shows the barge next to a jack-up vessel with a Tetrahedron crane installed onto it. The location where the heave motion is recorded is indicated with the red square and is just eccentric of the x- and y-axis, causing the heave motion to consist of heave motion and elevation difference due to roll and pitch motions of the barge.

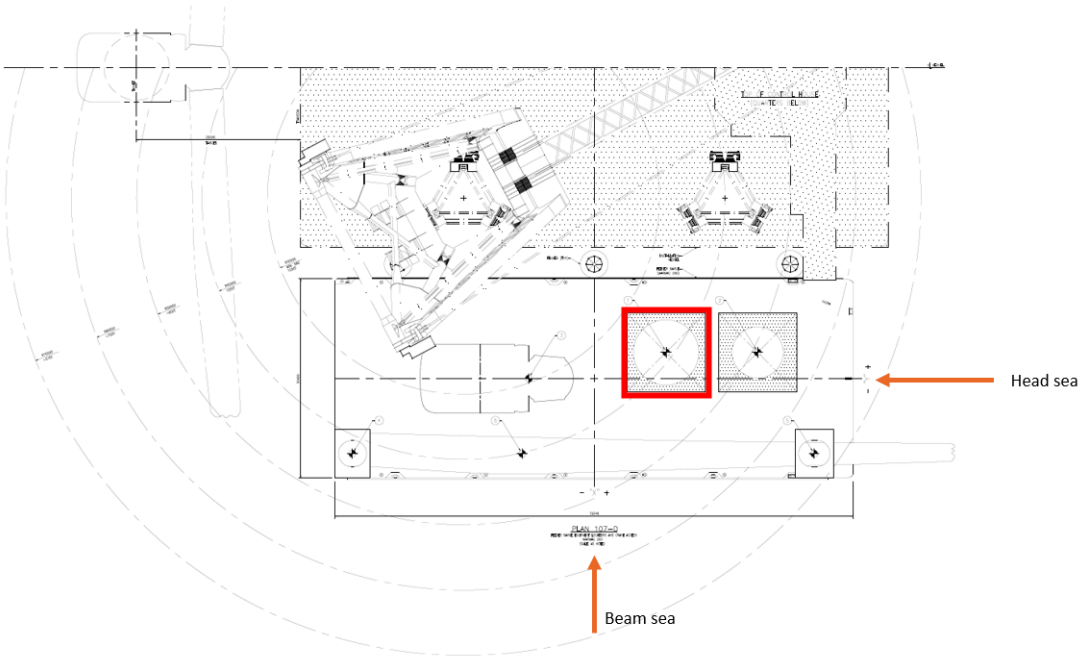

Figure 3.15: Location of heave motion measurements together with the wave directions were the motion is caused by.

3.3. Critical activities

First, the jack-up with the tetrahedron crane must arrive safely at the location of the pre-installed substructures on which the turbines will be installed. For this, the jack-up vessel has to sail across the Atlantic ocean with all the dangers that entail.

Secondly, a vessel feeding the components to this jack-up vessel sailing under the flag of the United States must be used. Otherwise, transport to and from the American port where the parts will come from will not be possible. Due to the Jones Act, the jack-up vessel cannot sail back and forth to the marshalling yard or port.

Furthermore, the lift of each part can be considered critical in its way. For example, the lift of the blade rack is less critical due to the weight, but due to the length and fragility of the components, so this lift must be handled with extreme care. The two lifts of the tower sections are critical because these components have to be lifted standing up and have a considerable length in this direction. Lifting the nacelle is critical because the weight of the nacelle in combination with the transport frame and the rigging approaches the crane's maximum capacity. The following chapters look at the most extreme situation where weight of 900 tons, the maximum capacity of the Tetrahedron 45, has to be lifted from a moving deck.

4

Single Degree of Freedom Model

The previous chapter describes a case study with details, values, and constraints regarding a feeder-lift operation. In this chapter, a single degree of freedom (SDOF) model is set up, an equation of motion for this model is derived, and some tests with this model are done to understand the problems that come with feeder lifting. Furthermore, the effects of the crane stiffness and the hoisting velocity on feeder-lift operations are examined. The limiting factors for these operations, including the dynamic amplification factor (DAF), are addressed. In the further course of this thesis, this model will be referred to as the 1D model.

4.1. Model description

4.1.1. Assumptions

To simplify the tetrahedron crane to a one degree of freedom model, some assumptions have to be made. The first assumption is that the crane and the cables are weightless. Masses of the structure are disregarded in this model and do not effect the deflection of the crane hook. The second assumption is that the vertical motion of the load is the only dependent variable and is why the one degree of freedom crane system experiences dynamic motions. Thirdly, it is assumed that the effect of load pendulation is not present in the system. To avoid pendulation of the load in the crane, it would mean that load, crane hook, and hoisting cable are perfectly aligned in the vertical direction. Furthermore, the assumption has been made that the main structural components, such as, among others, the slew bearing, the pedestal, and the jib, are sufficiently stiff in comparison with the slender truss structure of the crane and the flexible hoisting cables. In this case, the inertia of the stiffer components can be neglected, and the single degree of freedom model can be assumed as two springs aligned in series. The final assumption is that snap loads are not considered in this model. However, the moments when they occur can be determined. Snap loads are large tensile forces that occur when a rope or cable transfers from a slack state to a taut state [26]. The faster the slack is removed from the rope or cable, the higher the snap load. Snap loads will only occur at the beginning of a lifting operation, between when the lifting operation starts and when the load is partially suspended in the crane. Therefore, it is assumed that the snap loads are not critical in the lifting operation and that at this moment, during the lift, the flexibility of the crane absorbs the most significant force.

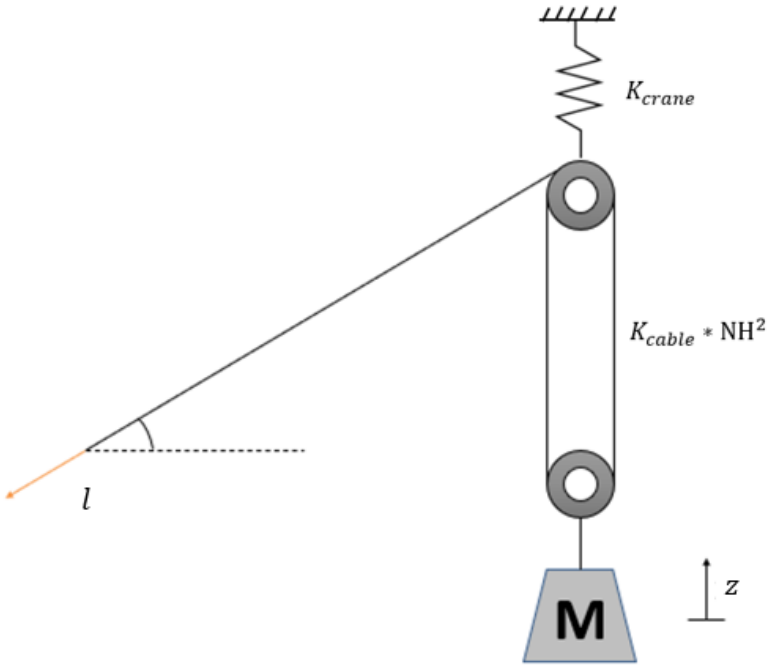

Figure 4.1: Simplification of a crane to a SDOF model

4.1.2. Derivation

The equation of motion for the load to be lifted from the deck of the feeder vessel will be derived based on the problem depicted in Figure 4.1. The designations in Figure 4.1 mean the following: z describes the vertical displacement of the load measured in meters from the position at which the load is lifted clear from the vessel deck. The number of falls of the hoisting cable is depicted in the figure with NH. With l being the displacement of the rope at the winch. The difference between length l and displacement of the the hook is caused by an force acting on the cables and crane. This force can be described as $K_{total}(l - NH * z)$ and depends on the cable- and crane stiffnesses; K_{cable} and K_{crane}. Figure 4.1 shows that the cable stiffness and crane stiffness relate to each other like two springs in series. Therefore, the total stiffness can be described with Equation 4.1. With the force in the cable and on the crane known, the equation of motion (EOM) for the load becomes Equation 4.2.

$$\frac{1}{K_{total}} = \frac{1}{K_{crane}} + \frac{1}{K_{cable,total}} \tag{4.1}$$

$$M\ddot{z} = K_{total}(\frac{l}{NH} - z) \tag{4.2}$$

Furthermore, l can be described as the velocity of the hoisting cable multiplied with the time; $l = V_{line} * t$. This can be substituted into Equation 4.2 and divided by the mass to obtain Equation 4.3. Equation 4.4 introduces ω into the EOM, $\omega = \sqrt{\frac{K_{total}}{M}}$ and describes the natural frequency in rad/s.

$$\ddot{z} + \frac{K_{total}}{M} z = \frac{V_{line}}{NH} * t * \frac{K_{total}}{M} \tag{4.3}$$

$$\ddot{z} + \omega^2 z = \omega^2 * \frac{V_{line}}{NH} * t \tag{4.4}$$

In order to obtain the general solution from the equation of motion, the initial conditions need to be used. The general solution for the model is only applicable if the entirety of the mass is hanging in the crane, the moment of lift-off. This lift-off moment takes place at $t = 0$, and the initial conditions for the location and the velocity at this moment are known. The load location at the moment of lift-off can be assumed to be zero, so $z(t = 0) = 0$. The velocity of the load relative to the crane hook is the difference in the velocity of the vessel deck, where the load was situated, and the hoisting velocity. The hook moves with a velocity of $\frac{V_{line}}{NH}$ and the vessel deck moves with a velocity of $V_{deck}(t = 0)$, so the initial condition for the velocity is; $\dot{z}(t = 0) = \frac{V_{line}}{NH} - V_{deck}(t = 0)$. Inserting the initial conditions into the equation of motion (Equation 4.4) results in the general solution, found in Equation 4.5.

$$z(t) = \frac{1}{\omega}(\frac{V_{line}}{NH} - V_{deck})sin(\omega t) + \frac{V_{line}}{NH}t \tag{4.5}$$

However, the exact moment of lift-off is hard to determine. It may occur that the entirety of the load is suspended in the crane but the location of the vessel deck prohibits a lift-off to occur. This keeps the load a fraction longer on the vessel deck. In this case, the initial condition of the load location being precisely zero at the moment of lift-off is not valid. The series of springs that represent the crane is stretched a little further, resulting in an extra force that is not accounted for in Equation 4.5. For now, the length of this extra elongation of the springs at the moment of lift-off is named z_0, resulting in the initial condition for the location of the load to become; $z(t = 0) = z_0$. With this new initial condition, the general solution changes as well. The new general solution is described in Equation 4.6.

$$z(t) = \frac{1}{\omega}(\frac{V_{line}}{NH} - V_{deck})sin(\omega t) + z_0 cos(\omega t) + \frac{V_{line}}{NH}t \tag{4.6}$$

4.1.3. Operations model

The purpose of the model is to determine whether the load can or cannot be lifted from the feeder vessel at a specific moment in time. A lift from the feeder vessel can either result in a good, 'clear' lift-off or a re-hit. This second result is undesirable. A clear lift-off means that the load is lifting of the vessel deck without any disturbances or hick-ups. A re-hit is when the load, after it has a lift-off, comes in contact with the vessel deck again. A re-hit can result in damage to wind turbine components, the feeder vessel or the crane. To determine the extent of this damage, the velocity at the moment of impact will be determined. Other significant numbers to retrieve from the model are the lift-off time from when the crane starts the lifting procedure and the dynamic amplification factor (DAF) for the lifting operation. The DAF needs to be determined because the crane and wind turbine components have specific limits for the DAF.

Visualizing a lift is done based on a lifting graph. This graph shows the location of the vessel deck, the load and other essential indicators as a function of time. It is essential to keep in mind that, even though the load appears to be moving sideways, the movement only occurs in the vertical direction. The first line introduced in the graph is shown in Figure 4.2, this line describes the location of the vessel deck. As can be seen in the figure, for this example, the vessel deck moves sinusoidal over time with a period of six seconds and an amplitude of half a meter. Figure 4.3 introduces the height of the hook, which is the hoisting velocity times the time. This line would be the load location during a lift if either the mass of the load was minimal or both lifting cables and crane were infinitely stiff. As can be seen in Figure 4.3, the location of the hook starts below the location of the vessel deck. If the hook's location is below the vessel deck, there is slack in the rigging, and the vessel deck supports the entire mass of the load.

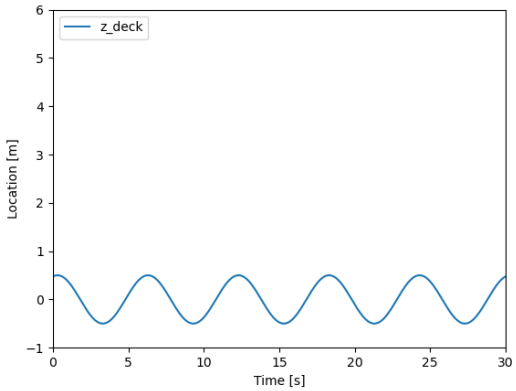

Figure 4.2: Location of the feeder vessel's deck over time.

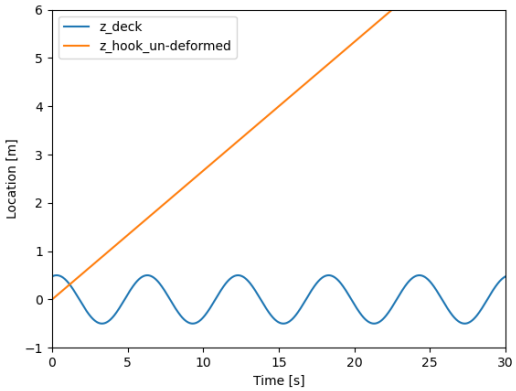

Figure 4.3: Unloaded hook location over time.

The red line depicted in Figure 4.4 resembles the relative distance between the travelled distance by the crane hook (orange line) and the location of the vessel deck (blue line). The moment of a wave trough results in a relatively large distance between load and hook, and a wave crest causes a relatively small distance between the location of the crane hook and the vessel deck. Because both the hoisting cable and the Tetrahedron crane have a specific stiffness, the jib will deflect downwards under the mass of the load, and the hoisting cables will elongate. The winches must first reel in this "extra" distance before a lift-off can occur. The difference in deflection of the crane hook between having zero kilograms hanging in it or having the entire mass hanging in the crane is shown by the green line in Figure 4.5. Thus the green line represents the total downward deflection of the crane hook at the moment of lift-off.

The moment of lift-off can be indicated by the intersection of the green and red line because this is the point where the distance between the hook and the vessel deck exceeds the bending of the crane and the elongation of the hoisting cables.

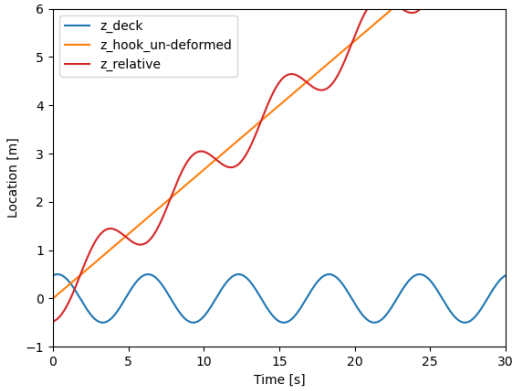

Figure 4.4: Relative distance between hook and deck.

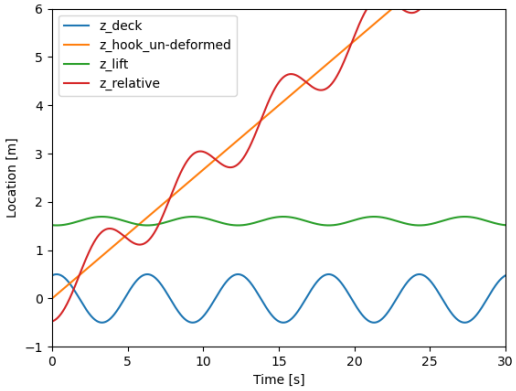

Figure 4.5: Bending and elongation of crane and cable.

To finalise the lifting graph and the way the model can visualise each lift, the location of the load is introduced. Figure 4.6 shows this load location with the black line. From $t = 0$ until the red and green line intersects, the load follows the location of the vessel deck. In this stage, the crane, hook, and cables gradually take over the weight of the load. From the moment the red and green line intersect, the moment of lift-off, the black line describes the motion of the load hanging in the crane as described by the general solution from Equation 4.6.

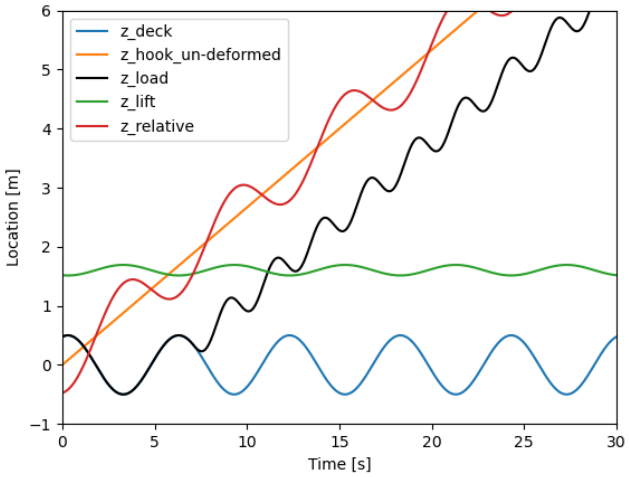

Figure 4.6: Complete lifting graph.

From the moment of lift-off onwards, two things can happen. The lift-off does not result in a re-hit with the vessel deck, a clear lift. A situation without a re-hit is desired. As shown in Figure 4.7 on the left side, the moment of lift-off is indicated by a vertical red line. The figure on the right-hand side shows the situation where the load and the vessel deck experience a re-hit. The re-hit can cause damage to load, vessel, and maybe even to the crane and is therefore not desired. The first red vertical line indicates the moment of lift-off, the second vertical red line indicates the moment of re-hit. The results from the moment of impact onwards are no longer used in further analysis. The line, representing the location of the load after the re-hit, as can be seen on the right-hand side of Figure 4.7 is a possible trajectory of the load suspended in the crane. But not necessarily correct.

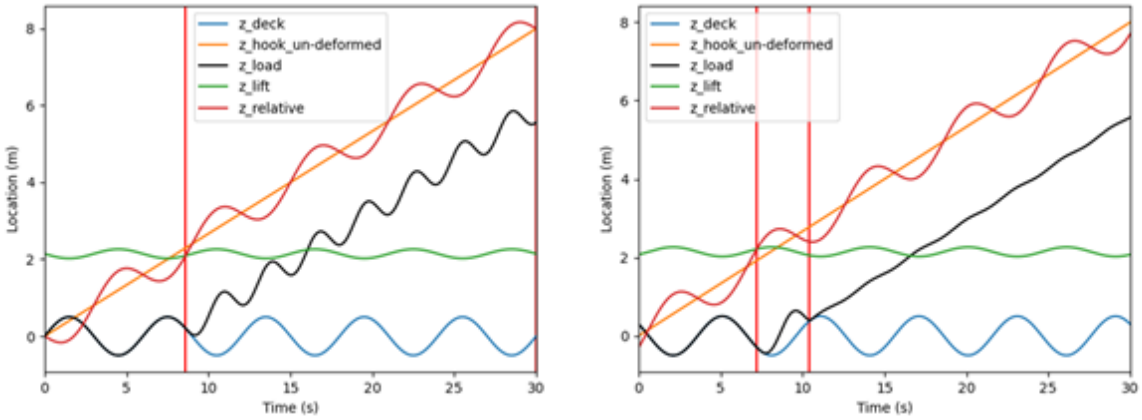

Figure 4.7: Clean lift-off case on the left, re-hit case on the right.

4.2. Parametric contemplation

4.2.1. Load

The masses of the loads, representing the wind turbine components, are discussed in Chapter 3 and summarised in Table 4.1, sorted by weight. In the table also the maximum lifting capacity of the crane is included. The maximum lifting capacity of the Tetrahedron 45 is 900 tonnes at a radius of 38 meters.

Load	Weight [tons]
max. Crane capacity	900
Nacelle	841
Tower component 1	611
Tower component 2 & 3	575
Blade rack (3 blades)	300

Table 4.1: Weight of the loads in the crane, in static conditions.

4.2.2. Stiffness

The stiffness of the simplified crane used in the 1D model is characterized by two different stiffnesses that together account for almost all the deflection that the load experiences. These two stiffnesses are the cable stiffness and the crane stiffness.

Cable stiffness

The cable's stiffness is defined by the amount of force needed to elastically deform the cable one meter. The stiffness of the main hoist cable can be calculated using Equations 4.7 and 4.8. In this equation, E is defined as the elastic modulus of the cable in N/m^2, L is the length of the cable in meters, and A is the surface area of the cross-section of one cable in m^2. Entering the values as used on the Tetrahedron 45 results in a total cable stiffness of $K_{cable,total} = 13327\ kN/m$. The cable's stiffness is virtually uniform over the lifting radius, which means that if a lift is executed at a 30-meter radius or a 50-meter radius, the cable elastically deforms with approximately the same amount. The orange line displays the cable stiffness as a function of the lifting radius in Figure 4.8.

$$K_{cable,single} = \frac{E * A}{L} \tag{4.7}$$

$$K_{cable,total} = K_{cable,single} * NH^2 \tag{4.8}$$

However, during the lifting operation, the length of the cables in the system changes. Part of the cable length is wound around the winches. The cable length decreases and reduces the cable's extension due to the load being placed in the hook. According to Equation 4.7, a decreasing length results in a higher rope stiffness. The flexibility of the system thus decreases during a lifting operation, which results in a change of frequency. The decreasing cable length can be taken into account by changing the equation for the cable stiffness such that Equation 4.9 can be derived. With a low lifting velocity, it takes longer for a lift-off to occur than with a higher lifting speed. As a result, the term $V_{line} * t$ remains virtually the same until the moment of lift-off and with it the influence this has on the cable stiffness. Simulations in the model show that the time-dependent cable stiffness (Equation 4.9) and the initial cable stiffness (Equation 4.7) give approximately the same results. Hand calculations show a difference in cable stiffness between the start of the lift and the moment of lift-off to be less than 0.2%. The influence on the total stiffness is even smaller. Based on these calculations and computations of the model, it has been assumed that the changes due to cable reeling have an insignificant change on the rope stiffness and can therefore be neglected. So in the further calculation of the cable stiffness Equation 4.7 is used. It will also keep the computation time low because the cable stiffness in the model does not become a time-dependent factor, and thus the total stiffness will not become a time-dependent variable. Time-dependent stiffnesses would make the model unnecessarily more complex and would not promote efficiency.

$$K_{cable,single} = \frac{E * A}{L - (V_{line} * t)} \tag{4.9}$$

Crane stiffness

In-house software Automatic Crane Engineer or ACE for short is used to determine the jib-top deflection. ACE is a program that, based on the given input values, determines the cross-sections of the members to minimise the weight of the crane and optimise the load curve for the Tetrahedron crane. By changing the input value for the load hanging in the crane, different jib-top deflections are obtained. By linearly extrapolating these output values, the stiffness of the crane structure can be obtained in force per meter (N/m). By executing this procedure for different radius resulted in a downward trend as the radius increased. In other words, the crane becomes less stiff and deflects more if the lifting radius is increased. The stiffness of the crane for the radius where the maximum lifting capacity of 900 tons can be reached is displayed by the blue line in Figure 4.8.

Total stiffness

The total stiffness of the crane and the cable together can obtained by assuming that the two stiffnesses originate from two 'springs' placed in series. Equation 4.1 shows how the total stiffness of the crane and cable together can be calculated. Entering the numbers calculated in the previous parts results in a total stiffness as displayed by the green line in Figure 4.8. In this figure, the stiffnesses are plotted as a function of the lifting radius. Only the radius' where the maximum loading capacity, of 900 tons, can be reached are shown in the figure.

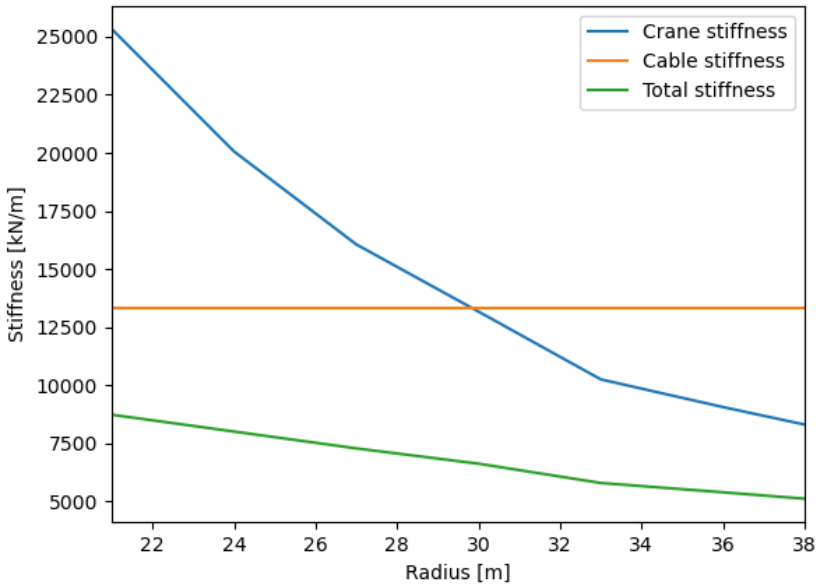

Figure 4.8: Stiffness diagram of the Tetrahedron 45.

4.2.3. Hoisting velocity

As mentioned above, the hoisting velocity impacts the moment of lift-off. A higher hoisting velocity causes an earlier moment of lift-off than a lower hoisting velocity. Because the total downward deflection that the crane experiences is reached sooner with a higher hoisting velocity. Cranes on most jack-up vessels have a hoisting velocity of 8 meters per minute when lifting total capacity. Through the use of the so-called "smart hoist", the hoisting speed of the Tetrahedron 45 is assumed to be 16 meters per minute, twice that of other cranes in the industry. The "smart hoist" uses an ingenious way of shearing and combining the main-hook and forward-hook. Therefore, the crane can achieve higher lifting velocities while lifting the maximum capacity. Increasing the power of the engines driving the winches could result in even higher hoisting velocities, up to 30 or even 40 meters per minute. However, this has yet to be proven, and therefore a hoisting velocity of 16 meters per minute is used in the simulations.

4.3. Dynamic Amplification Factor

As explained in Section 2.3, the dynamic amplification factor is used to multiply with the static load to account for dynamic effects. At the moment of lift-off, when the load is released from the feeder vessel, these dynamic effects are more significant when the load moves in the opposite direction of the crane hook rather than when the load is stationary. If the load moves in the direction of the crane hook at the moment of lift-off, then the dynamic effects are smaller than when the load is lifted in static conditions. The DAF can be expressed as shown in Equation 4.10.

$$DAF = \frac{F_{dynamic}}{F_{static}} = 1 + \frac{a}{g} \tag{4.10}$$

According to Equation 4.10, the DAF can be found using the acceleration of the load, and dividing it by the gravitational acceleration. The acceleration of the load is the second derivative of the general solution shown in Equation 4.6. If the second derivative is filled in Equation 4.10, a new function for the dynamic amplification factor can be found. This function is shown in Equation 4.11 and differs not so much from the DAF of DNV-GL (Equation 2.2). The only difference is that the component that describes the relative velocity differs. This can be explained by the fact that Equation 2.2 uses estimates for the velocity of the crane hook and the velocity of the load at the moment of lift-off, both these estimates are dependent of the significant wave height where the feeder vessel is subjected to. Equation 4.11 uses the real values for the velocity of the hook and the velocity of the load. Therefor, this equation computes the relative velocity in the same way as described by the DAF equation of D.E. Charett in Equation 2.5. The equation derived from the simplified SDOF model slightly differs from this equation because the velocity of the crane hook is dependent on the number of hoisting falls.

$$DAF = 1 + \left(\frac{V_{line}}{NH} - V_{deck}\right)\sqrt{\frac{K_{total}}{M * g^2}} \tag{4.11}$$

For both the equation described by D.E. Charett as the derived equation for the DAF of the SDOF system holds that a low relative velocity between hook and load results in a lower DAF and thus lower dynamic forces. A situation where the feeder vessel moves up at the moment of lift-off results in a lower DAF. A situation where the feeder vessel moves downwards results in a higher force, the relative velocity between hook and load at the moment of lift-off is greater.

All the passed equations that describe the DAF only account for the relative motion between the wave and the hook. Additional motion can arise from slack slings, it is most likely that this does not effect the load dynamics because the flexibility of the crane prohibits this.

The DAF has a limit for either the crane or the wind turbine components that may not be exceeded. The Tetrahedron 45 is designed for a maximum DAF of 1.1 when lifting at total capacity, so at 900 tons. The maximum dynamic load the crane can endure is this 990 tons. Exceeding this maximum dynamic load can cause severe damage to the crane structure and results in hazardous situations. The maximum dynamic amplification factors on either the WTG components or their frames is summarized in Table 4.2 [27].

Component	Maximum DAF
Nacelle in transport frame	2.0
Tower section in transport frame	2.0
Tower section on grillage	2.0
Blades in transport frames	2.0
Full tower in grillage	1.5
Blade in blade rack	1.3

Table 4.2: Maximum dynamic amplification factor on either WTG components or their frames.

4.4. Performance in sinusoidal waves

Now that the general solution is derived, the suitable parameters are determined and calculated, and the equation for the DAF is obtained, some tests can be executed. First, this simplified dynamic model of a crane is assessed when the load, initially located at the deck of the supply vessel, is undergoing a sinusoidal motion. The additional assumption that the ship's heave motion follows the wave motion has been made in this part. Actual vessel motion in heave direction consists of the heave motion with a possible addition due to the roll and pitch motion of the vessel. Heave motion at, for instance, the vessel's stern can be considerably higher if pitch motion is taken into account. The ideal point for the load to have lift-off is located when the feeder vessel reaches its highest point in the cycle of oscillations because with sinusoidal motions, re-hits will not occur since the next crest in the vessel motion is as high as the one where the load is initially lifted. However, this point is hard to determine in practice because the crane operator is situated tens of meters above the deck of the jack-up vessel and therefore even further away from the sea level. The location of the crane operator makes it very hard to judge the vertical heave motion of the feeder vessel.

For the test with sinusoidal waves, a wave period of six seconds is assumed to be comparable with the results that will be found from the wave data of Friede & Goldman from Section 3.2.5, which has an average motion period of 5.59 seconds. Furthermore, the motion amplitude is assumed to be 0.4 meters, which is similar to the highest recorded location of the vessel (0.37 meters above the equilibrium) and the lowest recorded location (0.41 meters below the equilibrium) in the head sea direction. The heave motion of the feeder vessel in these specific conditions is shown in Figure 4.9.

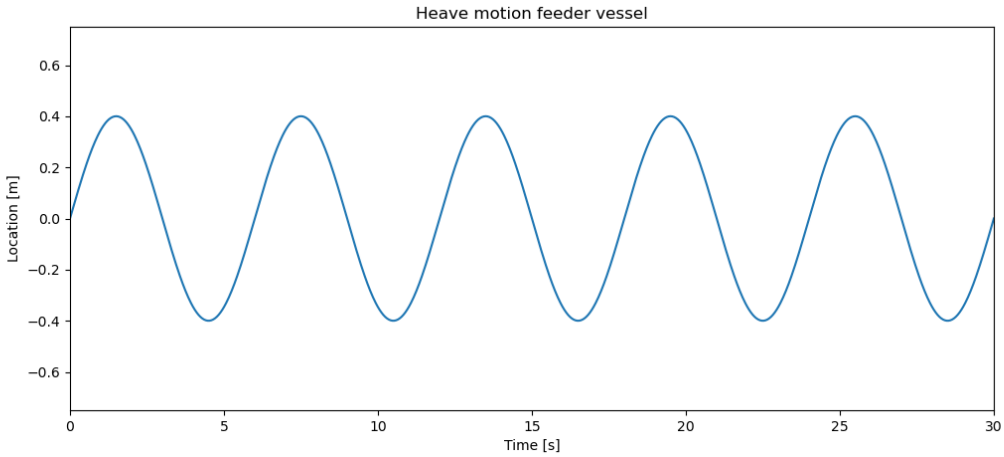

Figure 4.9: Sinusoidal heave motion of the feeder vessel.

The parameter from Section 4.2 are implemented under maximum conditions, so a load of 900 tons and the crane lifting this load at a radius of 38 meters. The motion period is then cut into a thousand pieces, and a run with the model was performed at each of these moments, either resulting in a re-hit or a clean lift. Figure 4.10 shows the moments where the start of a lift resulted in a re-hit (displayed by the red dots) or resulted in a clear lift (displayed by the green dots). In 32.1% of the cases, a lifting operation resulted in a re-hit. The chance that a re-hit will occur is far too high when it happens in one-third of the attempted lifts. Nevertheless, considering that the sinusoidal heave motion is made up of the most extreme amplitude of the heave motion data of Friede & Goldman, it would mean that this test performed on the data should result in lower re-hit percentages. From this figure, it can be concluded that the moment immediately after the wave trough is the worst moment to start the lift because a red area is visible here. However, it appears that this area shifts when parameters and conditions change. So this conclusion only applies to the specific conditions and parameters described above.

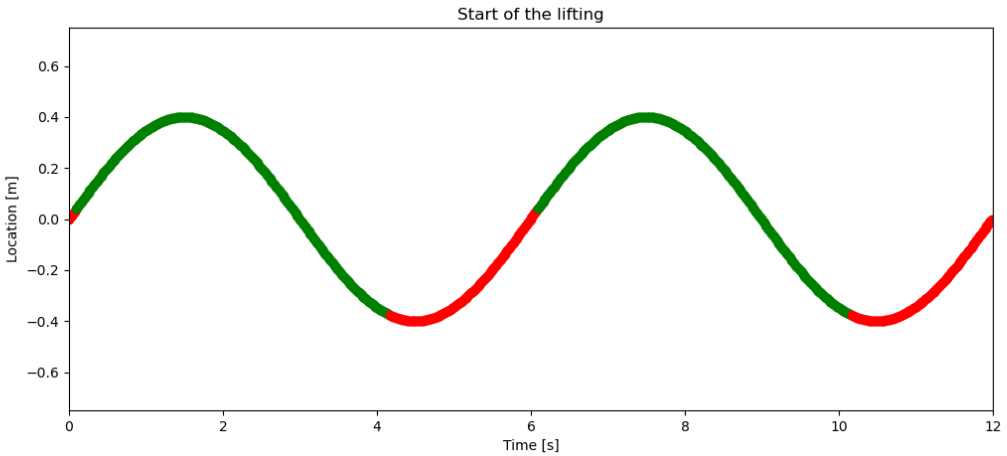

Figure 4.10: Lifts resulting in either a re-hit (red) or a clean lift (green).

In addition to its unique design, the tetrahedron crane has two features that vary significantly from a luffing boom crane. The Tetrahedron crane has a higher hoisting velocity and a lower crane stiffness than a luffing boom crane. To find out if this impacts the percentage of re-hits positively, first, the effects of the hoisting velocity will be examined, and then the impact of the crane stiffness on the percentage of re-hits is examined. The effects of the hoisting velocity on the percentage of re-hits are shown in Figure 4.11. In this figure, the case of the Tetrahedron 45 is displayed, and for comparison, a line for a luffing boom crane is drawn as well. In general luffing boom cranes have a higher crane stiffness and a lower hoisting velocity. For this fictional luffing boom case, a crane is taken with a total stiffness of exactly 10000 kN/m, which is a common crane stiffness for a luffing boom crane. If at a certain hoisting velocity, the Tetrahedron 45 has a lower re-hit percentage than the luffing boom crane, this is considered as positive for Tetrahedron B.V. However, Figure 4.11 shows that the designed hoisting velocity a Tetrahedron 45 crane has a higher re-hit percentage than the luffing boom crane at that same hoisting velocity. In practice luffing boom cranes can not achieve hoisting velocities this high.

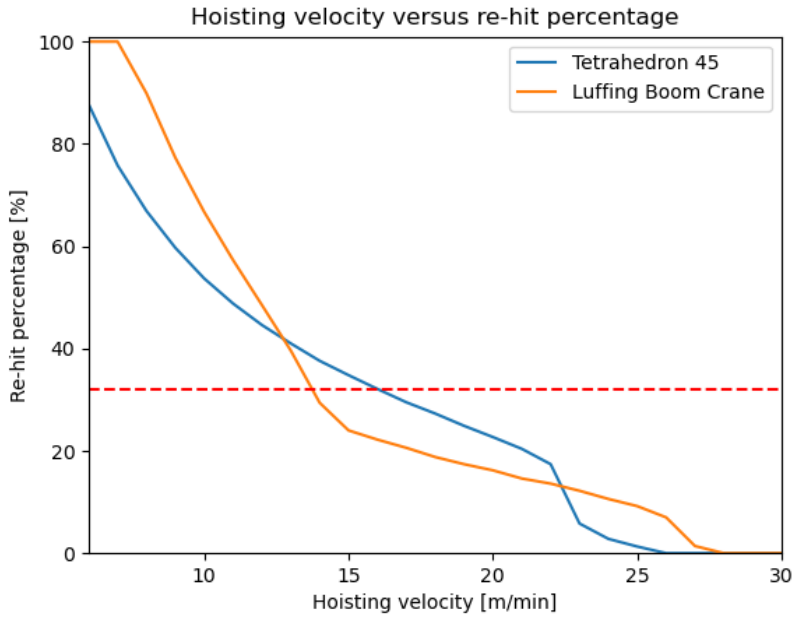

Figure 4.11: Re-hit percentage at different hoisting velocities.

The effects of the crane stiffness on the percentage of re-hits are shown in Figure 4.12. In this graph, the crane stiffness and the total stiffness are changed and displayed with the accompanying re-hit percentage. The graph shows results for both the hoisting velocity of the Tetrahedron 45 and the fictional luffing boom crane. The general trend in the figure is that with an increasing crane stiffness, the percentage of re-hits decreases. Only at very high stiffnesses, this trend is broken. Furthermore, a similar re-hit percentage can be obtained for the Tetrahedron 45 ($K_{total} = 5508\ kN/m$), lifting at 16 meters per minute, as with the luffing boom crane ($K_{total} = 10000\ kN/m$) that lifts with a hoisting velocity of 13.75 meters per minute.

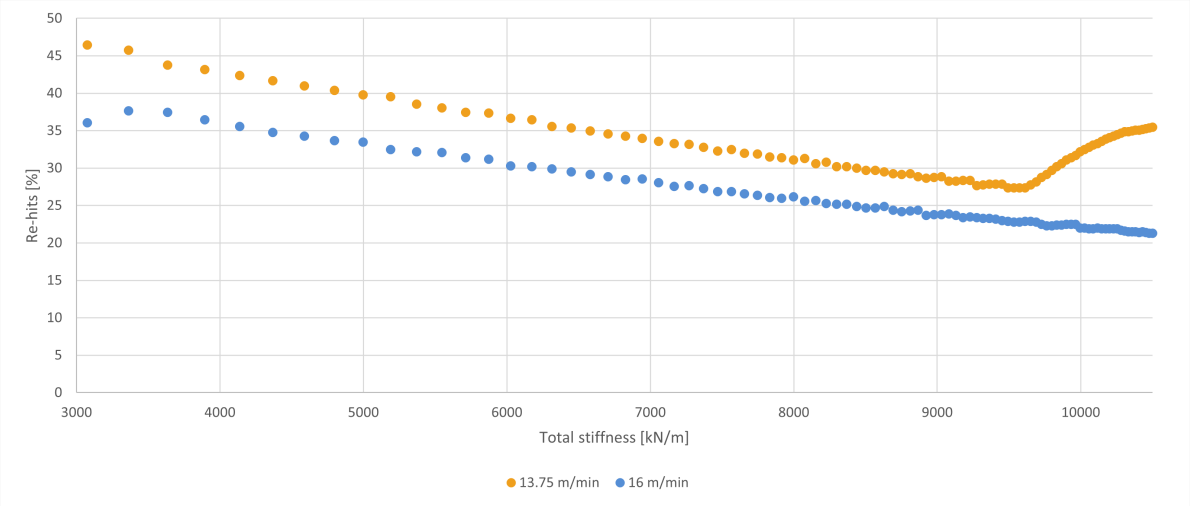

Figure 4.12: Re-hit percentage at different total stiffnesses.

A final way to compare the Tetrahedron 45 with the luffing boom crane is through the Dynamic Amplification Factor. If, in general, the DAF at lifting operations for the Tetrahedron 45 is lower than that of the luffing boom crane in a similar situation, it is positive. A lower DAF means that lower forces will occur during the lifting operations. The two chosen points where the DAF's will be compared with each other are indicated in Figure 4.11, at the location where the red-dotted line crosses the other two lines. This line is drawn at the percentage of re-hits with the Tetrahedron 45 when it lifts at designed hoisting velocity, at 32.1%. It crosses the line of the luffing boom crane at a hoisting velocity of 13.75 meters per minute. This means that the Tetrahedron lifting at 16 meters per minute achieves a similar successful lifting percentage as the luffing boom crane with a hoisting velocity of 13.75 meters per minute. The dynamic amplification factors of the luffing boom crane and the Tetrahedron 45 are shown in, respectively, Figure 4.13 and 4.14. In these figures, the orange bars represent the results obtained with Equation 4.11. The red vertical line represent the DAF according to DNVGL-ST-0378 from Equation 2.2. The bin width in these histograms is 0.025, so the two bins of the different equations within this domain represent the same values. In general, despite a higher hoisting velocity, the Tetrahedron 45 results in a lower DAF than the luffing boom crane. The average DAF, resulting from Equation 4.11, for the Tetrahedron 45 is 1.15. For the luffing boom crane, the average equals 1.21. Also, the maximum DAF that occurs during all the different lifting runs is higher for the luffing boom crane than for the tetrahedron, respectively 1.27 and 1.20. For the Tetrahedron 45, the value for the DAF and thus the maximum permissible dynamic load of 990 tons is exceeded in 56.3% of the cases. This leads to a total of 64.0% of the lifting operations being unsuccessful, meaning that the maximum DAF is exceeded or a re-hit occurs. According to DNV, the DAF that should be considered for the feeder lifts executed by the luffing boom crane and the Tetrahedron 45 are, respectively, 1.39 and 1.29. These values are obtained by using a significant wave height of 1.5 meters. The values that follow the 1D model for both cranes are significantly lower than the DAF calculated according to the DNV standard but still give a high rate of unsuccessful lifts when a load of 900 tons is lifted.

To conclude on the sinusoidal heave motion, the Tetrahedron 45 at a similar re-hit percentage as the luffing boom crane has a lower dynamic amplification factor. Assuming that the luffing boom crane has the same DAF limit as the tetrahedron 45, it can be said that the T45 outperforms the luffing boom crane under these specific conditions.

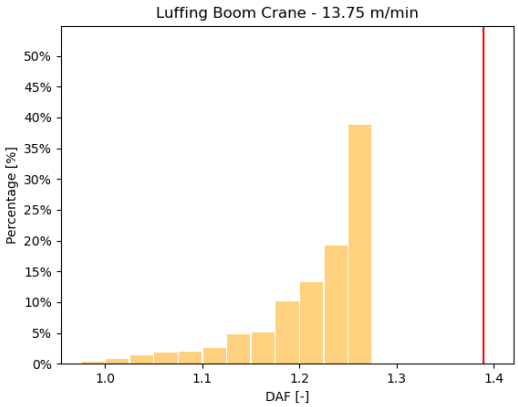

Figure 4.13: DAF for the Luffing Boom Crane case.

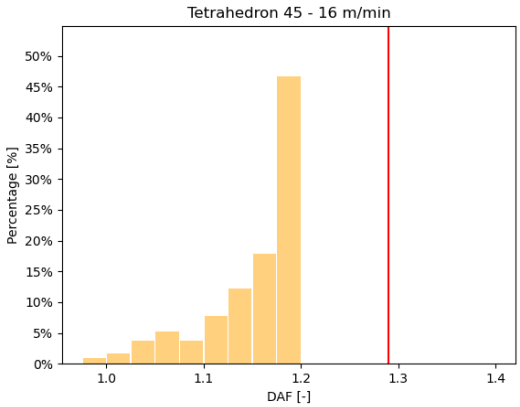

Figure 4.14: DAF for the Tetrahedron 45 case.

4.5. Performance in realistic sea state

More difficulties occur when the supply vessel in realistic sea conditions and is not dealing with a perfect sinusoidal movement of the sea surface. In realistic sea states the wave height and frequency are less predictable and can lead to precarious motion, it can result in resonance between waves, leading to more extreme sea conditions.

The performance in realistic sea states is done on the heave motion data described in Section 3.2.5. The complete data sets consists of 3-hour heave motion data, where the deck elevation is measured every 0.2 seconds. To perform a lifting test on each of these points with different hoisting velocities and crane stiffnesses, as done with the sinusoidal waves, would take days. However, after comparing several tests done with a 5-minute fragment from this heave motion data and an hour fragment of the same data, it could be concluded that shorter pieces of data gave a similar result to the longer pieces of data because the re-hit percentages differed less than two per cent. This is why all test in this section are executed on a 5-minute heave motion data set, displayed in Figure 4.15. The data point set contains 1500 data-point from where the lifts are executed and result in a clear lift or a re-hit. The highest point is located 0.37 meters above the average deck height, and the lowest point is located 0.41 meters below the average deck height. Furthermore, it can be seen that the amplitude changes considerably, and the period is not constant. The average period is 5.59 seconds.

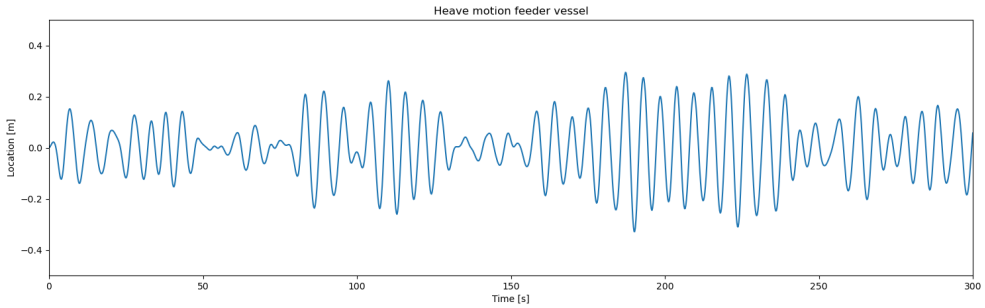

Figure 4.15: Realistic heave motion of the feeder vessel, head sea direction, Tp = 5.59 s, H_S = 1.5 m.

A run of the model is executed with every data point as a starting point of the lift operation, so every 0.2 seconds. The parameter from Section 4.2 are implemented under maximum conditions, so a load of 900 tons and the crane lifting this load at a radius of 38 meters. Figure 4.16 shows the data points where the start of a lift resulted in a re-hit (displayed by the red dots) or resulted in a clear lift (displayed by the green dots). In 0.66% of the cases, a lifting operation resulted in a re-hit. Significantly lower than the percentage of re-hits obtained at the sinusoidal heave motion data. Figure 4.16 shows that the red dots are very scattered. The figure shows that the start of a lift operation that results in a re-hit can often

be found before a relatively high crest in the motion spectrum. Furthermore, it can be observed that when the heights of the crests of the heave motion are relatively low, a lifting operation has a higher chance to result in a clear lift. This can be seen in the figure between seconds 0 and 80, 130 to 160 and 240 to 300. Thus, periods of calmer heave movements are more favourable when it comes to feeder lifts. Examples of individual lifting graphs can be found in Appendix D.

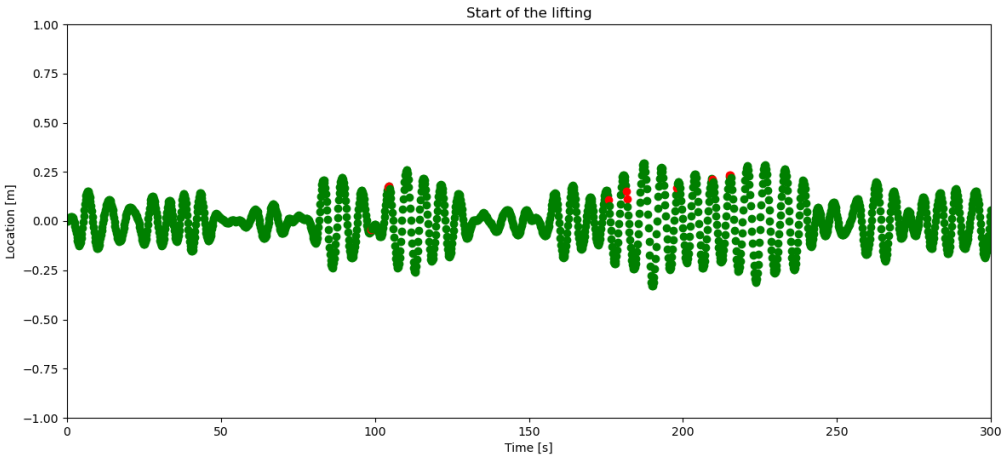

Figure 4.16: Lifts resulting in either a re-hit (red) or a clean lift (green).

As with the sinusoidal waves, an analysis of the hoisting velocity is executed for the realistic heave motion data for the Tetrahedron 45 and a fictional luffing boom crane with a total stiffness of 10000 kN/m. The re-hit percentages at different hoisting velocities are shown in Figure 4.17. A horizontal red-striped line is drawn at 0.66% to indicate the re-hit percentage of the Tetrahedron 45 with a hoisting velocity of 16 meters per minute. This red-striped line crosses the LBC line at a hoisting velocity of 14.25 meters per minute. This hoisting velocity happens to be close to the same velocity as with the sinusoidal heave motion. Again, hoisting velocities that luffing boom cranes use are generally much lower.

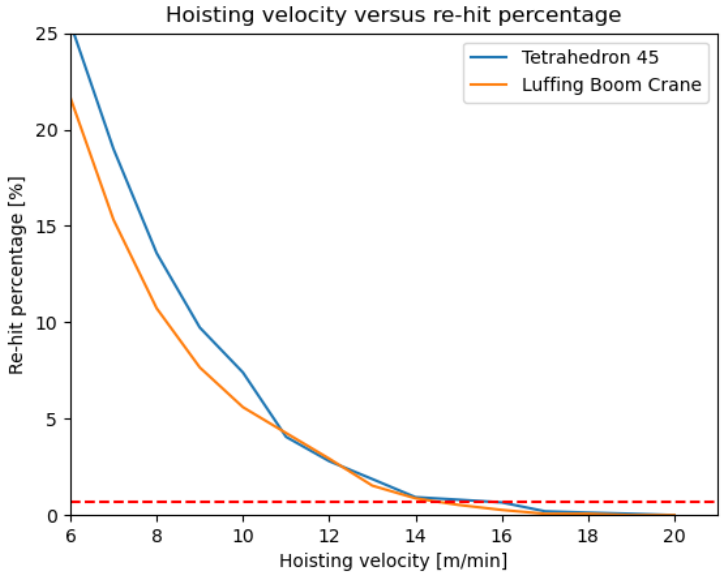

Figure 4.17: Re-hit percentage at different hoisting velocities.

The effects of the crane stiffness on the percentage of re-hits are shown in Figure 4.18. In this graph, the crane stiffness and the total stiffness are changed and displayed with the accompanying re-hit percentage. As with the sinusoidal heave motion, the realistic heave motion has a downward trend in the re-hit percentages over an increasing total stiffness. However, this pattern is going down a little less consistent. Furthermore, it can be seen that the total stiffness of the Tetrahedron 45 with a hoisting velocity of 16 meters per minute results in a similar re-hit percentage as the point where the 14.25 meters per minute data point and the total stiffness of the luffing boom crane.

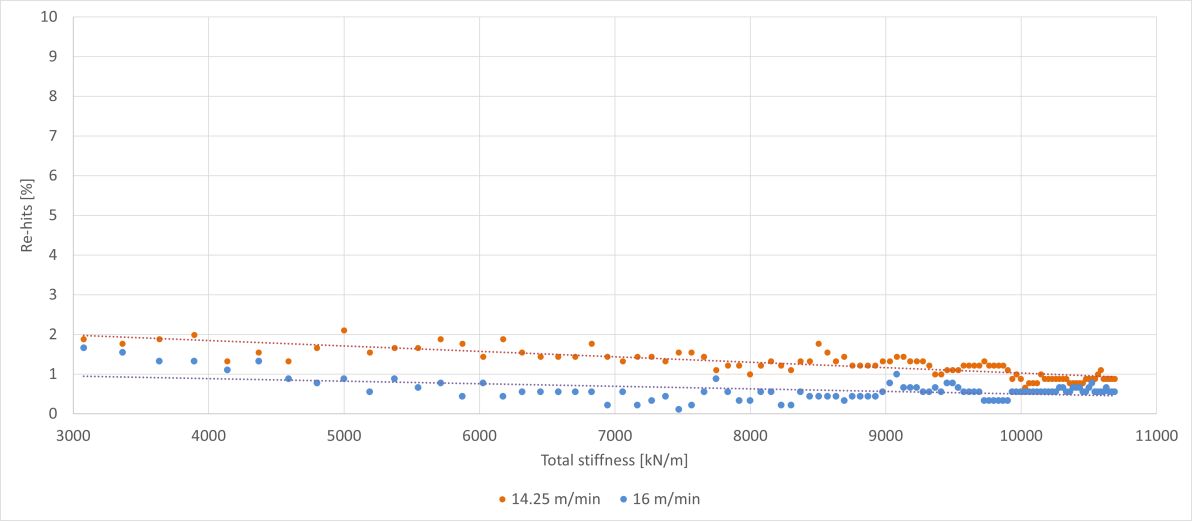

Figure 4.18: Percentage of re-hits on 5-min heave motion data at different total stiffnesses.

The last step to compare the Tetrahedron 45 with the luffing boom crane is using the Dynamic Amplification Factor. The same analysis is executed as with the sinusoidal heave motion, and the results are shown in Figure 4.19 and 4.20, respectively the LBC and the Tetrahedron 45. These figures show the DAF obtained from the 1D model, equal to the equation of D.E. Charett, displayed by the bars. These results are obtained with Equation 4.11. The average DAF, resulting from Equation 4.11, for the Tetrahedron 45 is 1.08. For the luffing boom crane, the average equals 1.10. Also, the maximum DAF that occurs during all the different lifting runs is higher for the luffing boom crane than for the tetrahedron, respectively 1.20 and 1.16. Thus, overall the resulting dynamic amplification factor is lower than the results from the previous section. This is very promising because the DAF are further away from the critical factor discussed in Table 4.2, but still some lifting operations experience higher dynamic loads than the T45 is designed for. In 26.4 % of the lifting operations the DAF limit for the crane is exceeded, a total of 27.0% of the lifting operations results in an unsuccessful lift. The red vertical lines represent the value for the DAF determined using Equation 2.2, these values are the same as with the sinusoidal waves since it is dependent on the significant wave height. The significant wave height stayed the same. The difference in the obtained DAF for the model and DNV are even further apart. The values obtained from the 1D model are way below the, conservative, value from the DNV standard.

To conclude on the realistic heave motion, the Tetrahedron 45 at a similar re-hit percentage as the luffing boom crane has a lower dynamic amplification factor. Under the assumption that the DAF limit for the luffing boom crane is the same as for the Tetrahedron 45, it outperforms the luffing boom crane under these specific conditions.

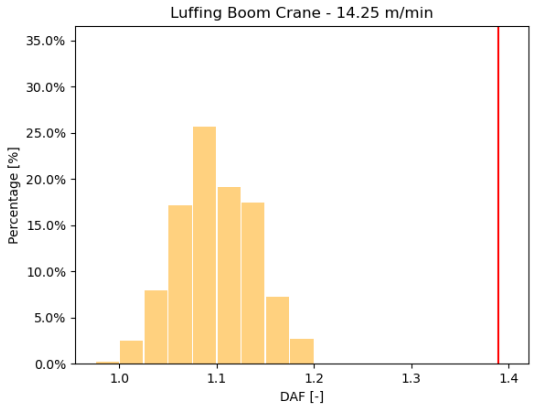

Figure 4.19: DAF for the Luffing Boom Crane case.

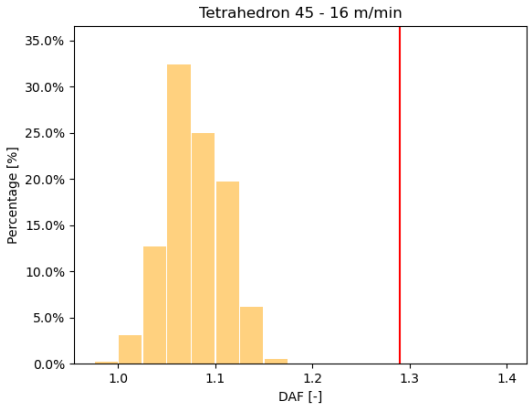

Figure 4.20: DAF for the Tetrahedron 45 case.

4.6. Verification of the single degree of freedom model

The goal of the 1D model was to determine if it is safe to lift a load, being a wind turbine component, from a feeder-vessel utilizing a Tetrahedron 45 crane. Save in the 1D model means that the load clears the vessel deck without having a re-hit and resulting in possible damage to load and crane. Furthermore, the 1D model aims to assess the feasibility of feeder lifting for data sets containing large quantities of data points in a relatively short period of time. An additional aim was to derive and determine the magnitude of the dynamic amplification factor when a load is undergoing sinusoidal- or realistic heave motion is lifted. The DAF should stay within limits set by the crane and turbine manufacturer. The 1D model offers a way to simulate lifting a load at a specific moment when the heave motion data of the feeder-vessel is put in. Furthermore, the model can simulate a lifting operation for every time step in a data series, so specific ranges in time can be pointed out where a lift is possible without the opportunity of a re-hit to occur. The DAF per lift can be determined, and when larges data series are examined, it is possible to statistically display the DAF data and determine changes exceeding the set limits. So the model can assess the goals which it was intended to.

Derivation of the equation of motion, from the dynamic model, to the function with which the dynamic factor is calculated (Equation 4.11) corresponds to what is mentioned in the literature. This feature can be found in a 1976 article, ”Dynamic Factors for Offshore Cranes,” by D.E. Charrett [28]. However, this equation differs from the most common equation used to calculate the dynamic factor (Equation 2.2) [18]. This difference can be explained by the fact that DNV calculates both the velocity of the crane hook and the velocity of the vessel based on the magnitude of the significant wave height the feeder vessel is located in. However, the equations used to determine these velocities are based on a probabilistic approach. This approach assumes a chance of exceeding the calculated velocities to be equal or less than 2%. Furthermore, DNV assumes the velocity of the feeder vessel to be equal to the velocity of the wave it is located in. This does not apply to larger vessels, such as feeder vessels that transport turbine components. These two reasons are mainly responsible for the fact that the DAF is much more conservatively determined by DNV than the values obtained by the 1D model.

$$z = -(\frac{1}{\tilde{p}})(\frac{V_{line}}{NH} + V_{deck}) * sin(\tilde{p} * t) + \frac{V_{line} * t}{NH} \tag{4.12}$$

$$where;\ \tilde{p}^2 = \frac{p^2}{(1 + NH\frac{K_{cable,single}}{K_{crane}})}\ and\ p^2 = NH^2\frac{K_{cable,single}}{M} \tag{4.13}$$

$$DAF = 1 + (\frac{NH}{g}) * (\frac{V_{line}}{NH} + V_{deck}) * \sqrt{\frac{K_{cable,single}}{M}} * \sqrt{(1 + NH\frac{K_{cable,single}}{K_{crane}})} \tag{4.14}$$

The dynamic amplification factor is also described in the article; ”The dynamic behaviour of offshore platform cranes” by D.G. Owen from 1979. In this article, a dynamic amplification factor is derived based on a dynamic model from which an equation of motion, and a general solution for an offshore crane are derived [29]. This article uses the same assumptions as those made in Section 4.1.1. However, this dynamic model uses the difference in acceleration between the crane hook and the jib top to derive the equation of motion from a similar system as shown in Figure 4.1. As a result, the equations differ from those mentioned in the sections above. Equation 4.12 and Equation 4.14 show respectively the general solution, and the DAF derived in this article. These obtained equations have not been compared with the values obtained in the previous sections because when NH and $K_{cable,single}$ are varied in such a way that $K_{cable,total}$ (according to Equation 4.8) remains the same, the outcome of the dynamic factor is different. Assuming that the DAF remains the same and reasoning backwards to $K_{cable,single}$ or K_{crane}, these values should increase or decrease in relation to each other when the value of NH is varied. But this is not the case. It is for this reason that these functions are assumed to be incorrect, and the results from the previous sections have not been compared with Equation 4.12 and 4.14.

4.7. Discussion regarding the single degree of freedom model

To reach the goal stated at the beginning of the previous section. First, a simplified dynamic model representing a tetrahedron crane has been set up. After this model is set up, the equation of motion and general solution of this model are derived. Next to that, an analysis of the dynamic amplification factor is executed. Results of the model can be examined and displayed per lifting operations or for larger quantities of starting point from the heave motions data sets from Friede & Goldman. In addition to assessing the feasibility of feeder lifting for heave motion where the amplitude and period of the heave motion are known, as seen with the sinusoidal waves, input data can also be used where the amplitudes and periods vary and are less predictable.

The model works on the basis that only the starting point of the lift operation is known. The exact moment of lift-off can be determined but is not known before the lifting operation. An estimate can be made when the load experiences a lift-off from the vessel’s deck, but the exact moment is not known in advance. This is because it depends on the vessel motions in the seconds after the lifting operation starts. However, this information would be of interest because the ideal situation for lifting a load of a feeder vessel is that the lift-off takes place precisely on the wave crest.

The label ”clear lift” is now given to a lifting operation where the load and the vessel’s deck do not come in contact after the lift-off. However, more objects are present on the deck of the feeder vessel with which the load can experience a re-hit after the lift-off. For example, motions such as surge, sway, roll and pitch could cause the feeder vessel to hit surrounding obstacles or other turbine components located on the vessel’s deck after the lift-off. Furthermore, it is highly likely that the jib top, crane hook and load are not perfectly aligned. Eccentric lifting of the load can lead to pendulation of the load whilst it is hanging in the crane. The 1D model can not simulate movements in the x- and y-direction. It can only simulate the movements in the z-direction, and the label ”clear lift” is therefore limited to the movements in this direction.

A final point under discussion is the reliability of the 1D model. The model is based on derivations and assumptions found in the literature. However, this model is a simplified representation of reality, and it is necessary to find out the correctness of the 1D model concerning reality. Furthermore, it is not yet clear whether the assumptions and simplifications contribute to the validity. One of the simplifications is neglecting the weight of the structure and the cables. Mass is an important parameter in determining the load trajectory and could load to significantly different results. In the next chapter, a 2D model is introduced to which the 1D model can be compared.

5

2D Tetrahedron Crane Model

In this chapter, an existing 2D model of the Tetrahedron Crane is modified, tuned and used to verify the results of the 1D model and put them in perspective. In the further course of this thesis, this model will be referred to as the 2D model. First, it is examined how the existing model is constructed, the parameters are obtained, what degrees of freedom the model has, and what output it gives. Secondly, the adjustments to the model are discussed so that comparison material for the 1D model can be obtained. Subsequently, a series of tests will be performed in which the 2D model is exposed to the same realistic heave motion data as the 1D model was in the previous chapter. Finally, this chapter ends with the verification and discussion of the 2D model.

Both models aim to generate an output that shows whether a lifting operation results in a re-hit or a clear lift. Based on the outputs of the two models, it can be concluded whether the limits set for the DAF are being exceeded or not. While the 1D model can generate the desired outputs for large amounts of data points relatively quickly, the 2D model can only retrieve outputs for one lifting operation at a time. Another fundamental difference between the models is that the 2D model can experience displacements in both the z-direction and the x-direction. The 1D model can only experience displacements in the z-direction. This difference may allow for load pendulation to occur in this additional range of motion. Load pendulation was assumed to be absent in the 1D model. The 2D model also differs from the 1D model because it accounts for the weight of the crane and the lifting cables. The own weight of the elements plays a role in the deflection of the crane hook. This deflection is not taken into account in the 1D model. The 1D model assumes that both crane and hoisting ropes are considered to be massless.

5.1. Static analysis

The static analysis aims to determine the displacement of the hook under the influence of static forces acting on the system. Furthermore, the static analysis serves to form a basis for the dynamic analysis. For this, the mass matrix, the stiffness matrix and the force vector must first be determined for the structure used in the 2D model. The displacement of, among other things, the crane hook can be found by solving Equation 5.1, where K and f can be determined. In this equation, K stands for the structure's stiffness matrix, the force vector is described by f, and the displacement vector, u, has to be found. First, the approach used in the existing model will be discussed, then the preformed adjustments will be explained to determine the displacement of the crane hook. Furthermore, the static forces that occur in the structure can be determined. These forces are essential to determine the dynamic amplification factor at a later stage of the analysis of the 2D model.

$$f = K * u \tag{5.1}$$

5.1.1. Initial 2D structure

The construction used for the analyzes of the 2D model consists of a system of elements and nodes. The initial system resembling the tetrahedron crane in the 2D model is shown in Figure 5.2. The elements with which the model is described are shown with blue lines, and the numbered green circles depict the nodes connecting the elements. An element always runs from one node to another. The locations of the nodes and the distances between them (lengths of the elements) are chosen so that the lengths of the elements and the entire shape of the structure corresponds to that of the Tetrahedron 45. In addition to the length, the elements are also given parameters for the cross-sectional area, inertia, density, elastic modulus that match the part of the Tetrahedron 45 represented by this element. The elements are modelled as Euler-Bernouilli beam elements with possible axial extension, as can be seen in Figure 5.1. This figure shows that for the extremities of each element, translation in the local x- and z-direction is possible and rotation around the local y-axis. The deformed state of a single element follows from 6 degrees of freedom, 3 for each end of the element. The mass of each element is described by the cross-sectional area times the length multiplied by the density. A six-by-six element mass matrix can be constructed by lumping the mass of an element to the two nodes it connects. It is assumed that half of the element's mass acts on each node it connects. The degree to which an element provides resistance to deformations in the six degrees of freedom is described in the element stiffness matrix. The content of this matrix depends on how the ends of the element are connected to the nodes. This connection can be either "fixed" or "pinned". When an element has a "fixed" connection to a node, this means that the element can give a form of resistance towards deformations in the local x- and z-direction and against moments rotating around the y-axis. When there is a "pinned" connection between the element end and the node, there is no resistance to deformation around the local y-axis, so for the corresponding entries in the element matrix this results in a zero. However, there is resistance to translation in the local x and z directions. The equation and shapes of these nodal constraints dependent stiffness matrices can be found in Appendix E. In this way, a local mass and stiffness matrix is drawn up for each element. Then, these local element matrices are converted into global element matrices using rotation matrices. The translation from local to global axis system results in one axis system in which all the element matrices are described. It follows that all the element matrices are now corresponding to the same system of axis.

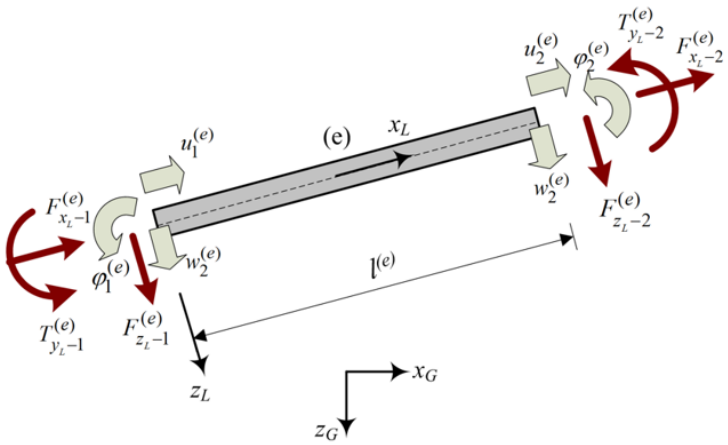

Figure 5.1: Forces and degrees of freedom on a beam element.

The next step is to merge all individual element mass and stiffness matrices to create a mass and stiffness matrix for the entire 2D structure. This merging is done using the direct stiffness method. Using the direct stiffness method means that when several elements are linked to a node, the mass and stiffness terms that operate in the same degree of freedom are joined through superposition. This results in each node having three degrees of freedom.

For the construction in Figure 5.2, consisting of 15 elements and 14 nodes, the 15, six-by-six, element mass matrices form a total mass matrix with a length and width of 42. The same applies to the total stiffness matrix. Every node has 3 degrees of freedom, and there are 14 nodes in total. Thus, the system has 42 degrees of freedom. When the design of the element matrices and the superposition of the DOFs has been done correctly, the mass and stiffness matrix should be symmetrical.

Now that the stiffness matrix have been obtained, only the force vector needs to be determined to solve Equation 5.1. The force vector has the same length as the number of degrees of freedom of the system. For the initial construction, this is 42. The forces in the force vector are built up from the summation of the forces caused by the weight of the structure, additional weights and external forces per degree of freedom. Additional weights are, for example, the weight of the hoisting blocks, the winch frame and the jib top. An example of an external force is the load suspended in the crane. In this example, the force would be linked to the degree of freedom in the z-direction of node number 15. When drawing up the force vector, the direction of the force is carefully considered. The positive x- and z-directions are indicated in Section 3.2.1, a positive force in the rotational direction acts anti-clockwise.

All information needed to compute the displacement vector has been determined with the force vector and the stiffness matrix. This displacement vector, just like the force vector, has a length of 42. However, some of the entries in this vector are already known. The nodes connecting the crane to the slewing platform cannot experience translation in the x- and z-direction but only rotate, and thus the displacement is zero for these degrees of freedom. The nodes connected to the slewing platform are represented by the numbers 1, 4 & 6 in Figure 5.2. In the model, these degrees of freedom are described as restrained degrees of freedom. The initial structure has six restrained degrees of freedom. The corresponding rows and columns can be removed from the mass and stiffness matrices, as can the corresponding entries in the force and displacement vector. The length of the vectors and dimensions of the matrices is now reduced to 36. Using Equation 5.1 a system of 36 equations of motions with 36 unknown displacements is constructed, so it is solvable. A deformed construction can be depicted by moving the nodes using these 36 displacements in the direction of the free degrees of freedom. An example of this is shown in Appendix E.

5.1.2. Modified 2D structure

The 1D model, introduced in the previous chapter, is dependent on the stiffness of the crane and the stiffness of the main hoist cable. The initial 2D structure from Figure 5.2, resembling just the crane, had no input that resembled the main hoist or the crane hook. Figure 5.3 shows the initial structure modified to have a 15^{th} element resembling the main hoist and a 16^{th} node that resembles the crane's hook. The parametric values that describe the added element match the values used to calculate the cable stiffness in Section 4.2.2. These parameters are the cross-sectional area, density, length and Young's modulus.

In the 1D model, the assumption is made that jib, hook and load are perfectly aligned and that the only displacement of the hook takes place in the z-direction. In order to be able to compare this 2D model with the 1D model, the same assumption is made. This assumption is reflected in the way the new element is linked to the new node. This connection is considered ”pinned”, so the only degree of freedom the hook can experience movement is the z-direction. Therefore, the main hoist cable is just as the 1D model, only subjected to extension. The addition of this extra degree of freedom means that, for the mass and stiffness matrices, the length and width become 37, where these were previously 36. The force-vector and displacement-vector also have a length of 37. Equation 5.1 yields a system of 37 equations of motions with 37 unknowns and is therefore solvable.

A force that resembles a load hanging in the crane would now be subjected to node 16 instead of node 15. The direction of the force stays unchanged.

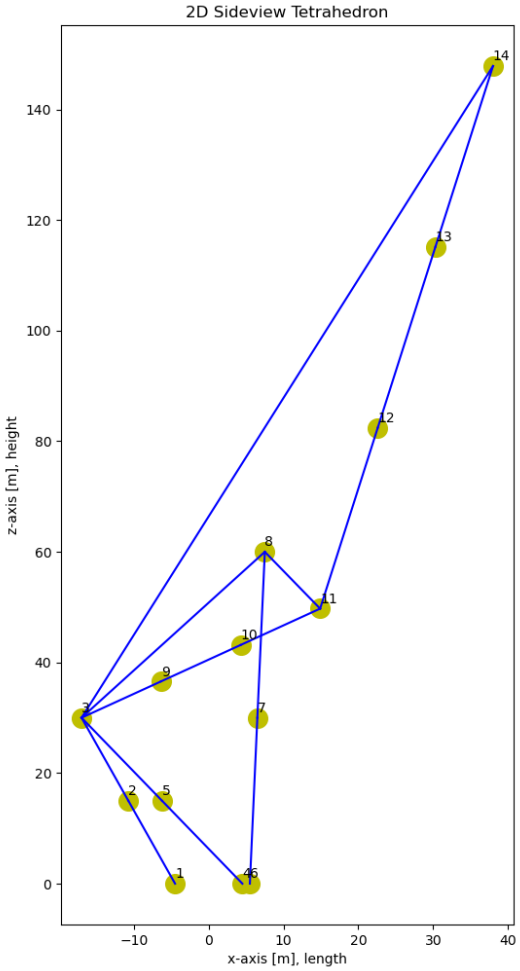

Figure 5.2: Initial structure 2D side-view Tetrahedron

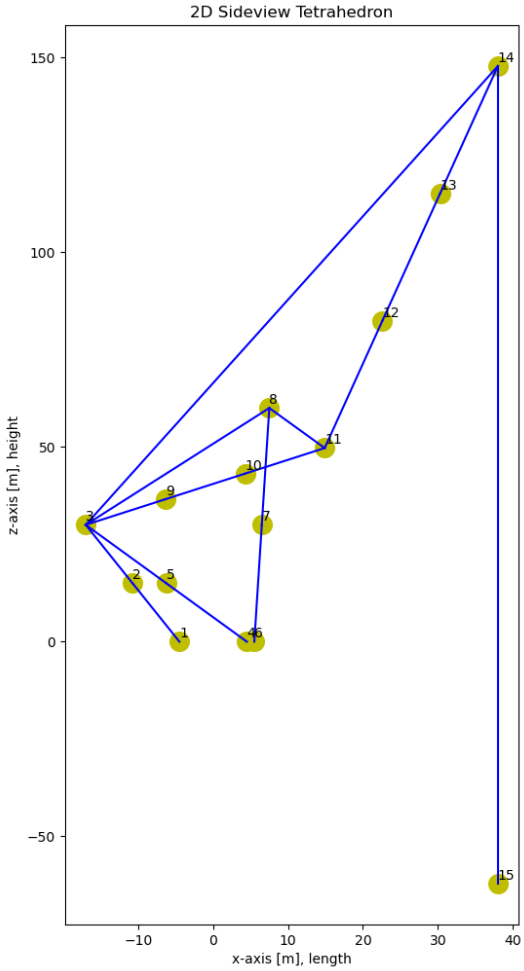

Figure 5.3: Modified structure 2D side-view Tetrahedron

5.2. Dynamic analysis

A result of interest for the assessment of the feeder lift feasibility is the hook's location over time. During this analysis, it is assumed that the location of the load, when suspended to the crane hook, is equal to the location of the hook. The location of the hook over time, together with the given wave data from Friede & Goldman, makes it possible to conclude whether a re-hit is taking place or whether the lifting operation results in a clear lift. The dynamic analysis also serves to determine the dynamic forces acting on the elements. It follows that from Equation 4.10 that the dynamic force divided by the static force from the previous section forms the dynamic amplification factor. By determining this for all elements, the normative DAF for the system can be determined.

The dynamic analysis determines the displacements of the nodes in the free degrees of freedom per time step. When the displacements over time are found, the velocity at which these displacements occur is also obtained. The dynamic method uses the state-space formulation to describe the unknown variables; these are the displacements and velocities of the free degrees of freedom. Instead of working with a system of n equations of motion for n degrees of freedom, the state-space formulation breaks the second-order equations into $2n$ first-order equations [30]. This means that the length and width of the mass and stiffness matrices becomes $2n$ and also the lengths of the force vector and displacement vector become $2n$. In the modified structure, n is equal to 37, so $2n$ equals 74. The first half of the displacement vector describes the velocities of the degrees of freedom, and the second half contains the displacements of the degrees of freedom.

After the equations of motions are rewritten according to the state space method, the Runge-Kutta 4th order method is applied as a numerical integration method. The applied numerical integration aims to determine the yet unknown displacements and velocities of the degrees of freedom as accurately as possible for the next time step. An advantage of using the Runge-Kutta method for the numerical integration is that this method converges faster in comparison to, for example, Euler's method and is, therefore, a suitable integration method for this model [31]. A disadvantage of this method is that it is computationally heavier than integration methods that converge less quickly. As a result, the 2D model generates results a fraction slower than when a lower order integration method is used. Since the 2D model is intended to analyze a single lifting operation at a time, this is only a minor inconvenience. When larger quantities of lifting operations have to be analysed, as is possible with the 1D model, this can cause more significant difficulties because running the script will take a long time.

5.3. Response of the system

5.3.1. Location of the load over the time

The 1D model uses the initial displacement and initial velocity at the moment of lift-off as input for the general solution, which computes the trajectory of the load hanging in the crane. The 2D model also requires initial conditions at the moment of lift-off to determine the load's trajectory. However, the initial conditions for all degrees of freedom are needed, which means that an initial displacement vector is needed as an input. The length of this vector is $2n$.

Through the static analysis, the exact deflection of the crane hook at lift-off can be determined due to the 900 tons load hanging in the crane. This value is almost the same as the deflection experienced by the 1D model at the moment of lift-off. The defection at the moment of lift-off was shown in the lifting graph by the green line. Examples of these lifting graphs can be found in Appendix D. The deflection of the hook at the moment of lift-off is around 1.6 meters. During the pre-loading phase of the 1D model, the crane hook gradually takes over the load from the moving feeder vessel. During this pre-loading phase the load remains located on the deck of the feeder vessel. By comparing the amount of load suspended in the crane hook with the total load, a list can be drawn up containing the percentages of the total load hanging in the hook at any moment in the pre-loading phase. The percentage of the total load hanging in the crane hook is proportional to the percentage of the deflection the hook experiences under maximum load. This list is then adjusted to the step size of the 2D model using linear interpolation and exported. The next step is to load this list into the 2D model and use it as an input for the displacement of the crane hook. This displacement acts on node 16 in the negative z-direction, node 16 resembles the crane hook. This node is moved during the pre-loading phase in the same way that the 1D model experiences it at the same time. This means that the 2D model is pre-loaded at the same rate as the 1D model. An example of a lifting graph from the 1D model and the corresponding imposed displacement of the crane hook during the pre-loading phase, used as input for the 2D model, are shown in Figure 5.4 and 5.5.

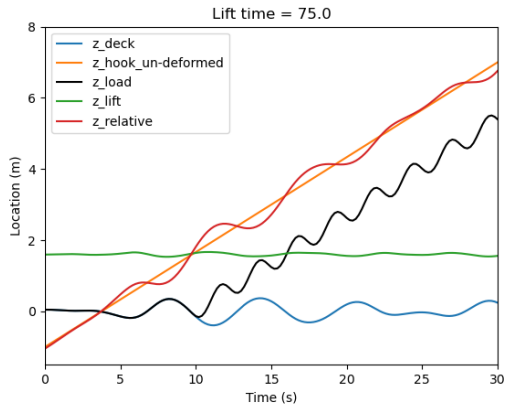

Figure 5.4: Lifting graphs for $t_{start} = 75\ s$.

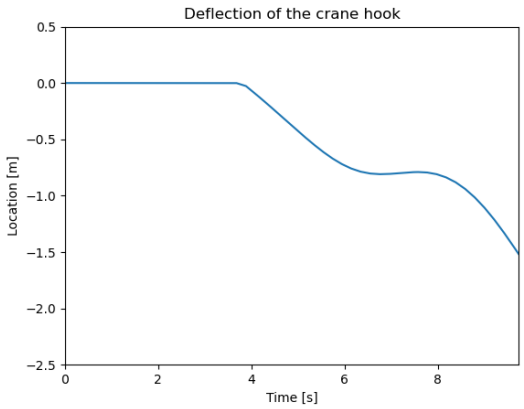

Figure 5.5: Imposed displacement of the crane hook.

The last displacement vector, obtained from the 2D model, before lift-off, containing a value for the displacement and the velocity of every degree of freedom, is then used as the initial condition at the moment of lift-off for the 2D model. From the moment of lift-off, the situation changes. The first difference with the pre-loading phase is that the displacement of the hook is no longer considered a given and no longer experiences imposed changes. A second change is that the mass of the load is suspended in the crane hook from the moment of lift-off. Therefore, this mass becomes part of the system of nodes and elements that describes the crane. This changes the mass matrix. The mass at the hook's location was first described by the mass of the hook and half the mass of the element representing the hoisting cables. It accounts for half of the weight of the hoisting cables due to the way the masses of the elements are lumped onto the nodes in the 2D model. From the moment of lift-off, the mass of the load is added. Now that the initial conditions are known at lift-off, and the mass matrix has been adjusted, the load trajectory over time can be determined. The trajectory of the load from the moment of lift-off can then be compared with the 1D model and the conclusion can be drawn if the lifting operation results in a re-hit or not.

5.3.2. Dynamic Amplification Factor

The 1D model uses a general solution that describes the location of the load during the lift. The second derivative of this general solution expresses the acceleration experienced by the load during the lift, which can then be used to calculate the DAF. For the 2D model, it is not possible to determine the maximum acceleration of the load during the lift. Nevertheless, the 2D model can determine the static and dynamic forces per element. The static forces per element are found by statically loading the system. The dynamic force per element follows from the maximum force that an element experiences during the lifting operation. As described in Equation 4.10, the DAF can be determined based on the ratio between the dynamic and static force. The element with the highest value of the DAF is normative.

5.4. Performance in realistic sea state

The 2D model is pre-loaded, as described in the previous section, to obtain the initial conditions for every degree of freedom at the moment of lift-off. Furthermore, the trajectory of the load whilst it is suspended in the crane is obtained. This section describes the results of the 2D model and how they relate to the 1D model. In contrast to the 1D model, where an entire data series can be analyzed in a single run of the model, the 2D model can only extract results for a single lifting operation at a time. Two situations are highlighted in this section. First, a situation is considered where the load on the feeder vessel moves downwards at the moment of lift-off. So, the relative velocity between load and crane hook at the moment of lift-off is high. Then a situation is considered where, at the moment of lift-off, the load is moving upwards. So, the relative velocity at the moment of lift-off is low. More examples of lifting operations can be found in Appendix E.

5.4.1. Lift-off at downwards heave velocity

The first situation that will be looked at is when the load experiences a downward motion at the moment of lift-off. As a result, the load moves in the opposite direction from the hook. In this situation, the highest forces are expected to occur, resulting in large amplitudes when the load oscillates in the crane after lift-off. Figure 5.6 shows an example of such a situation. In this example, the lifting operation has started at 75 seconds from the beginning of the data series, displayed in Figure 4.15. At the moment of lift-off, the load has a velocity of 0.35 m/s in the negative z-direction. The crane hook moves in the positive direction with a velocity of 16 meters per minute, resulting in a relative velocity of 0.62 m/s.

Figure 5.6 shows that the lines representing the load trajectory for the 1D and 2D models are initially very similar, but as time goes by, they start to deviate more from each other. This divergence is due to the difference in the period of the two motions. The period of the 2D model is slightly larger than the period of the 1D model. A larger period results from a lower frequency because $T = \frac{2\pi}{\omega}$, where T is the period of the motion in seconds, and ω is the natural frequency of the motion in rad/s. The natural frequency can be described by; $\omega = \sqrt{\frac{K}{M}}$, where K is the stiffness and M represents the mass. Because the 2D model considers the dead weight and the weight of additional masses, the mass in this last equation is higher than in the 1D model. Examples of these additional masses are the weight of the hinge mechanism, weight of the winch frame, weights of the upper and lower block of the main hoist. As seen in the figure, this higher mass results in a lower frequency and, therefore, a larger period. The natural frequency of the 1D model is equal to 2.47 rad/s, while the natural frequency of the 2D model is equal to 2.13 rad/s. It follows that the location of the load after seven oscillations of the 2D model is equal to that of the 1D model after six oscillations. Figure 5.6 confirms this.

Furthermore, it can be seen that the oscillations occurring in the 2D model are less smooth than those in the 1D model. Some peaks of the oscillations are sharper, and others are smoothed out. This is caused by different modes of vibration caused by different natural frequencies. The 2D model can determine the other natural frequencies but not the magnitude of the load trajectory per natural frequency. The 2D model follows that, as mentioned earlier, the first natural frequency is equal to 2.13 rad/s, the second natural frequency is equal to 5.02 rad/s, and the third natural frequency is equal to 9.48 rad/s.

The magnitude of dependence of the load trajectory on these second and third natural frequencies can be determined with the Fast Fourier Transform. The Fast Fourier Transform (FFT) is an algorithm that computes the Discrete Fourier Transform (DFT). The Fourier analysis converts the load trajectory from its original time domain to a frequency domain. Subsequently, the power spectrum density (PSD)

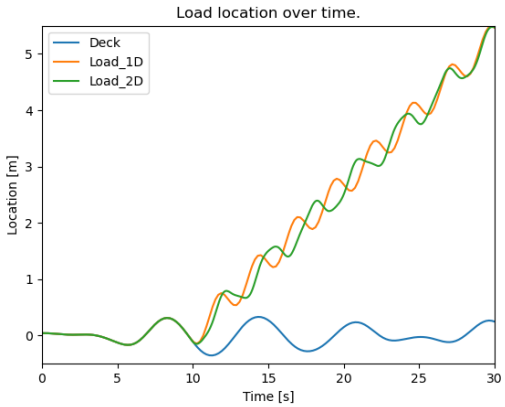

Figure 5.6: Comparing load location between 1D- and 2D-model, start-time = 75 s.

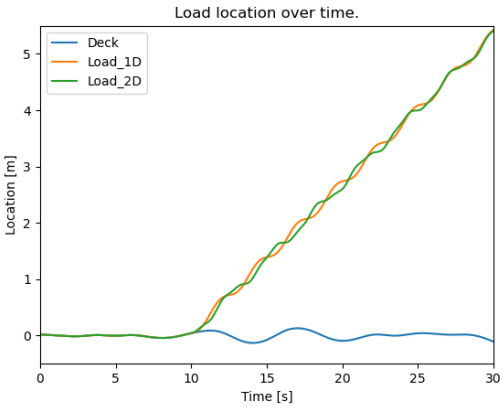

Figure 5.7: Comparing load location between 1D- and 2D-model, start-time = 50 s.

can be determined. From this, it can be read from which frequencies the signal is composed and the dependence on these frequencies. This can be seen in Figure 5.6. It can be seen that the load trajectory of the 2D model is more than 95% dependent on the first natural frequency. Furthermore, a small peak can be observed around 5.02 rad/s, the second natural frequency. Since there is no peak at the third natural frequency, it does not affect the load's trajectory. The disturbance in the load trajectory, resulting in the load trajectory of the 2D model in Figure 5.6 having less smooth oscillations than that of the 1D model, is therefore caused by the second natural frequency.

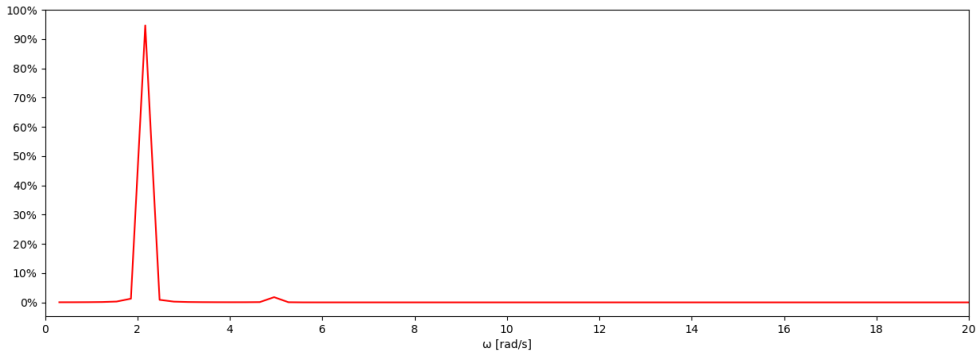

Figure 5.8: Power density spectrum of the 2D load trajectory.

5.4.2. Lift-off at upwards heave velocity

The second situation examined is when the load located on the feeder vessel is moving upwards, in the positive z-direction, at the moment of lift-off. In this situation, the load and the crane hook move in the same direction and the relative velocity is lower than the hoisting velocity of 16 meters per minute. These examples result in less severe oscillations representing the load's location over time. An example of such a lift is the result of a lifting operation commencing at 50 seconds from the beginning of the data series of the realistic heave motion from the previous chapter, shown in Figure 5.7. At the moment of lift-off, the load experiences an upward velocity of 0.05 m/s. The relative speed between hook and load is 0.21 m/s.

The same observations can be made as for the previous situation. The natural frequencies do not change if the moment that the lifting operation commences changes. The lines representing the load trajectory of the 1D and the 2D model start similar but start to divergence when time passes. As in the previous situation, the load location after six oscillations according to the 2D model is almost identical to the load location according to the 1D model after seven oscillations. Furthermore, the load location over time of the 2D model is less smooth than that of the 1D model. This is caused by the mode vibrations from the second natural frequency. Additional lifting graphs can be found in Appendix E.

5.4.3. Resulting DAF

The dynamic amplification factor to be taken into account during a lifting operation can be determined with the method explained in Section 5.3.2. The situation that is considered is the same as can be seen in Figure 5.6, where the load moves in the opposite direction of the crane hook at the moment of lift-off. From the 1D model, it followed that the dynamic forces occurring in this lifting operation were a factor of 1.16 higher than the static forces. In order to find the DAF of the 2D model, the static force per element must first be acquired. Then the maximum dynamic force per element is determined. This dynamic force is then divided by the static force that occurs in the element due to a load of 900 tons. The results of this can be seen in Table 5.1, in which the elements are numbered, and in the second column, you can see between which two nodes the element is located. The numbered nodes that correspond to the modified crane structure as can be seen in Figure 5.3.

The values in this table are based on the axial forces that occur in the elements. The shear forces are disregarded because they contain relatively low values for the static consideration of the forces and are given a much higher value during the dynamic consideration. When this is represented as a ratio between the dynamic and static forces, dynamic amplification factors arise that can be two or higher, with outliers of 25 and 38. Despite these huge factors, the forces themselves are not sufficient to lead to the structure's failure.

According to DNV, the DAF that must be taken into account in the case of a significant wave height of 1.5 meters is equal to 1.29. This value for the DAF represents the actual dynamic amplification factor according to the 2D model better than the factor that follows from the 1D model.

After performing several runs with different start times, the value of the DAF found from the 1D model is always lower than the normative DAF from the 2D model. The DAF found in the 1D model matches better with the DAF found for element 16, the main hoist cable. According to the 1D model, the DAF for the lifting operation from the table below is equal to 1.16, while a DAF of 1.17 is found for the main hoist cable (element 16) in Table 5.1.

Element	Node	DAF
1	1-2	1.25
2	2-3	1.24
3	4-5	1.28
4	5-3	1.29
5	6-7	1.24
6	7-8	1.24
7	3-8	1.23
8	3-9	1.23
9	9-10	1.22
10	10-11	1.21
11	11-12	1.18
12	12-13	1.17
13	13-14	1.17
14	3-14	1.23
15	8-11	1,23
16	14-15	1.17

Table 5.1: DAF per element for the lifting operation with start-time = 75 s.

5.5. Verification of the 2D Tetrahedron crane model

The composition that forms the structure of the crane used in the model has not been shown and described in literature before because it is specific to the crane designed by Tetrahedron B.V. However, the way the structure is built and the methods used in the 2D model are thoroughly described in the literature. For example, the Direct Stiffness Method is described in detail in books such as ”Structural Dynamics” by M. Paz and Y.H. Kim or in ”Matrix Structural Analysis” by W. McGuire, R.H. Gallagher and R.D. Ziemian [32] [33]. The method used for the numerical integration, the Runga Kutta 4 method, is described in ”Numerical Methods for Ordinary Differential Equations” by C. Vuik [31].

Apart from the model itself and the methods used for the model being heavily described in the literature, there is a way to check the numerical values obtained by the model. This is done by using the in-house software ACE. ACE, in turn, is verified with commercial software NASTRAN. NASTRAN is a finite element analysis program used for the analysis of linear and nonlinear stress, dynamics and heat transfer characteristics of structures and mechanical components [34].

The changes made to obtain the 2D model with the modified Tetrahedron crane structure are done so that the model keeps working in the same way only with different input values and with an additional element and node. The additional element representing the main hoist cable is implemented such that it reflects the situation of the cable in the 1D model. The elongation of the main hoist cable due to a load of 900 tons suspended in the crane for the 1D model is 0.66 meters. The elongation of the main hoist cable under the same load conditions in the 2D model equals 0.71 meters. The larger elongation of the cable in the 2D model can be explained by the extra weight that hangs in it. This extra weight is partly the weight of the cable and partly due to the weight of the main hoist lower block of the Tetrahedron 45. The weight of the main hoist lower block is 45 tons, and the part of the weight of the cables is about 17 tons, half of the total weight of the main hoist cables. This brings the total weight hanging in the cables to 962 tons. When this load value is entered into the 1D model, an elongation of the cables is obtained equal to 0.71 meters.

Differences in the load trajectory of the 1D and 2D models are explained in the previous section. Both the difference in natural frequency and the difference in the shape of the oscillations are explainable. The difference in the shape of the oscillations will even get smaller over time since the energy from higher frequency modes transfers to lower frequency modes. This transfer in energy means that the first natural frequency will even get more dominant, and the effects of the second natural frequency will disappear.

5.6. Discussion regarding the 2D Tetrahedron crane model

As discussed in Section 5.3, the way the 2D model determines what the initial conditions are at the moment of lift-off is based on the force transfer from vessel deck to crane hook of the 1D model. By expressing this in percentages of the total force that ultimately hangs in the crane, both models are loaded at the same rate, and the lift-off takes place simultaneously. However, when looking at absolute numbers, the forces that hang in the crane at a specific time are different for the 1D and 2D models. This is mainly caused by the fact that the 2D model includes the self-weight of the crane structure and the hoisting cables. Additionally, the 2D model includes the inertia of the nodes and elements that represent the structure.

As mentioned before, the frequency of the 2D model differs from the 1D model. As shown in the figures above, the lines of the 1D and 2D models are not far apart just after the lift-off but diverge quickly after the moment of lift-off. During the lifting operation, there are periods where the two lines have considerable differences and moments where they differ not that much, for example, after six oscillations of load trajectory of the 1D model and after seven oscillations of the load trajectory of the 2D model. This difference in load location is caused by the fact that the 2D model takes self-weight and extra masses into account, where the 1D model does not. In order to be able to compare the entire trajectory of the load, the 1D model will have to be also adapted to take self-weight and additional masses into account.

The graphs that are shown in Figure 5.7 and 5.6 and Appendix E all show the effects of the second natural frequency in addition to the first natural frequency that is mainly responsible for the shape of the load trajectory has after the lift-off. It is also known that energy from the higher frequency will transfer to the lower frequency. This effect is not reflected in the load trajectory, and the 2D model does not consider it. The speed at which this shift in energy takes place can influence the re-hit percentage and the dynamic forces occurring in the crane. Another effect that is not included in the 2D model is the effect of damping. In the current model, there is no damping, so the oscillations retain the same size over time. In reality, the oscillations experienced by the load hanging in the crane will decrease due to damping in the system.

Another point for discussion is how the DAF is determined for the 2D model. It is now assumed that because the crane is dimensioned for a maximum DAF of 1.1 that this also applies to each element. Thus, the element with the highest value for DAF is now normative. While it may be the case that one or more elements have a maximum DAF of 1.1 and that there are also elements that can withstand a higher dynamic factor than 1.1. In the example mentioned in the previous section, it could be that the base frame can tolerate a higher DAF and therefore is not normative, whereas according to the current reasoning, it is.

In order to be sure about results from the computations, for instance, the deflection of the jib-top in the z-direction, experiments with prototypes have to be executed. This is possible, for example, in research facilities such as Deltares and Marin, where waves in basins can be simulated. Such an experiment could, for example, consist of a feeder barge that experiences movements caused by waves in a wave pool, from which a prototype Tetrahedron crane tries to lift a load. No similar experiments have been performed before, and it is still unclear whether the obtained results described in this thesis correctly simulate reality. However, these models are designed so that they, in all probability, approximate reality reasonably. By monitoring the displacement of critical nodes in the pre-loading phase, it can be determined if the way the hook and thus the structure is now pre-loaded is correct. Perhaps it emerges here that different nodes experience pre-loading at a different rate and behave differently than currently assumed. This could alter the results currently obtained with the 2D model.

6

Assessment on the Case Study Results

In this chapter, the models from chapters 4 & 5 are used to assess the case study. The 1D model is adjusted to better match the 2D model and, therefore, reality. Results related to the case study, described in chapter 3, are obtained. Subsequently, these results and the case study itself are discussed.

6.1. Case Study results

In Chapter 4, it emerged that when the Tetrahedron 45 and a luffing boom crane perform the same 900-tonnes lifting operation. That the occurring forces in the Tetrahedron crane are lower than those occurring at the luffing boom crane under the conditions that they have a similar re-hit percentage but differ in crane stiffness and hoisting velocity. The crane stiffness and the hoisting velocity are both crane-specific parameters and impact the case study results. Apart from these parameters, some more parameters are essential for the case study but do not affect the crane itself. These parameters are the differences in the weight of the turbine components and the heave motion data of Friede & Goldman. To determine the effect of these parameters on the case study results, the 1D model, described in chapter 4, must first be adapted. This has to be done because chapter 5 showed that the crane's dead weight has a considerable effect on the results. Initially, the dead weight of the crane and cables was neglected in the 1D model.

6.1.1. Adjustments 1D model

In the previous chapter, it emerged that the shortcomings of the 1D model were mainly due to the missing dead weight of the crane and cables. This shortcoming resulted in a considerable difference in the natural frequency of the two models. Adjusting the 1D model should therefore be done so that the natural frequency of the 1D model matches that of the 2D model. The natural frequency of the 1D model, operating under maximum load capacity, was initially 2.47 rad/s. The natural frequency of the 2D model is equal to 2.13 rad/s.

The natural frequency, described by $\omega = \sqrt{\frac{K}{M}}$, can be decreased by either decreasing the stiffness or increasing the mass. It has been chosen to adjust the value of mass such that $\omega = 2.13\ rad/s$. It can be seen in Equation 4.6 that by adding this extra mass, the load trajectory gets not only a lower natural frequency but also the term $\frac{1}{\omega}$ increases due to the lower frequency. This increase means that the amplitude has increased due to this change. However, adding the self-weight to the model should not affect the amplitude of the motion. This is solved by only modifying the ω that is inside the brackets of the sine and leaving the term $\frac{1}{\omega}$ unchanged. An example of the load trajectory for the 1D and 2D models before and after adjusting the 1D model can be found in Figure 6.1. This figure shows how the 1D model, after the adjustments approximates the 2D model well. The shortcoming of the 1D model regarding the effects of the second natural frequency remain.

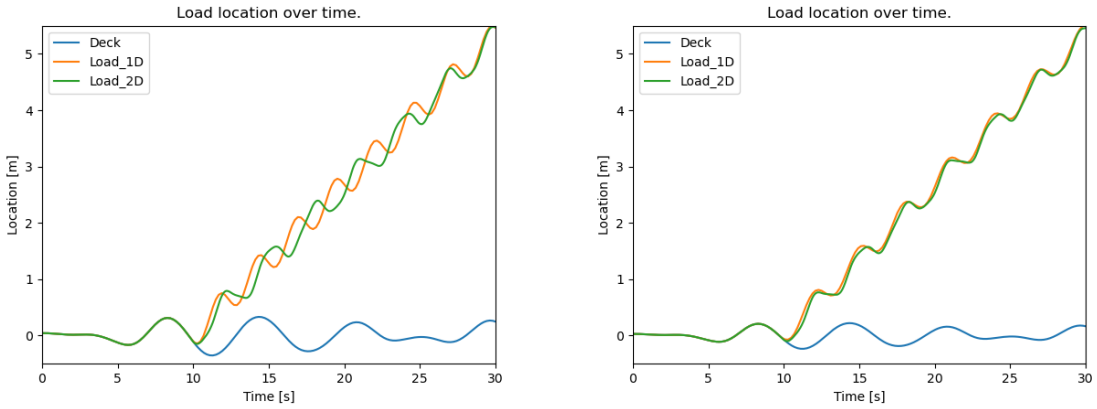

Figure 6.1: Comparison of load location between 1D- and 2D-model before adjusting the 1D model (left) and after adjusting (right).

6.1.2. Results

Now that the 1D model has been modified and the dead weight of the crane and hoisting cables are taken into account, the feasibility of performing feeder lifts for the case study described in Chapter 3 can be assessed.

The influence that the different masses of the components have on the percentage of unsuccessful lifts can be seen in Table 6.1. This table shows the percentage of lifting operations in which a re-hit occurs, the percentage of lifting operations in which the crane's DAF limit is exceeded, or the DAF limit of the component is exceeded, and the total percentage of failed lifting operations. Here, lifting operations that both exceed the DAF limit and result in a re-hit count as one unsuccessful lift. For the computations of these percentages, the Tetrahedron 45 is used with a hoisting velocity of 16 meters per minute. The heave motion where it is subjected to is the same as used in Section 4.5, having an average motion period of 5.59 seconds and caused by waves with a significant wave height of 1.5 meters.

As described above, a larger mass results in a lower frequency, a lower mass results in a higher frequency and thus a shorter period. Furthermore, a higher frequency results in a lower amplitude of the oscillations. Table 6.1 shows that a decrease in the component mass does not instantly cause the re-hit percentages to go down. This table does not consider that when lifting lower masses, a higher hoisting velocity can be used. A higher hoisting velocity results in the few re-hits that still occur being prevented. Furthermore, Table 6.1 shows that only at a maximum capacity of 900 tons is the DAF limit of the crane is exceeded. The weights of the components in combination with the given data on the heave motion do not lead to a situation where the DAF limit of the crane is exceeded. The lower the weight, the higher the DAF must be to exceed the crane's limit.

Load	Mass [tons]	Re-hit [%]	DAF T45 [%]	DAF comp. [%]	Total [%]
max. Crane capacity	900	0.40	15.06	0.00	15.46
Nacelle	841	0.20	0.00	0.00	0.20
Tower component 1	611	0.20	0.00	0.00	0.20
Tower component 2 & 3	575	0.40	0.00	0.00	0.40
Blade rack (3 blades)	300	0.27	0.00	2.93	2.93

Table 6.1: Percentage of unsuccessful lifting operations per turbine component.

The DAF limits set by the turbine manufacturer are summarised in Table 4.2. From this table, it follows that the DAF on the blade rack should not exceed 1.3. However, in Table 6.1 it can be seen that in 2.93% of the lifting operations of the blade rack, this DAF limit is exceeded. This would result in the conclusion that the Tetrahedron 45 with a lifting velocity of 16 meters per minute is not able to lift the blade rack of the feeder vessel. However, this is not due to the high possibility of a re-hit taking place. Instead, the forces that occur during the lift of the blade rack are too high and can damage the blade

rack or the turbine blades located in the blade rack. This exceedance of the DAF limit can be mitigated by placing a passive heave compensator (PHC) between the crane hook and the blade rack during the lifting operation. A passive heave compensator works as a giant shock absorber and absorbs external forces that influence the system. In this case, the external forces are caused by the feeder vessel that moves up and down. The passive heave compensator absorbs these external forces partly and reduces the peak loads that occur during lift operation. The downside of a PHC is that it decreases the maximum lifting height of the crane because it is located between hook and load. Hereby adding additional weight to the crane. This does not matter much for the lighter components because they are far from the maximum lifting capacity. However, for the heavier components, such as the nacelle, this can make the difference between exceeding the maximum lift capacity or not. In the case of the lift of the blade rack, a passive heave compensator could make it possible for the Tetrahedron 45 to execute these feeder lifts. However, this does not mean that all lifting operations benefit from being performed with a PHC.

Table 6.2 and 6.3 shows the re-hit percentages and information on the probability of DAF exceedance, for the Tetrahedron 45 described before, for the different wave periods in the two different wave directions, respectively the head sea direction and the beam sea direction, as displayed in Figure 3.15. Although the re-hit percentages between the different motion periods differ considerably, there seems to be no direct relationship between them. These differences are more likely caused by the 5-minute fragment from the entire data series of Friede & Goldman containing rougher or less rough motions. From Appendix C it follows that at higher periods, the velocity of the heave motion is not necessarily lower because the wave heights of the heave motions are higher. What does follow from these data is that the re-hit rates for all periods are higher in the beam sea direction than in the head sea direction. Also, the probability is higher in beam sea directions that the DAF limit of the crane is exceeded. The wave coming from the beam sea direction results in a higher re-hit percentage and higher values for the DAF because the heave motions are larger in the beam sea conditions. In addition, they have higher velocities than for the head sea direction. This is mainly due to the pitch motion that has a more significant influence on the motion height and velocity in the beam sea direction than in the head sea direction.

Period [s]	Re-hit [%]	DAF crane [%]	DAF comp. [%]	Total [%]
5.59	0.40	15.06	0.00	15.46
7.64	3.60	31.58	0.00	34.84
9.13	3.00	33.38	0.00	36.04

Table 6.2: Percentage of unsuccessful lifting operations for different wave periods for the head sea direction.

Period [s]	Re-hit [%]	DAF crane [%]	DAF comp. [%]	Total [%]
5.59	3.20	34.04	0.00	36.78
7.64	3.86	36.51	0.00	39.71
9.13	3.66	30.18	0.00	33.38

Table 6.3: Percentage of unsuccessful lifting operations for different wave periods for the beam sea direction.

In addition to the direction from which the waves come and their period, the wave height can also vary. The significant wave height is modified by factoring the measured heave motion data points from Friede & Goldman with the same factor in which the significant wave height changes. The effects of the significant wave height on the percentages of re-hits and the percentage of DAF limit exceedance can be found in Table 6.4. The values in this table are based on the Tetrahedron 45 loaded at maximum loading capacity. The heave motion has a period of 5.59 seconds and is coming from the head sea direction. This data shows that a higher significant wave height results in a higher percentage of re-hits. Higher waves result in more significant heave motions within the motion period, which stays the same. As a result, higher velocities occur, and the chance that a re-hit will occur increases.

A higher velocity of the load at the moment of lift-off causes the Dynamic Amplification Factor to rise, possibly exceeding the maximum acceptable DAF. This increase in DAF and the increase in the percentage f DAF limit exceedance for the Tetrahedron crane can also be seen in Table 6.4.

H_S [m]	Re-hit [%]	DAF crane [%]	DAF comp. [%]	Total [%]
2.50	9.76	39.91	0.00	48.03
2.25	5.06	35.31	0.00	39.37
2.00	3.06	29.38	0.00	31.05
1.75	1.13	21.99	0.00	22.32
1.50	0.40	15.06	0.00	15.46
1.25	0.07	6.60	0.00	6.67
1.00	0.00	1.87	0.00	1.87

Table 6.4: Percentage of unsuccessful lifting operations at different significant wave heights (H_S).

A number of examples in which the re-hits as a result of the of the feeder lifts are graphically displayed can be found in Appendix F. In every situation, one parameter is adjusted compared to the initial case.

6.2. Conclusion regarding the Case Study

The purpose of the case study is to assess the feasibility of installing wind turbines by lifting the components for the turbine from a feeder vessel. All this within the constraints and boundaries for the case study described in Chapter 3. The case study outlines are purely aimed at lifting operations in the heave direction. Other additional problems are disregarded and do not affect the lifting operations to be performed. Examples of such problems are sailing the jack-up vessel from Europe across the Atlantic ocean to US waters or the location keeping of the feeder barge next to the jack-up vessel. A conclusion that can be drawn concerning the boundary conditions is that it is advisable to position the feeder barge so that the waves come from the head sea direction, because forces and re-hit percentages are lower when the waves come from this direction.

Based on the results described in chapter 4 and the previous section, it can be concluded that the re-hit percentages are low but not completely zero. There is, therefore, a chance that a re-hit will take place with all its consequences. However, the analyzes on the heave motion data were performed without considering the crane operator controlling the crane. It is not usual for the crane operator to just start lifting at a moment in time. In practice, a crane operator will take the sea conditions into account and adjust the starting point of a lifting operation accordingly. Estimating the barge's movements based on incoming waves or with the help of advanced equipment could ensure that the moments when re-hits could take place are prevented.

In addition to the percentages concerning re-hits, there is an even more significant proportion of lifting operations where the DAF limit of the crane is exceeded. This is due to performing the tests under maximum load capacity. When a lower mass is hoisted as shown in Table 6.1 it no longer occurs that the crane's DAF limit is exceeded. Even in the circumstances where the above tables indicate that in almost 40 percent of the lifting operations the DAF limit of the crane is exceeded, these percentages are almost all equal to zero when a mass of 841 tons (mass of the nacelle) is used, and also with the other components the limit is not exceeded. Table 6.1 also revealed that there are lifting operations where the DAF limit of the blade rack is exceeded. From this it can be concluded that for lighter loads additional measures should be taken to reduce the dynamic forces on the components. An example of this is the use of a passive heave compensator.

Based on the data used for the case study and assuming that the start of a lifting operation is being considered by either the crane operator or technology, it is likely that in the situation described, it is feasible to install the wind turbines using a Tetrahedron 45 crane lifting the components from a feeder barge that is moving in the z-direction. However, in the current situation sketched in the case study it is not possible to perform feeder lifts of blade racks. The forces that can occur during these lifts are to high and could cause damage to the blades or the rack itself. Adding a passive heave compensator between hook and load would solve this problem. The values for the DAF during the lifts of the other components stay within the set maximums. So for the other components this means that the forces occurring during the operation remain within the norms and limits.

6.3. Discussion of methods

The case study has been compiled with care to form a realistic whole with all the separate components. For example, the wind farm location in combination with the chosen turbine is also linked in real life. There are plans to equip the chosen jack-up with a Tetrahedron 45 crane, and it is very likely that when this jack-up installs the turbines for the Vineyard wind project, a feeder barge for the supply will be used to circumvent the Jones Act. However, several components should or could be taken into account to make the case study more realistic. For example, it is not realistic that the feeder barge will only move in the heave direction. Movements in the x- and y-direction and rotations about the z-axis are plausible. However, the 1D model cannot take this into account, and its effects on the re-hit percentage cannot be determined. Another simplification included in the case study analysis is that the loads are assumed as point masses when they are of considerable size in reality. The effects of this are not taken into account. Lifting these components could potentially lead to resulting movements of the barge. These movements are not present in the analysis and are considered negligible, but this may not be a correct assumption. Besides the fact that the barge moves during lifting, the jack-up is not entirely stationary. This is now assumed to be the case. However, even when the jack-up vessel is on its legs, it still experiences forces in the cross direction from the waves that ensure that the jack-up with the Tetrahedron crane there does not stand entirely still.

A final point of discussion is the feeder barge's heave motion. Not only does the response to waves differ for each different barge, but also the heave motion comes from a different location than the location where the Vineyard Wind project will be built. Therefore, to achieve higher accuracy in the case study analyses, the heave motion data should be used for the correct feeder barge. In addition, the measurements should be taken at the location where the offshore wind farm will also be built.

7

Conclusions and Recommendations

In this chapter, the results are summarized and discussed, and some recommendations for further research on feeder lift execution with a Tetrahedron crane are proposed.

7.1. Conclusions

The goal of this research was to determine the feasibility of executing feeder lifts with a Tetrahedron crane. During this research, a feasible lift was referred to as a lifting operation where no re-hit took place, and dynamic force stayed within the set DAF limits of the crane and turbine manufacturers.

After the 1D model is adjusted to account for the weight of the crane structure and main hoist cables, it shows a great resemblance with the results obtained from the 2D model. Therefore, the 1D model that simplifies the crane structure to a single degree of freedom system can assess the feasibility of feeder lifting. However, the 1D model is only able to assess lift-motions in the z-direction. The current models cannot assess the motions resulting from a lifting operation in the x- & y-direction. In addition to determining whether a lifting operation results in a re-hit or not, the 1D model provides an approximation of the DAF that occurs in the main hoist cable. However, analysing the same lifting operation in the 1D model and the 2D model shows that this DAF is not normative, and there are elements in the 2D model where higher DAF apply. Therefore, the 2D model should be used to determine the dynamic forces that occur more accurately in the crane during lifting.

The results from the case study show that for a realistic situation, the re-hit percentages are very low. The re-hits that occur can be avoided if the crane operator tries to avoid short periods of heavier waves, resulting in rougher heave motions when the lifting operations starts. A higher lifting speed reduces the re-hit percentage and increases the chance of higher dynamic forces during a lifting operation. The same applies to crane stiffness. A higher crane stiffness decreases the chance of a re-hit but increases the DAF during the lifting operation. The difference in the weights of the wind turbine components has a minimal impact on the re-hit percentage. However, the feeder barge's heave motion has a significant influence on the chance of a re-hit. A higher significant wave height results in a higher percentage of re-hits. Also, the forces that occur at higher significant wave heights are more significant since the velocities of the load at the moment of lift-off can be more significant. Furthermore, the case study showed that the wave period has little influence on the percentage of re-hits. Larger wave periods result in higher heave motions but not in higher velocities of the feeder barge and, therefore, virtually no difference in re-hit percentages. The last factor that affects the percentage of re-hits is the direction of the waves relative to the feeder barge. Percentages are lower when the waves come from the head sea direction than from the beam sea direction. Therefore, it is advisable to consider this when positioning the jack-up vessel and feeder barge for a lifting operation.

An analysis of the dynamic forces during feeder lift operations of the heavier components, such as the nacelle, shows that the DAF limit for the crane is regularly exceeded. Additional measures should be taken to increase the feasibility of this type of lift. An example could be the use of a crane with a higher lifting capacity. In addition, it is common for the dynamic forces to exceed the limit of the lighter and more fragile components, such as the blade rack while performing feeder lifts. Again, additional measures should be taken to improve feasibility, such as adding a passive heave compensator between the load and the crane hook.

7.2. Recommendations

In this thesis, a model is developed that can be used to determine whether it is possible to perform a feeder lift in a specific situation with a tetrahedron crane. Through this, it can be proven if the load, when lifting off the feeder barge, has a clear lift or if it comes in contact with the vessel deck again. Also, the associated forces can be calculated. Finally, factors that positively or negatively affect the success rate of a feeder lift are indicated, and suggestions regarding these factors are made.

Despite fulfilling the objectives of the thesis, more can be done to get a better understanding, and further improve the feasibility of performing feeder lifts with a Tetrahedron crane.

First, it would be interesting to include the x- & y-direction into the model. However, this goes beyond the capabilities of the 1D model and the capabilities of the 2D model. The 2D model could include movements in the x-direction, but in the current model, this motion is restraint. A new model that also includes the movements in y-direction should be made. Motions, in addition to the motions in the z-direction, are of interest because they can, for example, result in swinging motions of the load in the crane. For example, it could be that when the load has lift-off, and according to the 1D model, no re-hit occurs with the ship deck. However, there could be clashes with other objects on the vessel deck. Furthermore, movements of the feeder vessel in the x-& y-direction could cause contact of the load hanging in the crane with the vessel deck or with objects situated on the vessel deck. Lateral motions can also result in higher forces on the crane elements, and therefore the probability of exceeding DAF limits could increase.

Secondly, instead of assuming the components as point masses, it is interesting to refer to their actual dimensions. For objects such as the turbine blades and the tower, which have a decent size, it is interesting that the cargo ends do not come into contact with the crane, the vessel's deck or other parts on the deck of the feeder vessel. While this can lead to damage to the object coming into contact. The addition of giving the components their actual dimensions could, for example, be an extension of the 3D model proposed above.

The third point for further research is to reduce the dynamic forces during lifting operations. This research has shown that for heavy components, the DAF limit of the crane is regularly exceeded and during the lifting operations of the fragile components, the DAF limits of the components are compromised. For the dynamic forces occurring in the crane, follow-up research can be done on performing feeder elevators operations with a larger crane with a higher lifting capacity. For the dynamic forces acting on the components, follow-up research can be done on the effects of passive or active heave compensators on the magnitude of the dynamic forces, the influence on the occurrence of re-hits and the extent to which the DAF is lowered.

A final recommendation for further research is to conduct experiments on a Tetrahedron crane in a controlled environment. Although no Tetrahedron cranes have been manufactured yet, this seems to be an option for further research. Because Tetrahedron has plans to build a 1 to 50 scale prototype, this prototype will probably have the ability to be controlled remotely using electronics. In a recent joint venture, connections are being made with research institute Marin. Marin has a wave pool where when the prototype crane is set up next to it. There is a setup to simulate feeder lifts. Similar experiments could provide more insights into the feasibility of feeder lifts, but new points of attention could arise that had not been thought of before.

A

Vineyard Wind project

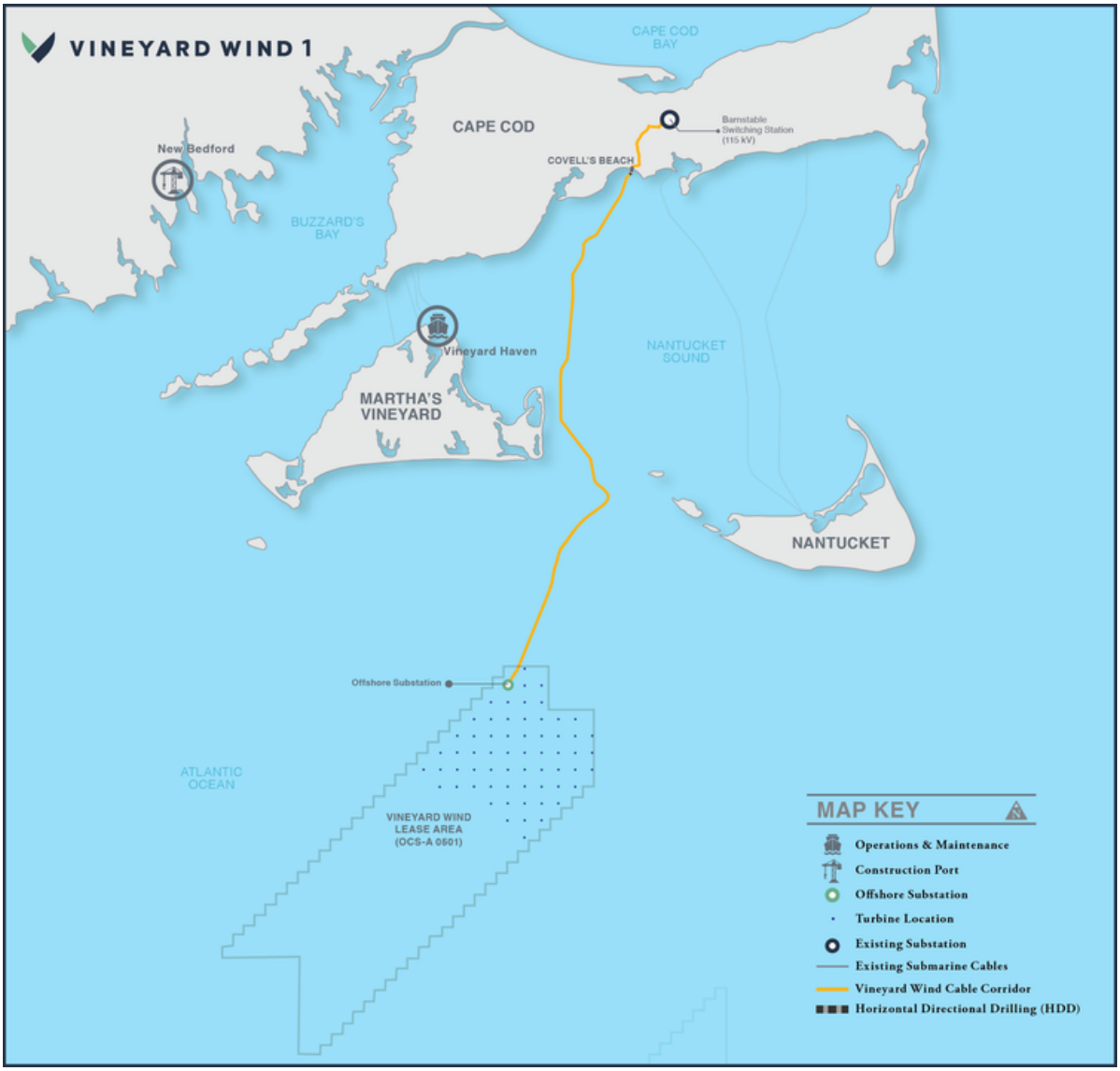

Figure A.1: Overview of Vineyard Wind project.

B

General Arrangements

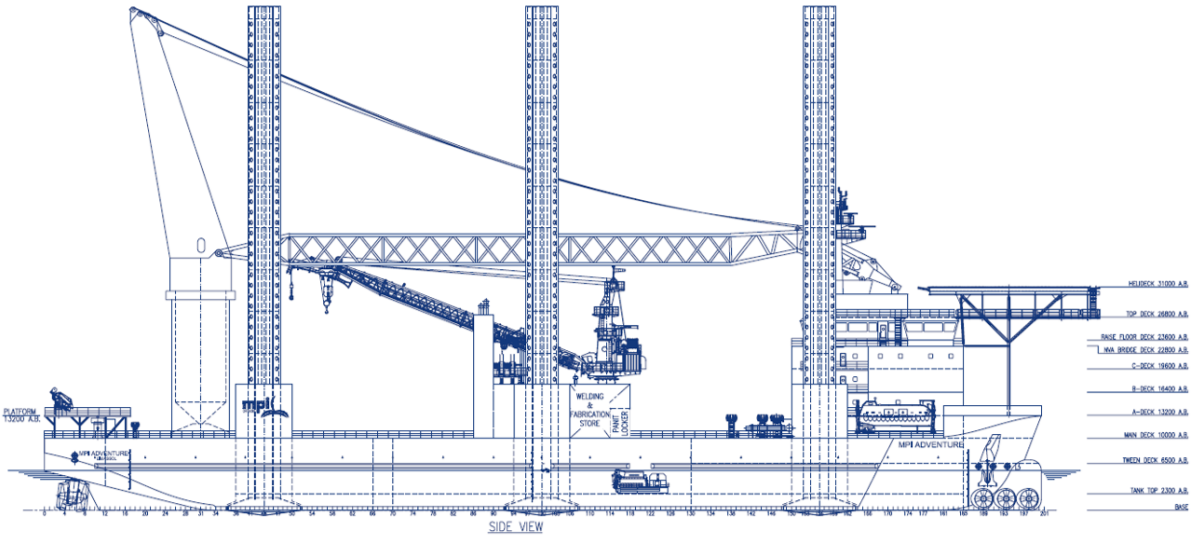

Figure B.1: Side view of the current Adventure jack-up vessel.

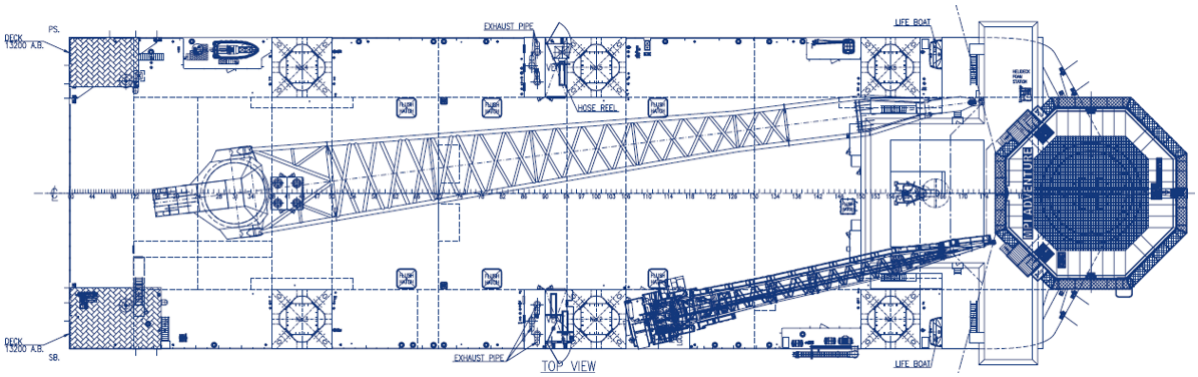

Figure B.2: Top view of the current Adventure jack-up vessel.

Tetrahedron B.V.
info@tetrahedron.tech
Klinkenagelstraat 2
3089 JP, Rotterdam
The Netherlands
Chamber of commerce:
73016608

Project:	TC 900-40-180 / TC 1260-26-130
Subject:	GENERAL ARRANGEMENT (drawn on VO-Adventure)

Subject:	Name	Date
Drawn:	RM	18-08-20
Checked:	WS	28-08-20
Approved:	AR	01-09-20

Scale: 1 :200 — Projection:

Drawing nr.: 2002-00-L101 — Rev.: 0

drawing size A0 (1189 x 841)

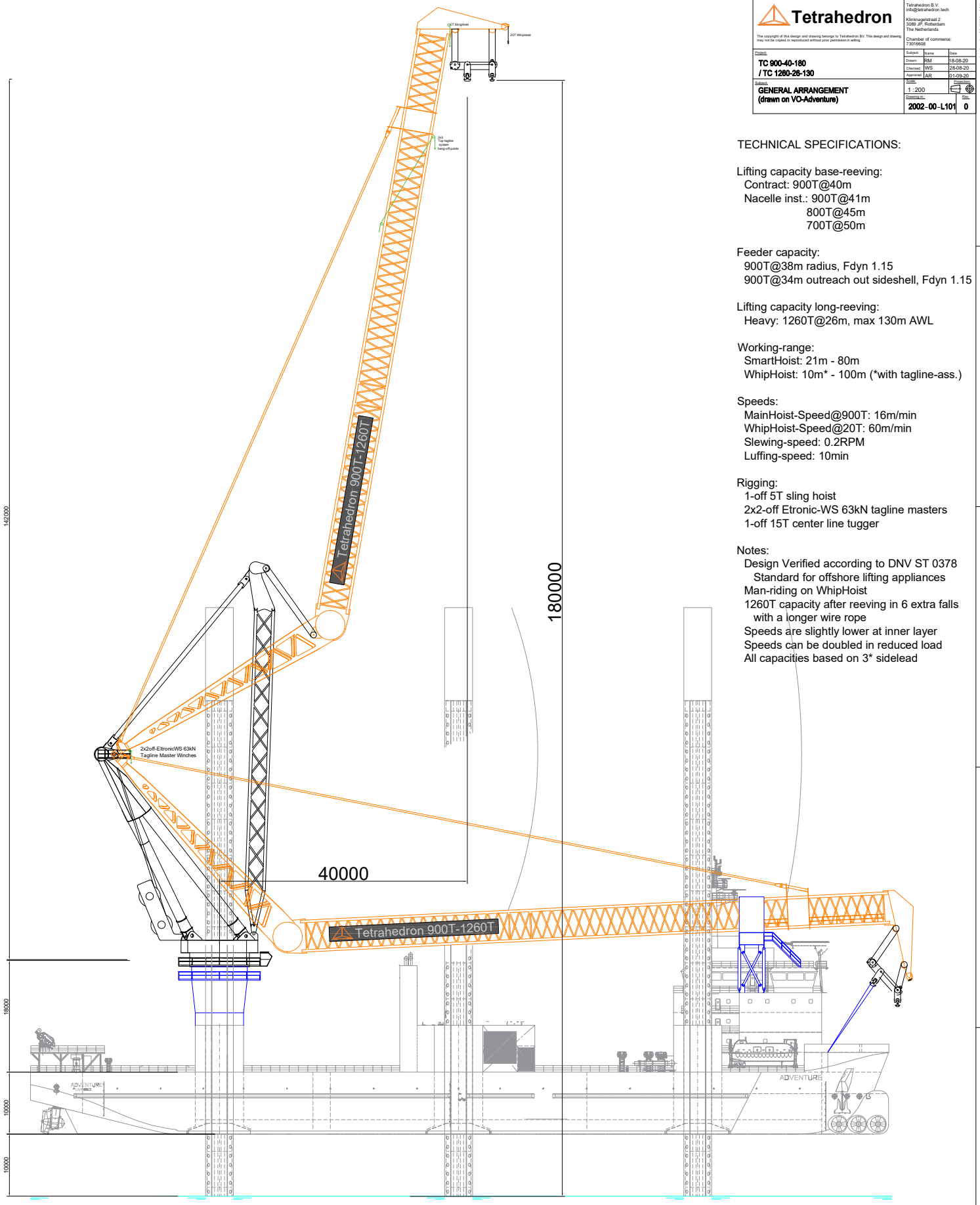

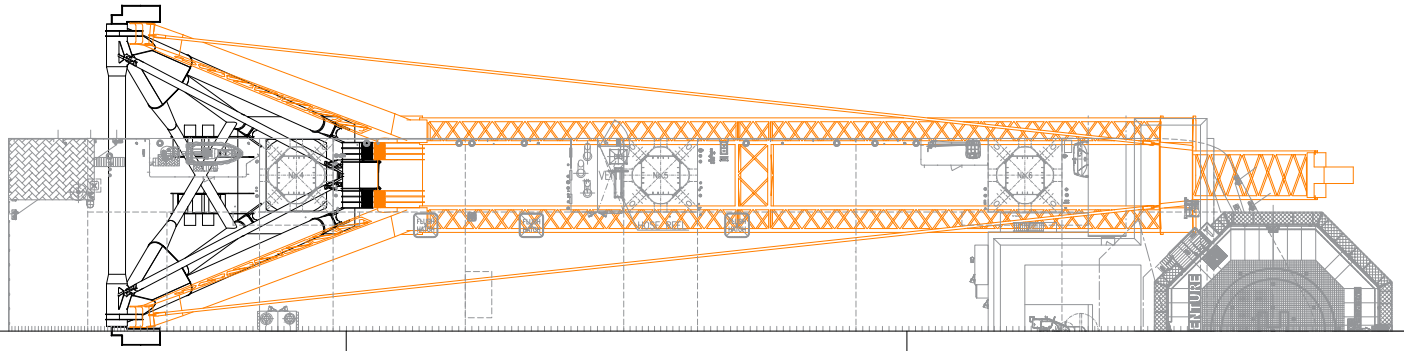

TECHNICAL SPECIFICATIONS:

Lifting capacity base-reeving:
- Contract: 900T@40m
- Nacelle inst.: 900T@41m
  800T@45m
  700T@50m

Feeder capacity:
- 900T@38m radius, Fdyn 1.15
- 900T@34m outreach out sideshell, Fdyn 1.15

Lifting capacity long-reeving:
- Heavy: 1260T@26m, max 130m AWL

Working-range:
- SmartHoist: 21m - 80m
- WhipHoist: 10m* - 100m (*with tagline-ass.)

Speeds:
- MainHoist-Speed@900T: 16m/min
- WhipHoist-Speed@20T: 60m/min
- Slewing-speed: 0.2RPM
- Luffing-speed: 10min

Rigging:
- 1-off 5T sling hoist
- 2x2-off Etronic-WS 63kN tagline masters
- 1-off 15T center line tugger

Notes:
- Design Verified according to DNV ST 0378 Standard for offshore lifting appliances
- Man-riding on WhipHoist
- 1260T capacity after reeving in 6 extra falls with a longer wire rope
- Speeds are slightly lower at inner layer
- Speeds can be doubled in reduced load
- All capacities based on 3* sidelead

C

Friede & Goldman heave motion data

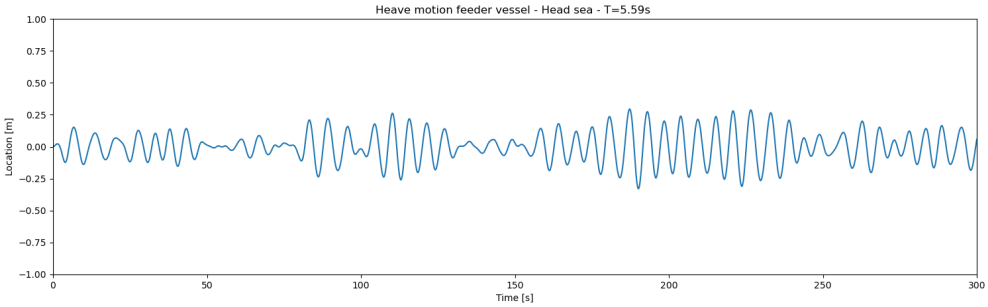

Figure C.1: Heave motion data induced due head sea waves ($T_{average} = 5.59s$)

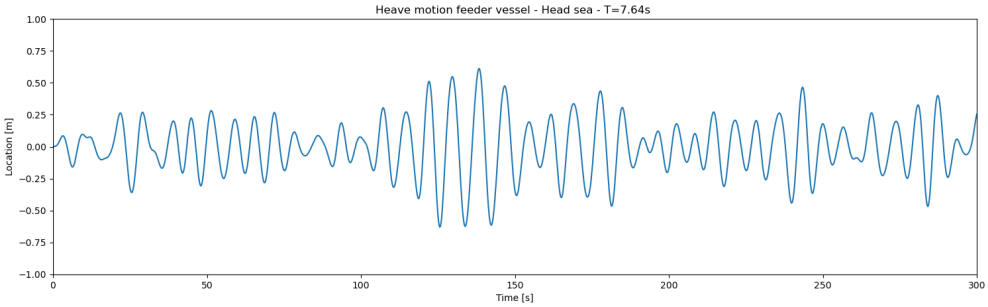

Figure C.2: Heave motion data induced due head sea waves ($T_{average} = 7.64s$)

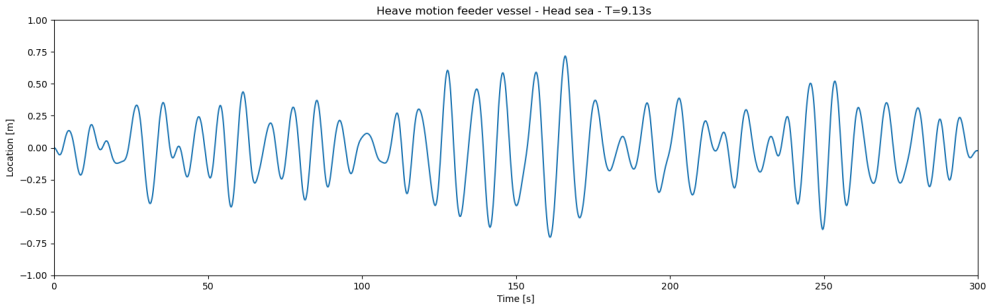

Figure C.3: Heave motion data induced due head sea waves ($T_{average} = 9.13s$)

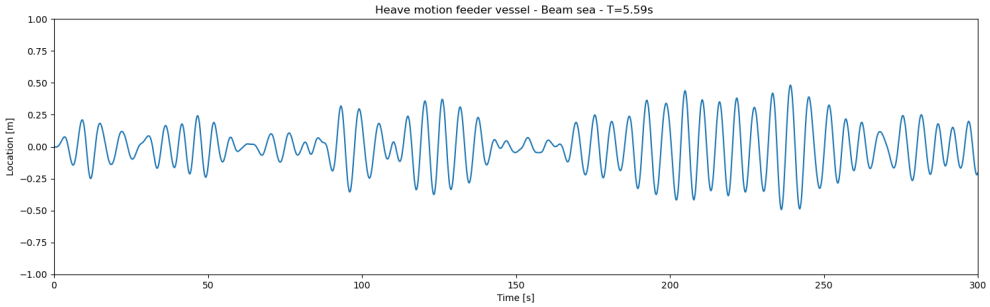

Figure C.4: Heave motion data induced due beam sea waves ($T_{average} = 5.59s$)

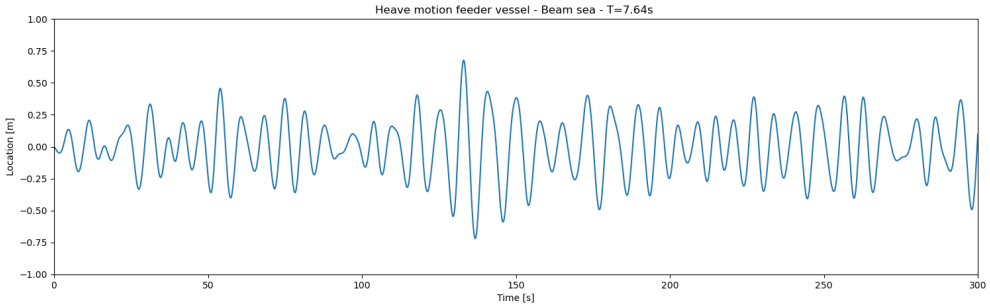

Figure C.5: Heave motion data induced due beam sea waves ($T_{average} = 7.64s$)

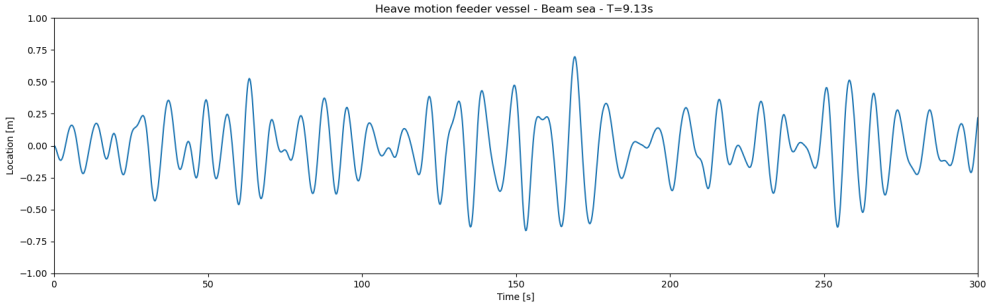

Figure C.6: Heave motion data induced due beam sea waves ($T_{average} = 9.13s$)

D

1D model

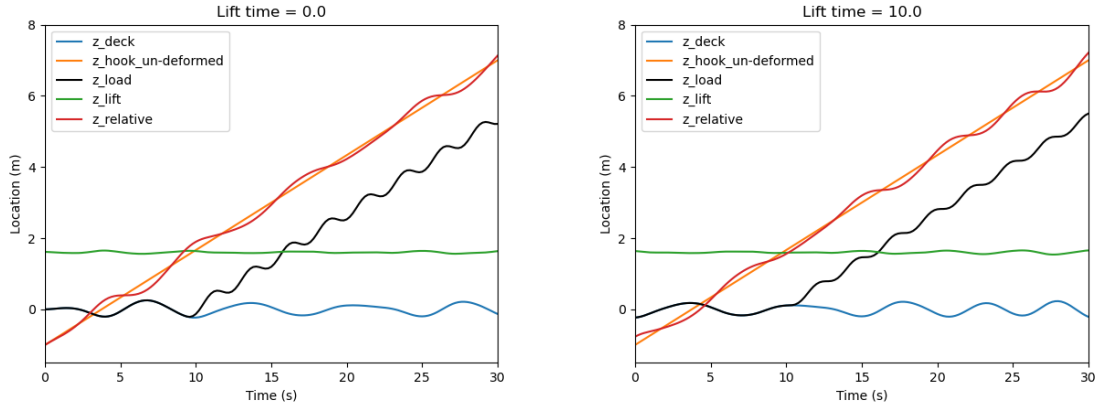

Figure D.1: Lifting graphs for $t_{start} = 0\ s.$ (left) and $t_{start} = 10\ s.$ (right).

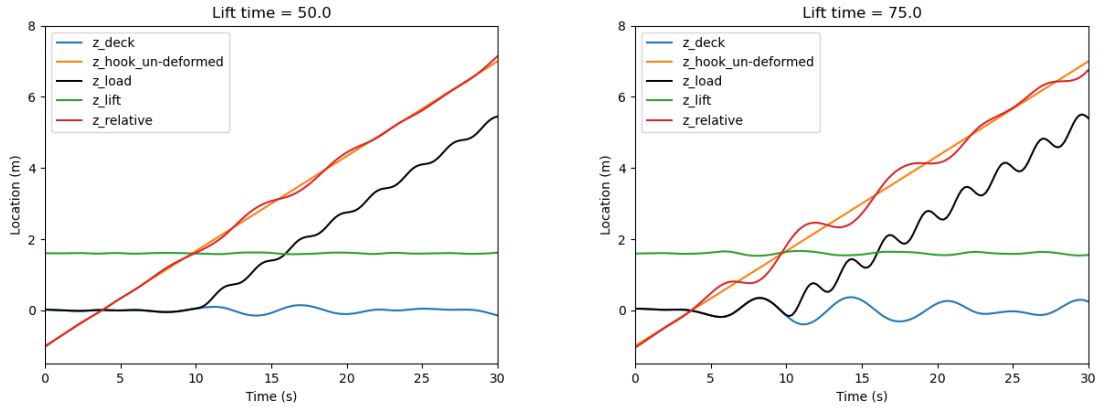

Figure D.2: Lifting graphs for $t_{start} = 50\ s.$ (left) and $t_{start} = 75\ s.$ (right).

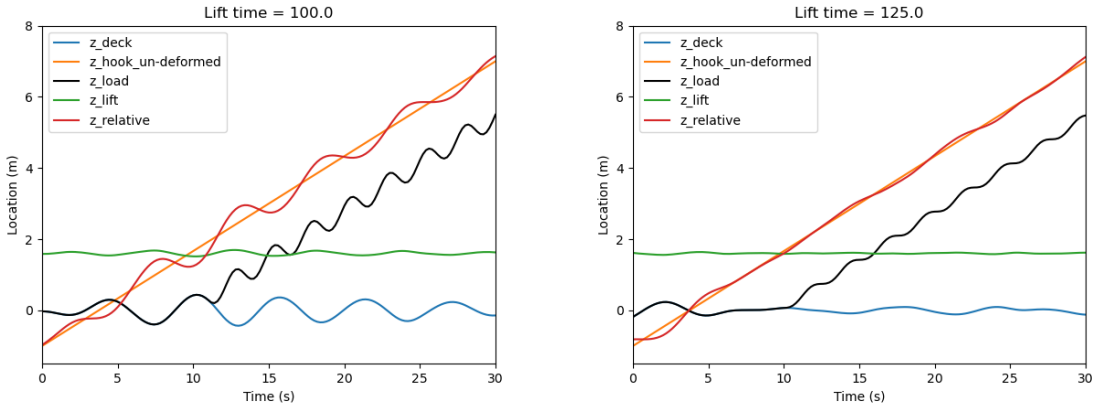

Figure D.3: Lifting graphs for $t_{start} = 100\ s.$ (left) and $t_{start} = 125\ s.$ (right).

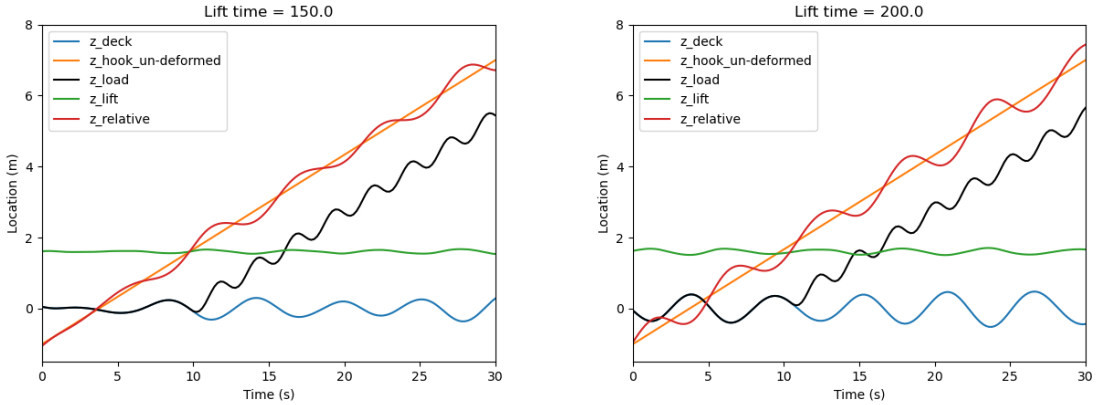

Figure D.4: Lifting graphs for $t_{start} = 150\ s.$ (left) and $t_{start} = 200\ s.$ (right).

E

2D model

Boundary conditions for a fixed-to-fixed beam element:

$$k_z^e = \begin{bmatrix} \frac{12EI_{yy}}{l^3} & \frac{-6EI_{yy}}{l^2} & \frac{-12EI_{yy}}{l^3} & \frac{-6EI_{yy}}{l^2} \\ \frac{-6EI_{yy}}{l^2} & \frac{4EI_{yy}}{l} & \frac{6EI_{yy}}{l^2} & \frac{2EI_{yy}}{l} \\ \frac{-12EI_{yy}}{l^3} & \frac{6EI_{yy}}{l^2} & \frac{12EI_{yy}}{l^3} & \frac{6EI_{yy}}{l^2} \\ \frac{-6EI_{yy}}{l^2} & \frac{4EI_{yy}}{l} & \frac{6EI_{yy}}{l^2} & \frac{4EI_{yy}}{l} \end{bmatrix} \quad \text{(E.1)}$$

Boundary conditions for a fixed-to-pinned beam element:

$$k_z^e = \begin{bmatrix} \frac{3EI_{yy}}{l^3} & \frac{-3EI_{yy}}{l^2} & \frac{-3EI_{yy}}{l^3} & 0 \\ \frac{-3EI_{yy}}{l^2} & \frac{3EI_{yy}}{l} & \frac{3EI_{yy}}{l^2} & 0 \\ \frac{-3EI_{yy}}{l^3} & \frac{3EI_{yy}}{l^2} & \frac{3EI_{yy}}{l^3} & 0 \\ 0 & 0 & 0 & 0 \end{bmatrix} \quad \text{(E.2)}$$

Boundary conditions for a pinned-to-fixed beam element:

$$k_z^e = \begin{bmatrix} \frac{3EI_{yy}}{l^3} & 0 & \frac{-3EI_{yy}}{l^3} & \frac{-3EI_{yy}}{l^2} \\ 0 & 0 & 0 & 0 \\ \frac{-3EI_{yy}}{l^3} & 0 & \frac{3EI_{yy}}{l^3} & \frac{3EI_{yy}}{l^2} \\ \frac{-3EI_{yy}}{l^2} & 0 & \frac{3EI_{yy}}{l^2} & \frac{3EI_{yy}}{l} \end{bmatrix} \quad \text{(E.3)}$$

Boundary conditions for a pinned-to-pinned beam element:

$$k_z^e = \begin{bmatrix} 0 & 0 & 0 & 0 \\ 0 & 0 & 0 & 0 \\ 0 & 0 & 0 & 0 \\ 0 & 0 & 0 & 0 \end{bmatrix} \quad \text{(E.4)}$$

Axial degree of freedom:

$$k_u^e = \begin{bmatrix} \frac{EA}{l} & \frac{-EA}{l} \\ \frac{-EA}{l} & \frac{EA}{l} \end{bmatrix} \quad \text{(E.5)}$$

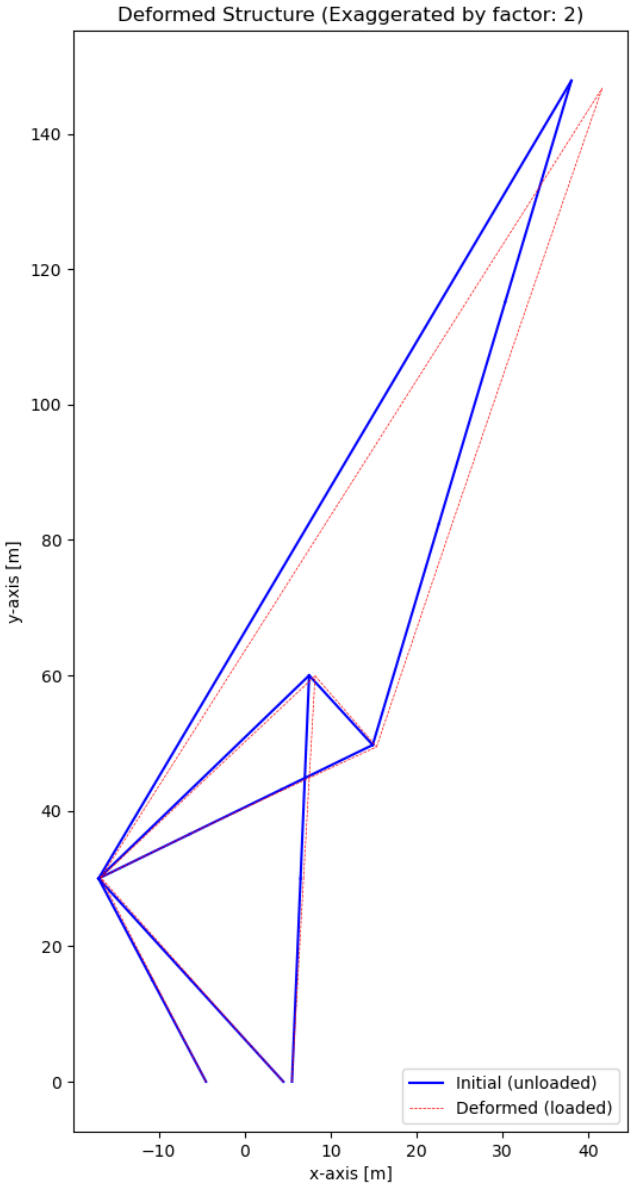

Figure E.1: Initial structure 2D side-view Tetrahedron displaced due to loading.

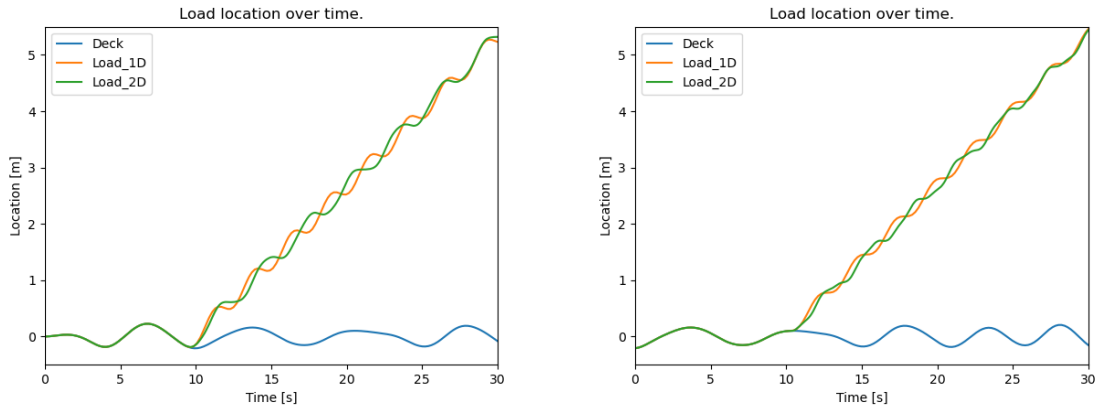

Figure E.2: Comparing load location between 1D- and 2D-model for $t_{start} = 0\ s.$ (left) and $t_{start} = 10\ s.$ (right)

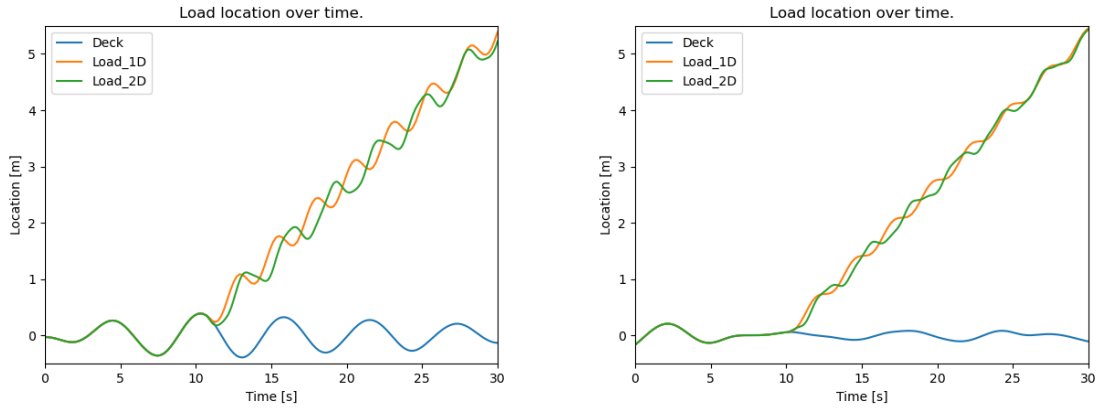

Figure E.3: Comparing load location between 1D- and 2D-model for $t_{start} = 100\ s.$ (left) and $t_{start} = 125\ s.$ (right)

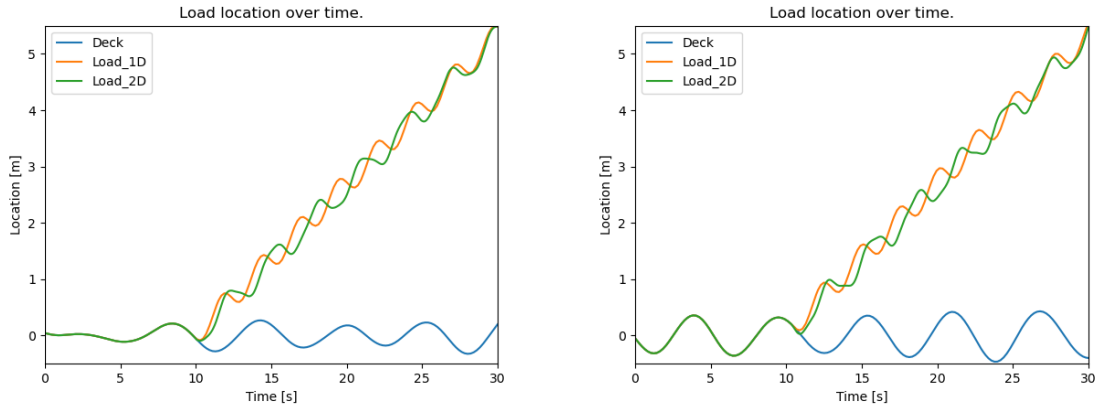

Figure E.4: Comparing load location between 1D- and 2D-model for $t_{start} = 150\ s.$ (left) and $t_{start} = 200\ s.$ (right)

Case study results

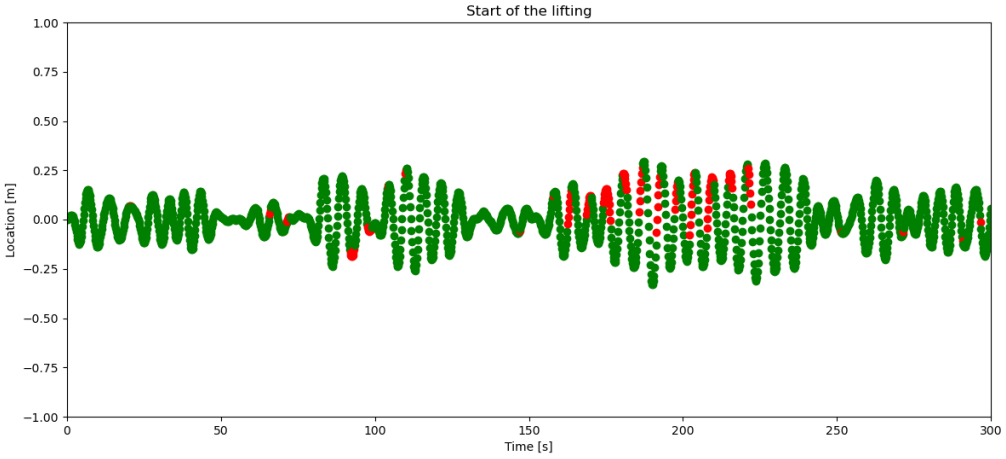

Figure F.1: Lifting results with a lower hoisting velocity (10 m/min) compared to the case study.

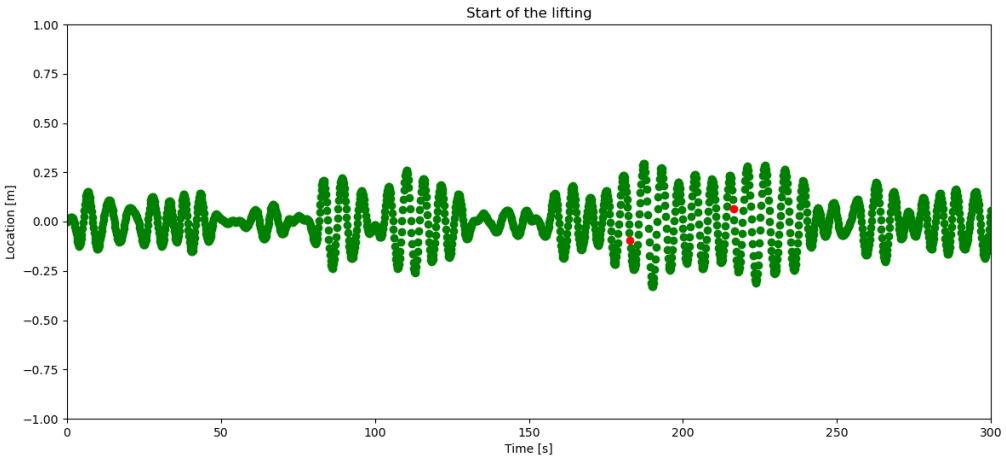

Figure F.2: Lifting results with a higher hoisting velocity (18 m/min) compared to the case study.

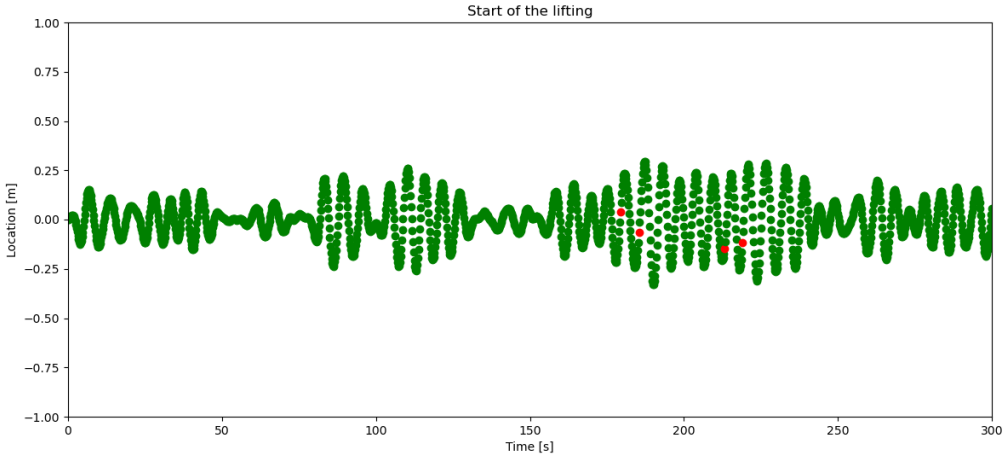

Figure F.3: Lifting results when the load weighs 300 tonnes (representing the blade rack).

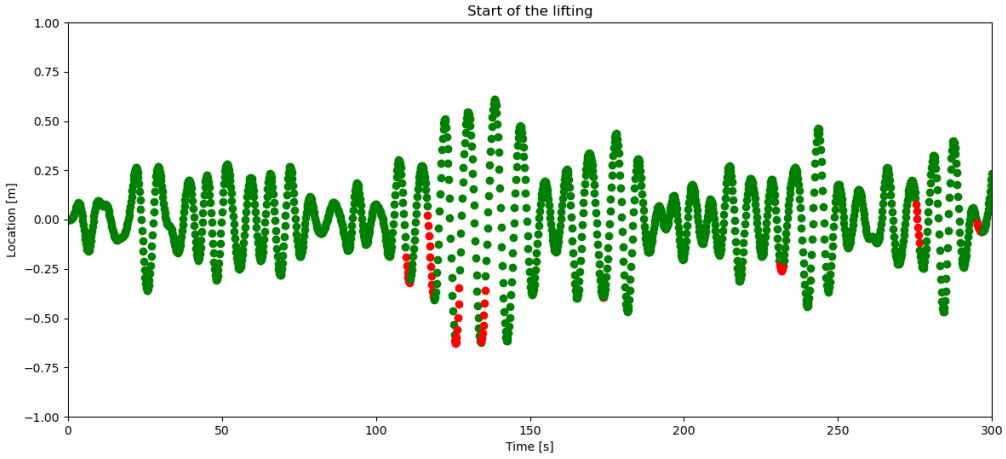

Figure F.4: Lifting results when average wave period is 7.64 s.

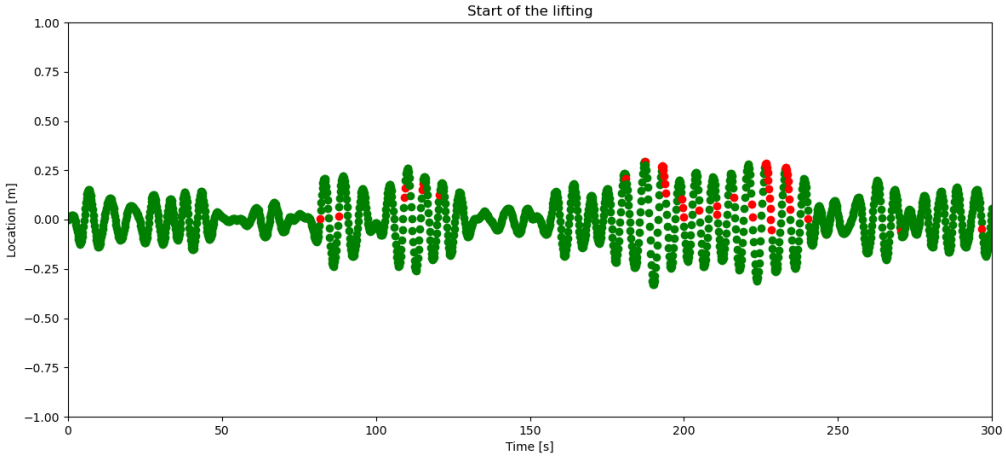

Figure F.5: Lifting results when the waves are coming from the beam sea direction.

Bibliography

[1] L. Ramirez, D. Fraile, G. Brindley, "Annual offshore statistics 2019.," February 2020.

[2] A. Von Ah, "*Offshore Wind Energy: Planned Projects May Lead to Construction of New Vessels in the U.S., but Industry Has Made Few Decisions amid Uncertainties*." https://www.gao.gov/products/gao-21-153. (visited: 10-05-2021).

[3] Tetrahedron B.V., "*Tetrahedron, Simply Lifting Higher*." https://www.tetrahedron.tech/. (visited: 17-02-2021).

[4] H. Slager, "*Netherlands Maritime Technology, Jones Act*." https://maritimetechnology.nl/standpunten/jones-act-ernstige-vorm-van-protectionisme/. (visited: 03-05-2021).

[5] M. Peeters, G. Santo, J. Degroote, and W. V. Paepegem, "The concept of segmented wind turbine blades: a review," *Energies*, vol. 10, 2017.

[6] Power Technology, "*London Array Offshore Wind Farm, Thames Estuary*." https://www.power-technology.com/projects/london-array/. (visited: 18-05-2021).

[7] Ørsted, "*Hornsea One is the largest offshore wind farm in the world*." https://hornseaprojectone.co.uk/about-the-project#project-timeline-2020. (visited: 18-05-2021).

[8] RWE Innogy, "*World's 2nd largest offshore wind farm Gwynt y Môr officially inaugurated*." https://www.group.rwe/en/investor-relations/news-and-ad-hoc-announcements/news/archive-ir-announcements/2015/World-s-2nd-largest-offshore-wind-farm-Gwynt-y-M-r-officially-inaugurated. (visited: 18-05-2021).

[9] A. Durakovic, "*South Korea Launches EUR 36 Billion Offshore Wind Project*." https://www.offshorewind.biz/2021/02/05/south-korea-launches-eur-36-billion-offshore-wind-project/. (visited: 18-05-2021).

[10] Navingo, "*Offshore WIND Vessel Directory 2018*." https://issuu.com/navingo/docs/ow_vd_def. (visited: 14-05-2021).

[11] Scaldis SMC, "*Transport and Installation of two 5MW Wind Turbine Generators for the Beatrice Demonstrator Project*." http://www.scaldis-smc.com/en/projects/groen-2007-jul-beatrice/. (visited: 02-11-2020).

[12] Saipem, "*Hywind Project.*." https://www.saipem.com/en/projects/hywind. (visited: 03-11-2020).

[13] GE Renewable Energy, "*Getting Block Island Shipshape*." https://www.ge.com/renewableenergy/stories/block-island-construction-process. (visited: 20-05-2021).

[14] Fred. Olsen Windcarrier AS, "*Case Study: Block Island*." https://windcarrier.com/block-island-15. (visited: 20-05-2021).

[15] GE Renewable Energy, "*GE Haliade Turbines Stand in China*." https://www.offshorewind.biz/2018/04/23/ge-haliade-turbines-stand-in-china/. (visited: 20-05-2021).

[16] A. Durakovic, "*First Turbine Up at Yangjiang Nanpeng Island Offshore Wind Farm*." https://www.offshorewind.biz/2019/07/11/first-turbine-up-at-yangjiang-nanpeng-island-offshore-wind-farm-video/. (visited: 20-05-2021).

[17] G. A. Stenhouse, R. J. Hilton, *et al.*, "Method for rating high pedestal cranes for lifting from supply boats in various sea states," in *SPE European Petroleum Conference*, Society of Petroleum Engineers, 1978.

[18] DNV-GL, *Offshore and platform lifting appliances (DNVGL-ST-0378)*. 2019.

[19] SAE-International, *Rating Lift Cranes on Fixed Platforms Operating in the Ocean Environment (J1238)*. 2017.

[20] API-Specification-2C, *Specification for Offshore Cranes*. 1995.

[21] Power Technology, "*Wind turbines continue to grow in size*." https://www.power-technology.com/comment/wind-turbines-continue-grow-size/. (visited: 07-05-2021).

[22] R. Wiser, M. Hand, J. Seel, and B. Paulos, "*The future of wind energy.*." https://emp.lbl.gov/news/future-wind-energy-part-3-reducing-wind. (visited: 09-05-2021).

[23] M. Schuler, "*First Large-Scale Offshore Wind Project in U.S. Selects DEME-Foss Partnership for Wind Turbine Installation Work*." https://gcaptain.com/first-large-scale-offshore-wind-project-in-u-s-selects-deme-foss-\partnership-for-wind-turbine-installation-work/. (visited: 10-05-2021).

[24] A. Durakovic, "*GE Haliade-X Wind Turbine Now Typhoon-Proof*." https://www.offshorewind.biz/2021/04/29/ge-haliade-x-wind-turbine-now-typhoon-proof/. (visited: 11-06-2021).

[25] Vineyard Wind, "*Vineyard Wind Receives Record of Decision for First in the Nation Commercial Scale Offshore Wind Project*." https://www.vineyardwind.com/press-releases/2021/5/11/vineyard-wind-receives-record-of-decision. (visited: 13-06-2021).

[26] J. M. Niedzwecki and S. K. Thampi, "Snap loading of marine cable systems," *Applied Ocean Research*, 1991.

[27] V. Cazenave, *WOS-T&I-RFE-026-Haliade-X-WIV Requierements for Installation*. GE Renewable Energy, 2019.

[28] D. Charrett, A. Hyden, *et al.*, "Dynamic factors for offshore cranes," in *Offshore Technology Conference*, Offshore Technology Conference, 1976.

[29] D. Owen, "The dynamic behaviour of offshore platform cranes," *Structural Engineer*, vol. 57, no. 4, 1979.

[30] J. L. Mendoza Zabala, *State-space formulation for structure dynamics*. PhD thesis, Massachusetts Institute of Technology, 1996.

[31] C. Vuik, F. J. Vermolen, M. B. van Gijzen, and M. J. Vuik, *Numerical methods for ordinary differential equations*. Delft Academic Press, 2015.

[32] M. Paz and Y. H. Kim, *Structural Dynamics - Theory and Computation, sixth edition*. Springer, 2019.

[33] W. McGuire, R. H. Gallagher, and R. D. Ziemian, *Matrix Structural Analysis, 2nd Edition*. Faculty Books 7, 2000.

[34] MSC Nastran, "*Multidisciplinary Structural Analysis*." https://www.mscsoftware.com/product/msc-nastran. (visited: 14-08-2021).